

## BIROn - Birkbeck Institutional Research Online

Marschall, H.R. and Wanless, V.D. and Shimizu, N. and Pogge von Strandmann, Philip A.E. and Elliott, T. and Monteleone, B.D. (2017) The boron and lithium isotopic composition of mid-ocean ridge basalts and the mantle. *Geochimica et Cosmochimica Acta* 207 , pp. 102-138. ISSN 0016-7037.

Downloaded from: <https://eprints.bbk.ac.uk/id/eprint/18628/>

*Usage Guidelines:*

Please refer to usage guidelines at <https://eprints.bbk.ac.uk/policies.html>  
contact [lib-eprints@bbk.ac.uk](mailto:lib-eprints@bbk.ac.uk).

or alternatively

# The boron and lithium isotopic composition of mid-ocean ridge basalts and the mantle

Horst R. Marschall<sup>1,2\*</sup>, V. Dorsey Wanless<sup>3</sup>, Nobumichi Shimizu<sup>1</sup>,  
Philip A.E. Pogge von Strandmann<sup>4</sup>, Tim Elliott<sup>5</sup>, Brian D. Monteleone<sup>1</sup>

<sup>1</sup> Dep. Geology and Geophysics, Woods Hole Oceanographic Institute, Woods Hole, MA 02543, USA

<sup>2</sup> Institut für Geowissenschaften, Goethe Universität Frankfurt, Altenhöferallee 1, 60438 Frankfurt am Main, Germany

<sup>3</sup>Dep. Geosciences, Boise State University, Boise, ID 83725, USA

<sup>4</sup>London Geochemistry and Isotope Centre (LOGIC), Institute of Earth and Planetary Sciences, University College London and Birkbeck, University of London, Gower Street, London WC1E 6BT, UK

<sup>5</sup>School of Earth Sciences, University of Bristol, Wills Memorial Building, Queen's Road, Bristol BS8 1RJ, UK

\*Corresponding author.

Tel: +49-69-798-40124

Fax: +49-69-798-40121

E-mail: marschall@em.uni-frankfurt.de

Short title: Boron and Li isotopes in MORB

Submitted to **Geochimica et Cosmochimica Acta** on 24. April 2016

Revised version submitted on 30. September 2016

2<sup>nd</sup> revised version submitted on 19. December 2016

3<sup>rd</sup> revised version submitted on 17. March 2017

Accepted for publication on 22. March 2017

DOI: 10.1016/j.gca.2017.03.028

## Abstract

A global selection of 56 mid-ocean ridge basalt (MORB) glasses were analysed for Li and B abundances and isotopic compositions. Analytical accuracy and precision of analyses constitute an improvement over previously published MORB data and allow a more detailed discussion of the Li and B systematics of the crust-mantle system. Refined estimates for primitive mantle abundances ( $[\text{Li}] = 1.39 \pm 0.10 \mu\text{g/g}$  and  $[\text{B}] = 0.19 \pm 0.02 \mu\text{g/g}$ ) and depleted mantle abundances ( $[\text{Li}] = 1.20 \pm 0.10 \mu\text{g/g}$  and  $[\text{B}] = 0.077 \pm 0.010 \mu\text{g/g}$ ) are presented based on mass balance and on partial melting models that utilise observed element ratios in MORB.

Assimilation of seawater (or brine) or seawater-altered material beneath the ridge, identified by high Cl/K, causes significant elevation of MORB  $\delta^{11}\text{B}$  and variable elevation in  $\delta^7\text{Li}$ . The B isotope ratio is, hence, identified as a reliable indicator of assimilation in MORB and values higher than  $-6\text{‰}$  are strongly indicative of shallow contamination of the magma.

The global set of samples investigated here were produced at various degrees of partial melting and include depleted and enriched MORB from slow and fast-spreading ridge segments with a range of radiogenic isotope signatures and trace element compositions. Uncontaminated (low-Cl/K) MORB show no significant boron isotope variation at the current level of analytical precision, and hence a homogenous B isotopic composition of  $\delta^{11}\text{B} = -7.1 \pm 0.9\text{‰}$  (mean of six ridge segments; 2SD). Boron isotope fractionation during mantle melting and basalt fractionation likely is small, and this  $\delta^{11}\text{B}$  value reflects the B isotopic composition of the depleted mantle and the bulk silicate Earth, probably within  $\pm 0.4\text{‰}$ .

Our sample set shows a mean  $\delta^7\text{Li} = +3.5 \pm 1.0\text{‰}$  (mean of five ridge segments; 2SD), excluding high-Cl/K samples. A significant variation of  $1.0 - 1.5\text{‰}$  exists among various ridge segments and among samples within individual ridge segments, but this variation is unrelated to differentiation, assimilation or mantle source indicators, such as radiogenic isotopes or trace elements. It, therefore, seems likely that kinetic fractionation of Li isotopes during magma extraction, transport and storage may generate  $\delta^7\text{Li}$  excursions in MORB. No mantle heterogeneities, such as those generated by deeply recycled subducted materials, are invoked in the interpretation of the Li and B isotope data presented here, in contrast to previous work on smaller data sets.

Lithium and boron budgets for the silicate Earth are presented that are based on isotope and element mass balance. A refined estimate for the B isotopic composition of the bulk continental crust is given as  $\delta^{11}\text{B} = -9.1 \pm 2.4\text{‰}$ . Mass balance allows the existence of recycled B reservoirs in the deep mantle, but these are not required. However, mass balance among the crust, sediments and seawater shows enrichment of  $^6\text{Li}$  in the surface reservoirs, which requires the existence of  $^7\text{Li}$ -enriched material in the mantle. This may have formed by the subduction of altered oceanic crust since the Archaean.

Keywords: boron, lithium, chlorine, MORB, assimilation, mantle

## 1 Introduction

One of the central foci of modern geochemistry is tracing material in the Earth's mantle that had previously been at the surface. This puts constraints on the compositional structure and heterogeneity of the mantle and on its long-term and large-scale convection. Geochemical research on the volcanic output at mid-ocean ridges, ocean islands and at subduction zones revolves around elemental and isotopic tracers that allow estimates on the amount of crustal material that was entrained into the source region of those magmas. Ideal tracers for this purpose should possess isotopic signatures that are uniquely produced at the surface and concentrations that are high in crustal rocks, sediments or in altered rocks of the seafloor but very low in the mantle. The elements lithium and boron fulfil most or all of these criteria better than most other elements and their isotope systems have been employed to trace recycling of crustal rocks in the mantle (e.g., Elliott *et al.*, 2004; Ryan & Chauvel, 2014; Tomascak *et al.*, 2016b).

Boron is a quintessentially crustal element with high concentrations in rocks of continental affinity and in rocks that interacted with the hydrosphere. Oceanic sediments and altered oceanic basalts and peridotites show very high B abundances (10 – 200 µg/g), whereas the depleted mantle is characterised by very low B contents (< 0.1 µg/g; Leeman & Sisson, 1996). Fractionation of the two stable isotopes of boron ( $^{10}\text{B}$  and  $^{11}\text{B}$ ) at low temperatures is responsible for surface reservoirs that are strongly enriched in the heavy isotope, with  $\delta^{11}\text{B}$  of seawater at the high end of the scale (+39.6‰; Foster *et al.*, 2010). Entrainment of seawater-altered material into the mantle via subduction should, therefore, potentially be detectable by anomalous- $\delta^{11}\text{B}$  domains in the mantle. However, the key to establishing this tracer critically depends on a well-defined geochemical baseline, i.e., the isotopic composition of the mantle that does not contain recycled components; yet, this value has so far been afflicted with large uncertainties. In this paper we present a study on a global set of mid-ocean ridge basalt (MORB) glasses to evaluate the absolute value and the variability of the B isotopic composition of these mantle-derived magmatic products and, by inference, that of the depleted mantle itself.

Boron isotope analyses of silicate materials with low B concentrations are not trivial, and the very low abundances of B in pristine, unmetasomatised mantle samples are not accessible with current analytical techniques at the level of precision required for a geologically meaningful interpretation. Alternatively, however, MORB glasses have been used to indirectly determine the elemental and isotopic composition of the convecting mantle. Attempts to determine the B isotopic composition of unaltered basalts and, by inference, the primitive and depleted mantle were made in a number of previous studies (e.g., Spivack & Edmond, 1987; Chaussidon & Jambon, 1994; Moriguti & Nakamura, 1998). The results are based on a restricted number of samples and span a wide range of  $\delta^{11}\text{B}$  values from approximately –10 to 0‰ (e.g., Ishikawa & Nakamura, 1992; Roy-Barman *et al.*, 1998; Chaussidon & Marty, 1995). In addition, it is not clear to what degree the lack of suitable B isotope reference materials and the limited analytical capabilities for B isotope analysis in the 1980s and early 1990s may have caused the discrepancy among the published studies (see Gonfiantini *et al.*, 2003). International reference materials for micro analysis are available today, and an improved mass spectrometric method was recently developed for the determination of the B isotopic composition of volcanic glasses with boron concentrations of as low as 0.4 – 2.5 µg/g, as is typical for MORB glasses (Marschall & Monteleone, 2015).

The light alkali metal lithium with its two stable isotopes,  $^6\text{Li}$  and  $^7\text{Li}$ , has gained similar attention in geochemistry to boron, with a similar range of possible applications. Yet, there are also some notable differences between these two trace elements that could lead to a combined geochemical application of the two isotope systems for a complementary approach (e.g., Gurenko & Schmincke, 2002; Kobayashi *et al.*, 2004; Genske *et al.*, 2014). Lithium is less incompatible than boron in mantle minerals and during partial melting of the mantle, and its enrichment in the continental crust and altered oceanic crust compared to the depleted mantle is much less extreme (Tomascak, 2004; Elliott *et al.*, 2004; Sauzéat *et al.*, 2015). Both elements show a high mobility in hydrous fluids and silicate melts, show a strong enrichment of the heavy isotope in seawater ( $\delta^7\text{Li} = +30.8\text{‰}$ ; Rosner *et al.*, 2007) and are enriched in low-temperature altered

crust. Yet, lithium diffusivities are high in minerals and melts, second only to H, and a strong kinetic isotope fractionation has been documented for many high-temperature systems, producing much greater isotopic excursions than any equilibrium fractionation process (e.g.; Richter *et al.*, 2003; Lundstrom *et al.*, 2005; Teng *et al.*, 2006; Parkinson *et al.*, 2007; Jeffcoate *et al.*, 2007).

The lithium isotopic composition of MORB and the mantle has been addressed in a number of studies. Published analyses for fresh MORB samples range from  $\delta^7\text{Li} = +1.5$  to  $+5.6\text{‰}$  (Chan *et al.*, 1992; Moriguti & Nakamura, 1998; Elliott *et al.*, 2006; Nishio *et al.*, 2007; Tomascak *et al.*, 2008). The majority of analyses, however, fall between  $+3.0$  and  $+4.0\text{‰}$ . The same range with a mean value close to  $+3.5\text{‰}$  has been found for equilibrated peridotites (Seitz *et al.*, 2004; Jeffcoate *et al.*, 2007; Pogge von Strandmann *et al.*, 2011; Lai *et al.*, 2015), and for mantle-derived carbonatites from the late Archaean to the present (Halama *et al.*, 2008). There is general agreement that this value is representative of normal MORB and the depleted upper mantle. However, it is unclear how much of the  $> 4\text{‰}$  range in  $\delta^7\text{Li}$  observed for MORB is the result of limited analytical precision, accuracy and interlaboratory comparability, and how much of it is an actual isotopic variability in these rocks. Furthermore, if real variability exists, it is a matter of debate by what process it was generated: does it reflect Li isotopic variability in the MORB-source mantle, or is it introduced by magmatic and metasomatic processes at the mid-ocean ridges?

In this study we analysed B and Li concentrations and isotopic compositions of a selection of 56 global MORB glasses, which had been well characterised in previous studies for their major, minor and trace element contents, as well as their radiogenic isotope compositions. They are fresh, unaltered basaltic glasses, ranging from depleted to enriched compositions. Halogen concentrations (F, Cl) were analysed for samples for which these had not previously been published to monitor assimilation of seawater-altered materials or brines by the MORB magma beneath the ridge (Michael & Schilling, 1989; Michael & Cornell, 1998; le Roux *et al.*, 2006; Kendrick *et al.*, 2013). The B and Li isotopic variability of mid-ocean ridge basalts is evaluated based on this new dataset, and effects of partial melting, fractionation and assimilation of seawater-altered materials by the MORB magmas at the ridge are addressed. Estimates for the abundances of Li and B and the B and Li isotopic compositions of the primitive and depleted mantle are presented, as well as estimates for the B isotopic composition of the continental crust, based on global mass balance. Mass balance among the surface reservoirs for Li argues for the enrichment of  $^7\text{Li}$  in at least part of the mantle.

## 2 Investigated samples

Fifty-six mid-ocean ridge glass samples were selected for this study. All samples are natural glasses from pillow basalt margins that have been investigated previously in a number of studies (see references in Table 1). Their major element, trace element and isotopic compositions were reported by various authors and are listed in the PetDB database (<http://www.earthchem.org/petdb>). In this study, we present new data for glasses from three different sections of the East-Pacific Rise (EPR), two localities on the Mid-Atlantic Ridge (MAR) and from one locality on the South-West Indian Ridge (SWIR). Samples were selected from well-investigated ridge segments far from the possible influence of hot spots (with the exception of two samples from the Kolbeinsey Ridge, which are close to Iceland). The samples represent depleted and enriched MORB having experienced various degrees of partial melting and fractionation, and they represent a range in radiogenic isotope space. All samples are listed in Table 1.

### 2.1 Mid-Atlantic Ridge, 26°S

The 26°S segment of the MAR is bounded by two transform fracture zones (see map in Supplement) and comprises depleted MOR basalts (N-MORB) that show a small degree of low-pressure differentiation with MgO contents of 8.9 – 6.6 wt% and Mg# of 63 – 51 (Niu & Batiza, 1994). Pieces of glass from 16 samples were selected that cover the full range in MgO content and the full length of the segment from dredges

D12 to D27 near the two bounding transform faults, respectively (see map in Supplement). Nine of these samples have  $Mg\# > 60$  with  $MgO = 7.8 - 8.9$  wt%. All dredges sampled on-axis basalts at approximately equal spacing along the  $\sim 100$  km long section. Spreading in this section is slow and slightly asymmetrical at  $19.3$  mm/a to the west and  $16.3$  mm/a to the east (Carbotte *et al.*, 1991). The segment shows an intermediate high of the ridge axis (the “ $26^\circ$  axial swell”; see map in Supplement) with a depth of  $2500$  m, whereas the depth of the ridge north and south of that swell is close to  $4000$  m (Table 1). Samples from off-axis seamounts were not analysed. There is no hot-spot volcanism within  $1300$  km of this ridge segment.

Incompatible trace elements in the basalts are depleted, and radiogenic isotopes show a depleted mantle source (Fig. 1; Table 2; Castillo & Batiza, 1989; Graham *et al.*, 1996; Regelous *et al.*, 2009). The Mid-Atlantic Ridge  $26^\circ$ S samples best represent depleted N-MORB from a slow-spreading ridge.

## 2.2 Kolbeinsey Ridge (Atlantic, $67^\circ$ N)

The Kolbeinsey Ridge is located north of Iceland and is a very shallow ridge ( $< 1000$  m). It stretches from the Tjörnes Fracture Zone in the south that separates it from northern Iceland to the Jan Mayen Fracture Zone at  $71^\circ$ N (Devey *et al.*, 1994). The spreading rate of the ridge is  $20$  mm/a (Devey *et al.*, 1994). The two samples investigated here were dredged in 1989 during *Polarstern* cruise ARKV/Ib from a locality near  $67^\circ$ N at a depth of  $< 200$  m (Table 1; Devey *et al.*, 1994).

The two samples investigated have high  $MgO$  contents (Table 2). Their radiogenic isotopes show high  $^{87}\text{Sr}/^{86}\text{Sr}$ , but the lowest  $^{207}\text{Pb}/^{204}\text{Pb}$  among all samples investigated, and they have depleted incompatible trace elements (Fig. 1; Table 2; Mertz *et al.*, 1991). The Kolbeinsey Ridge samples represent depleted MORB produced by high degrees of partial melting at a very shallow ridge segment. The ridge is located adjacent to the Iceland plume.

## 2.3 South-West Indian Ridge, $57^\circ$ E

The  $57^\circ$ E segment of the South-West Indian Ridge is located directly to the east of the Atlantis-II Fracture Zone, north of the Atlantis Bank core complex (see map in Supplement). It comprises MOR basalts that are less depleted in incompatible elements than typical N-MORB and are interpreted as the product of lower degrees of partial melting compared to most other MORB as a result of the very low total spreading rate of  $13 - 16$  mm/a (Jestin *et al.*, 1994; Robinson *et al.*, 2001). The samples were dredged from a depth of  $4325 - 4800$  m below sea level (Table 1). The chemistry of the glasses shows evidence of a small degree of differentiation by low-pressure fractional crystallisation to various degrees with  $MgO$  contents of  $7.5 - 5.9$  wt% and  $Mg\#$  of  $58 - 49$  (Robinson *et al.*, 1996). Five samples were selected for this study that cover the full range in composition.

Incompatible trace elements in the basalts are only moderately depleted, and radiogenic isotopes show a depleted mantle source very unradiogenic Pb that plots to the left of the Geochron (Table 2; Robinson, 1998). There is no hot-spot volcanism within  $1000$  km of this ridge segment. The samples from the South-West Indian Ridge  $57^\circ$ E best represent depleted MORB generated by low-degree melting at a very-slow spreading ridge.

## 2.4 East-Pacific Rise, $10.5^\circ$ N and $11.4^\circ$ N

The segment of EPR between the Clipperton Fault Zone ( $10.3^\circ$ N) and the overlapping spreading center (OSC) at  $11.8^\circ$ N (see map in Supplement) was subject to a number of geophysical and geochemical studies (e.g., Thompson *et al.*, 1989; Regelous *et al.*, 1999; Pan & Batiza, 2003; Elliott *et al.*, 2006; White *et al.*, 2006). In particular, two sample series taken at  $10.5^\circ$ N and  $11.4^\circ$ N, respectively, were subject to geochemical studies. The section at  $10.5^\circ$ N was sampled by dredging and rock coring, and it covers an across-ridge traverse out to  $50$  km on the Pacific and Cocos Plates, representing a history of on-axis volcanism over the past  $800$  ka (Batiza *et al.*, 1996; Regelous *et al.*, 1999). The section was previously used to demonstrate the

temporal evolution of the axial magma chamber, and it was demonstrated that this section of the EPR has relatively low magma supply rates producing more differentiated (low-Mg) magmas over certain periods (Regelous *et al.*, 1999). Six samples were selected from the 10.5°N across-ridge section (Table 1). It has been speculated that the magma chamber beneath this segment of the EPR between the Clipperton Fault Zone and the OSC at 11.8°N may be built from one elongated magma chamber that is supplied from the area near 11.4°N (Regelous *et al.*, 1999). This, however, would require extensive horizontal dyking and magma transport and may not be physically feasible. The possibility of smaller magma-chamber sections with more local magma supply, therefore, seems more likely. Five samples were selected from the 11.4°N across-ridge section (Table 1).

The 10.5°N samples show very little variation in Sr, Nd and Pb isotopes, and there is no correlation among Sr, Nd and Pb isotopes (Table 2; Regelous *et al.*, 1999; Niu *et al.*, 1999). The 11.4°N samples show a much larger variation in Sr, Nd and Pb isotopes, and Nd isotopes shows a weak correlation with Sr isotopes ( $R^2 = 0.59$ ) for the set of 24 samples reported by Niu *et al.* (1999). In particular, two high- $^{87}\text{Sr}/^{86}\text{Sr}$ , low- $^{143}\text{Nd}/^{144}\text{Nd}$  samples from near the active ridge define this correlation and the large spread. One of these samples (PH108-1) was investigated in this study. No correlation exists between Nd isotopes and any of the Pb isotope ratios ( $R^2 < 0.1$ ).

Incompatible trace elements in these samples range from moderately depleted to enriched (Fig. 1a; Table 2; Supplement). The samples are differentiated to various degrees with MgO contents of 7.49 – 3.90 wt % (Mg# = 58 – 32) that correlate with the magnitude of Eu/Eu\* (1.0 – 0.8), i.e., negative Eu anomalies in the more differentiated samples.

## 2.5 East-Pacific Rise, 9–10°N

The 9 – 10°N segment of the East Pacific Rise is probably the best investigated section of oceanic crust on the planet and has seen numerous geophysical, petrological and geochemical studies (e.g., Carbotte & Macdonald, 1992; Fornari *et al.*, 1998; Von Damm, 2004; Soule *et al.*, 2007; Key *et al.*, 2013). It is bounded by the Siqueiros Fault Zone (8.3°N) to the south and the Clipperton Fault Zone (10.2°N) to the north (see map in Supplement). The samples investigated here were collected by the submersible *Alvin* during various cruises between 1991 and 1994 from within the axial summit trough of the EPR (Sims *et al.*, 2002). They were all sampled from young lava flows that were erupted in the twentieth century, some of them within only a few years of sampling (Sims *et al.*, 2002). Eighteen samples were selected from this segment for this study. The selected samples show a relatively narrow compositional range with relatively high MgO contents (Table 2; Sims *et al.*, 2002). Eight of these samples have MgO > 8 wt % with Mg# = 59 – 64.

Incompatible trace elements in the basalts are depleted, and their radiogenic isotopes show a depleted mantle source with the lowest  $^{87}\text{Sr}/^{86}\text{Sr}$ , the highest  $^{143}\text{Nd}/^{144}\text{Nd}$  among all samples (Fig. 1; Table 2; Sims *et al.*, 2002). The samples from the East-Pacific Rise 9.5°N best represent depleted MORB generated by on-axis volcanism at a fast-spreading ridge.

## 2.6 East-Pacific Rise, Siqueiros Fracture Zone (8.3°N)

The Siqueiros transform fault zone located at 8.3°N is approximately 20km wide and offsets the EPR by 140km in a left-lateral sense (see map in Supplement; Crane, 1976; Perfit *et al.*, 1996). Three of the four samples were collected by the submersible *Alvin*, whereas the fourth (sample D20-2) was dredged. Two of the *Alvin* samples and the dredge sample are picritic basalt from a relatively fresh lava flow (< 100 a), whereas the remaining *Alvin* sample (2390-5) is an older and more differentiated basalt (Sims *et al.*, 2002).

The three depleted MORB samples from the Siqueiros Fault Zone show radiogenic isotopes typical of a depleted mantle source (Fig. 1; Table 2; Sims *et al.*, 2002). These picritic basalts are primitive with 9.6 – 10.1 wt % MgO and Mg# of 67 – 69, and they are highly depleted in incompatible trace elements (Fig. 1a; Table 2; Sims *et al.*, 2002). These samples are among the most incompatible-element depleted samples reported from the global mid-ocean ridges. They best represent highly depleted, undifferentiated

MORB produced by relatively high degrees of partial melting (Perfit *et al.*, 1996; Saal *et al.*, 2002; Sims *et al.*, 2002).

The fourth sample from the Siqueiros Fault Zone (sample 2390-5) is strongly enriched in incompatible trace elements and shows radiogenic isotopes that clearly reflect an enriched mantle source with high  $^{87}\text{Sr}/^{86}\text{Sr}$ , the lowest  $^{143}\text{Nd}/^{144}\text{Nd}$  and the most radiogenic Pb of all samples investigated here (Fig. 1; Table 2; Sims *et al.*, 2002). This glass sample best represents Pacific E-MORB.

### 3 Methods

New data for the samples investigated here include boron concentrations and boron isotopic compositions, lithium concentrations and lithium isotopic compositions, trace metal concentrations including those of beryllium, potassium, rare earth elements and a selection of other metals, and chlorine and fluorine contents.

Lithium isotope compositions were determined using a multi-collector inductively coupled plasma mass spectrometer (MC-ICP-MS) following lithium purification through chemical exchange columns after dissolution of powdered glass chips. Glass chips were hand picked and cleaned by ultrasonication in methanol and MilliQ  $\text{H}_2\text{O}$ . Powdered samples were dissolved in concentrated  $\text{HF} - \text{HNO}_3 - \text{HClO}_4$ , followed by stages of concentrated ( $\sim 15\text{M}$ )  $\text{HNO}_3$  and  $6\text{M}$   $\text{HCl}$ . For each sample,  $\sim 10\text{ng}$  Li were purified by a two-step cation column (AG50W X12) separation method using dilute  $\text{HCl}$  as an eluant, as described elsewhere (James & Palmer, 2000; Marschall *et al.*, 2007b; Pogge von Strandmann *et al.*, 2011). Li isotope measurements were performed on a Thermo-Finnigan Neptune MC-ICP-MS at the University of Bristol, as detailed in Jeffcoate *et al.* (2004). Multiple analyses of several international basalt reference materials over a period of nine years yielded a  $2\sigma$  SD external reproducibility of  $\pm 0.3\text{‰}$  (see Supplement), in keeping with previously cited reproducibility (Elliott *et al.*, 2006; Jeffcoate *et al.*, 2007; Pogge von Strandmann *et al.*, 2011). Results are presented as  $\delta^7\text{Li}$ , namely the deviation in per mil from the standard NIST RM 8545 (= L-SVEC; Flesch *et al.*, 1973):  $\delta^7\text{Li} = [({}^7\text{Li}/{}^6\text{Li}_{\text{sample}})/({}^7\text{Li}/{}^6\text{Li}_{\text{L-SVEC}}) - 1] \cdot 1000$ . Reported errors are two standard deviations of triplicate mass-spectrometer analyses (i.e., “internal precision”).

Boron isotopic compositions, and boron and halogen concentrations were determined by secondary-ion mass spectrometry (SIMS) on mounted and polished glass fragments using the Cameca ims1280 ion microprobe at the North-Eastern National Ionmicroprobe Facility (NENIMF) at the Woods Hole Oceanographic Institution (WHOI). Fragments of clean glass,  $0.5 - 2\text{mm}$  in diameter, were mounted in epoxy (Buehler Epothin) together with fragments of Herasil-102 pure silica glass and the reference materials B6 and GOR132 (Jochum *et al.*, 2000; Gonfiantini *et al.*, 2003; Marschall & Ludwig, 2004). All samples were located within a distance of  $8\text{mm}$  of the center of the  $12.7\text{mm}$  radius sample mount. Polishing was completed using a Buehler MiniMet 1000 polishing machine ( $1\text{ }\mu\text{m}$  diamond paste), which was set to produce a flat and even surface throughout the epoxy and glass samples. Alumina polish ( $0.3\text{ }\mu\text{m}$ ) was used for the final polish. All analysis were completed at a distance of at least  $100\text{ }\mu\text{m}$  from the edge of the samples. This includes the reference materials and MORB glasses. Prior to gold coating, the grain mounts were cleaned using  $96\%$  ethanol followed by an ultrasound bath using distilled water from a Millipore ultrapure water system ( $18\text{M}\Omega$ ). Samples were always cleaned and coated immediately before introducing them into the airlock of the mass spectrometer to reduce the possible deposition of contamination on the sample surfaces. Surface contamination was monitored by analyses of silica glass Herasil-102 ( $\leq 1\text{ ng/g B}$ ; Marschall & Ludwig, 2004) and was found to be below  $8\text{ ng/g}$ . The contribution of contamination to the boron signal was, thus, only  $0.3 - 2\%$ , introducing a potential systematic error of  $< 0.1$  to  $0.6\text{‰}$  to the measured boron isotope ratios of the MORB glass samples (Marschall & Monteleone, 2015).

The SIMS method for boron isotope analysis was recently improved at NENIMF to enable precise and accurate analyses of MORB samples, and is described in detail in Marschall & Monteleone (2015). Accuracy and reproducibility are estimated from analyses of glass reference materials to be  $\pm 1.5\text{‰}$  (Marschall & Monteleone, 2015). Boron isotope ratios are reported in the delta notation relative to NIST SRM 951 (Catanzaro *et al.*, 1970):  $\delta^{11}\text{B} = [({}^{11}\text{B}/{}^{10}\text{B}_{\text{sample}})/({}^{11}\text{B}/{}^{10}\text{B}_{\text{SRM 951}}) - 1] \cdot 1000$ . The reported B isotope ra-



tios are mean values of between three and eleven SIMS spot analyses. The error bars displayed in the figures for individual samples are two standard errors of the mean, i.e.,  $2SE = 2SD/\sqrt{n}$ , where  $n$  is the number of analysed spots.

Chlorine and fluorine were analysed following methods established at NENIMF for volatile analyses in volcanic glasses (e.g., Shaw *et al.*, 2010; Wanless & Shaw, 2012), building on methods established earlier by Hauri *et al.* (2002). Boron concentrations were determined using the Cameca ims1280 with the same setup for raster sizes and aperture, mass resolution, 40 nA  $^{16}\text{O}^-$  primary beam, and size of energy window with zero offset. Pre-sputtering lasted for 2 min. Ten analytical cycles were analysed including masses  $^{11}\text{B}^+$  and  $^{28}\text{Si}^{2+}$ . Reference glass GOR132-G (Jochum *et al.*, 2000) was used to determine  $^{11}\text{B}^+ / ^{28}\text{Si}^{2+}$  relative ion yields (Marschall & Monteleone, 2015). Precision of B concentration analyses ranged from 0.3 to 1.6 % ( $2\sigma$ ), with an average of 0.9 % for all samples. Reproducibility ranged from 0.2 % to 4.4 % on the reference materials, and was 2 % on average for the MORB glass samples. Two samples showed worse reproducibility of 7 % and 13 %, respectively, whereas reproducibility for all other samples was 5 % or better. Matrix effects between the komatiite reference glass (GOR132-G) and the basalt glass samples are negligible, as is demonstrated by indistinguishable relative ion yields for GOR132-G and the rhyolitic glass B6 (Marschall & Monteleone, 2015). Our B concentration data are, therefore, estimated to be accurate within 4.4 % or better, with a precision of typically 0.9 % ( $2\sigma$ ).

Lithium and beryllium concentrations were analysed using the newly refurbished Cameca ims3f at NENIMF. Analyses were performed using a nominally 10 kV/20 nA  $^{16}\text{O}^-$  primary ion beam. Positive secondary ions were accelerated through a nominal 4.5 kV. The energy window was set to 40 eV and an offset of 75 eV. The mass resolution  $m/\Delta m$  (10 %) was set to  $\sim 1170$ . Ten analytical cycles were analysed with integration times of 5 s for Li, 10 s for Be, and 3 s for Si. A 5 min presputtering time was applied to each spot. The internal precision (2 times relative standard error) of the Li and Be analyses was 2 – 6 % and 4 – 17 %, respectively. Two to three spots were analysed per sample with a reproducibility of  $< 6\%$  for Li and  $< 12\%$  for Be for most samples. NIST reference glass SRM612 was used to determine  $^7\text{Li}^+ / ^{30}\text{Si}^+$  and  $^9\text{Be}^+ / ^{30}\text{Si}^+$  relative ion yields using published concentrations (41.54  $\mu\text{g/g}$  Li; 37.73  $\mu\text{g/g}$  Be; Pearce *et al.*, 1997). International reference glasses were used to monitor Li and Be concentration analyses and the following concentrations were measured:  $7.70 \pm 0.25 \mu\text{g/g}$  Li and  $0.07 \pm 0.02 \mu\text{g/g}$  Be ( $n = 8$ ) in GOR132-G;  $20.6 \pm 0.5 \mu\text{g/g}$  Li and  $1.38 \pm 0.01 \mu\text{g/g}$  Be ( $n = 2$ ) in StHs6/80-G; and  $147.9 \pm 0.7 \mu\text{g/g}$  Li and  $8.5 \pm 0.2 \mu\text{g/g}$  Be ( $n = 2$ ) in IAEA-B6. These values agree with the recommended values (Tonarini *et al.*, 2003; Jochum *et al.*, 2006).

First row transition metals, rare earth elements (REE), and a range of other trace elements were analysed by laser-ablation inductively-coupled mass spectrometry (LA-ICP-MS) using a NewWave Ar-excimer laser (193 nm) coupled to a ThermoScientific Element-2 single-collector magnetic sector-field mass spectrometer at WHOI. The instrument was operated at low mass resolution ( $m/\Delta m \geq 300$ ). A laser spot diameter of 150  $\mu\text{m}$  was used, pulsed at 5 Hz. Masses  $^{43}\text{Ca}$ ,  $^{51}\text{V}$ ,  $^{52}\text{Cr}$ ,  $^{59}\text{Co}$ ,  $^{60}\text{Ni}$ ,  $^{85}\text{Rb}$ ,  $^{88}\text{Sr}$ ,  $^{89}\text{Y}$ ,  $^{90}\text{Zr}$ ,  $^{93}\text{Nb}$ ,  $^{133}\text{Cs}$ ,  $^{138}\text{Ba}$ ,  $^{139}\text{La}$ ,  $^{140}\text{Ce}$ ,  $^{141}\text{Pr}$ ,  $^{146}\text{Nd}$ ,  $^{147}\text{Sm}$ ,  $^{153}\text{Eu}$ ,  $^{157}\text{Gd}$ ,  $^{159}\text{Tb}$ ,  $^{163}\text{Dy}$ ,  $^{165}\text{Ho}$ ,  $^{166}\text{Er}$ ,  $^{169}\text{Tm}$ ,  $^{172}\text{Yb}$ ,  $^{175}\text{Lu}$ ,  $^{208}\text{Pb}$ ,  $^{232}\text{Th}$ , and  $^{238}\text{U}$  were measured and concentrations were quantified using  $^{43}\text{Ca}$  as internal reference based on published CaO contents for the sample glasses. Reference glass NIST-SRM612 was used as the external reference material (Pearce *et al.*, 1997). A range of natural glasses (BHVO-2G, BCR-2G, BIR-1G, GOR132G) was used to check accuracy, and it was found that oxide interferences affected the heavy REE to between 0.5 and 3 % of the total signal of any analysed isotope. The heavy REE concentrations were corrected accordingly. Sensitivity drift of the ICP-MS was monitored by analysing two spots on BHVO-2G at the start and end of the day, as well as after each ten to fifteen samples. All samples were analysed within a timeframe of eleven hours on the same day. The sensitivity drift for all trace elements was found to be linear at 0 to +1.6 %/h, and the analyses were corrected for this drift. Two spots were analysed per sample, and reproducibility and internal precision for all elements in all samples except Rb, Cs, Pb, Th and U was typically between 1.0 and 2.5 % (2 standard deviations; Supplement). For Rb, Pb, Th and U they were on average 3.0 to 6.0 %, and for Cs they were  $\sim 20\%$  (Supplement). Statistical detection limits (3 SD of

background signal) were typically better than 10 ng/g for most elements, and better than 2 ng/g in many cases (Supplement). Exceptions were V, Zr, Sr, Ba, and Pb for which detection limits were 20 – 30 ng/g, and Ni and Cr for which they were 150 – 660 ng/g. The signal for all analyses of all elements were at least three times above the detection limits, except for Cs, which was below the detection limit in the depleted MORB samples from the Siqueiros Fault Zone. All trace-element data including uncertainties and detection limits of all analysed samples and reference materials are provided in the Supplement.

Potassium contents of all samples were also analysed by LA-ICP-MS using the same setup as described for trace-element analyses, but operating the spectrometer at high mass resolution ( $m/\Delta m \geq 10,000$ ) to suppress oxide and hydride interferences, and natural basalt glasses (BHVO-2G, BIR-1G, BCR-2G) were used as external reference materials. The sensitivity drift for K was found to be linear at +0.4 %/h, and the analyses were corrected for this drift. Masses  $^{39}\text{K}$  and  $^{43}\text{Ca}$  were analysed and the latter was used as internal reference mass for quantification. Internal precision was on average 1.1 %, but ranged from 0.8 to 4 % (Supplement). Reproducibility for the two analysed spots was 2.5 % on average, and better than 6 % in all cases except for two glass samples, which showed 20 % discrepancy between the two respective spot analyses. The detection limit was 2.4  $\mu\text{g/g}$  on average, and less than 23  $\mu\text{g/g}$  in all cases. The lowest analysed K contents were  $203 \pm 3 \mu\text{g/g}$  in one sample glass and  $\sim 60 \mu\text{g/g}$  in NIST-SRM612 (Supplement).

The analytical sequence for each spot analysis of the LA-ICP-MS started in low mass resolution with a measurement of the background (10 cycles), followed by integration of the trace-element isotopes (23 cycles). Thereafter, the ICP-MS was switched to high mass resolution during continuing ablation, and K was analysed ( $\sim 35$  cycles), followed by wash-out time ( $\sim 40$  cycles) and analysis of the background ( $\sim 30$  cycles). Data reduction and conversion of count rates to concentrations was completed using an off-line spreadsheet provided by Cin-Ty Lee (Rice University).

## 4 Results

### 4.1 Trace metal concentrations

A set of trace-element analyses for all samples were available from the literature, but they comprised an incomplete collection of analyses completed over several decades by various methods and laboratories by a number of different authors. This increased the uncertainty on accuracy of the published data and led to a data set with highly variable accuracy and precision. Below, we compare the geochemical behaviour of Li and B with that of other trace metals, and in order to reduce uncertainties, we use the trace-element abundances of the glasses determined in our study in one analytical session using a single method (i.e., single collector, sector-field LA-ICP-MS). Our analyses provide a complete data set and are used in the discussion below; our data are generally in good agreement with the published data.

In particular  $\text{K}_2\text{O}$  contents available from the literature were afflicted with large uncertainties, because of the abundances in the MORB glasses that are close to or below the detection limit of the electron probe analytical methods employed several decades ago in some cases. The high-resolution LA-ICP-MS analyses completed here provide precise and accurate  $\text{K}_2\text{O}$  contents even for the most depleted MORB samples and enable a meaningful evaluation of B/K and Cl/K ratios.

### 4.2 Light element and halogen concentrations

Concentrations of Li in the glasses vary by a factor of 4 ranging from 3.1 to 13.1  $\mu\text{g/g}$  Li (Table 1), with a negative correlation of Li and MgO. The majority of the samples have between 7 and 9 wt % MgO and between 4 and 6  $\mu\text{g/g}$  Li (Fig. 2). Samples exceeding 9 wt % MgO, such as the depleted-MORB samples from the Siqueiros Fracture Zone, have Li abundances of less than 4  $\mu\text{g/g}$ , whereas differentiated, low-MgO glasses ( $< 7$  wt % MgO; EPR 10 – 12°N and SWIR) show higher Li contents ( $> 6.8 \mu\text{g/g}$ ). Li/Yb ratios of samples with Cl/K  $< 0.08$  vary in a narrow range between 1.4 and 2.1 (1.3 – 2.3 including all 56 samples).

No correlation is observed with Mg#, Li contents, nor with La/Sm ratios (Fig. 3a–c). The mean Li/Yb ratio is  $1.64 \pm 0.30$  (2SD;  $n=40$ ).

Concentrations of Be and B show a slightly larger variation than those of Li, both varying by a factor of  $\sim 7$  with a constant B/Be ratio of  $\sim 2$  (range 1.4 – 2.7; mean  $2.0 \pm 0.4$ , 2SD;  $n = 56$ ; Supplement). Boron and Be concentrations show a negative correlation with MgO. Concentrations of boron range from  $0.40 \mu\text{g/g}$  in depleted high-Mg samples from the Siqueiros Fracture Zone to  $2.0 - 2.5 \mu\text{g/g}$  in more differentiated, lower-Mg samples from the SWIR and the EPR  $10 - 12^\circ\text{N}$  section, and in the enriched-MORB sample from the Siqueiros Fracture Zone (Fig. 2). Beryllium contents vary from  $0.18$  to  $1.39 \mu\text{g/g}$  (Table 1). The SWIR samples and the Siqueiros enriched-MORB sample show a higher B (and Be) content at a given MgO content compared to the remaining samples.

Boron and Be contents show a positive correlation with incompatible trace elements, and ratios of B (and Be) over a range of trace elements show different systematic variations. Ratios of B over highly incompatible elements, such as Ba, Nb or K show large variabilities among various ridge sections, but much smaller variations within the sets of samples from particular ridge sections (Fig. 3d). For any given sample group from a particular locality, B/K is near-constant and does not correlate strongly with B content nor with Mg# (Fig. 3d,e). However, the global collection of the various sample groups shows a systematic decrease of B/K with increasing La/Sm (Fig. 3f). The most depleted members of our sample collection with primitive-mantle normalised  $(\text{La/Sm})_N = 0.3$  to  $0.5$  have  $\text{B/K} = 0.0020$ , and the most enriched MORB with  $(\text{La/Sm})_N = 1.8$  has  $\text{B/K} = 0.0004$  (Fig. 3f). The array crosses the primitive mantle value  $((\text{La/Sm})_N \equiv 1)$  at  $\text{B/K} = 0.0006 \pm 0.0002$  (Fig. 3f).

Ratios of B over moderately incompatible trace elements, such as the middle and heavy rare earth elements increase with increasing B content. Finally, ratios of B/Ce, B/Pr, B/P, and B/Be ratios show very little variation in the sample set and do not vary with B content. There is no variation of B/Ce or B/Pr with B content, nor Mg#, nor La/Sm (Fig. 3g–i; Supplement). The mean B/Pr of all low-Cl/K samples is  $0.57 \pm 0.09$ , and their mean B/Ce is  $0.10 \pm 0.02$ .

The variability of Cl contents are by far the greatest among all elements with variation by a factor of 1200 ( $2.9 - 3525 \mu\text{g/g}$ ), which is one to two orders of magnitude more than even the most incompatible trace metals (e.g., Rb, Ba, Th, Nb). Concentrations of F vary only by a factor of 17 and F/Cl ratios ( $0.19 - 32$ ) vary by a factor of  $\sim 170$ . F/Cl ratios show a weak positive correlation with MgO contents and a negative correlation with [Cl].  $\text{F/Cl} > 3$  were only found in samples with  $< 60 \mu\text{g/g}$  Cl.

### 4.3 Lithium and boron isotope ratios

Lithium isotope ratios range from  $\delta^7\text{Li} = +2.6$  to  $+5.1\text{‰}$  (Table 1). Low  $\delta^7\text{Li} \leq +3\text{‰}$  were found in all investigated areas and are not restricted to one particular location or subset of samples. High  $\delta^7\text{Li} \geq +4\text{‰}$  are restricted to samples from the EPR. In particular, only two investigated localities show  $\delta^7\text{Li} \geq +4\text{‰}$ : (1) samples from recent lava flows at  $9.85^\circ\text{N}$ , and (2) three on-axis samples at  $11.35^\circ\text{N}$  of the EPR (Fig. 4a,b). All of these high- $\delta^7\text{Li}$  samples were erupted on axis at relatively shallow water depths of approximately 2500m. No correlation was found between Li isotope composition and Li concentration or Li/Yb ratio, or between  $\delta^7\text{Li}$  and other geochemical parameters, such as La/Sm, Zr/Y, or MgO content.

Lithium isotopes also do not show any systematic variation with radiogenic isotope ratios, such as those of Sr, Nd or Pb (Fig. 4a,b; Supplement). However, the highest  $\delta^7\text{Li}$  values were found in samples from the EPR ( $11.35^\circ\text{N}$ ), which show elevated  $^{87}\text{Sr}/^{86}\text{Sr}$  (Fig. 4a). Yet, these samples do not differ from lower- $\delta^7\text{Li}$  samples of the EPR in Nd or Pb isotopes (Fig. 4b; Supplement). Instead they show highly elevated chlorine contents and Cl/K ratios (open symbols in Fig. 5). The other group of high- $\delta^7\text{Li}$  samples (EPR  $9.85^\circ\text{N}$ ) are not enriched in chlorine and have very low  $^{87}\text{Sr}/^{86}\text{Sr}$  (Fig. 4a).

Mean  $\delta^7\text{Li}$  for individual sections of the investigated ridges, excluding samples with high Cl/K ( $>0.08$ ), show resolvable variations (Fig. 6). Mean  $\delta^7\text{Li}$  values range from  $+2.9 \pm 0.2\text{‰}$  (2 SD) and  $+3.0 \pm 1.0\text{‰}$  for the lavas erupted before 1980 at the EPR  $9.5^\circ\text{N}$  section and the depleted Siqueiros samples, respectively, to  $+4.3 \pm 0.5\text{‰}$  for the lavas erupted after 1980 at EPR  $9.5^\circ\text{N}$  (Fig. 6; Table 3). The mean of all investigated

samples with  $\text{Cl/K} < 0.08$  is  $+3.6 \pm 1.2\text{‰}$  ( $n=25$ ), and the mean of the five different investigated ridge sections ( $\text{Cl/K} < 0.08$  only) is  $+3.5 \pm 0.9\text{‰}$  (Table 3). No correlations exist between lithium isotopic composition and Li concentrations among individual samples (not shown) nor among the mean values of the various ridge sections (Fig. 6).

Boron isotope ratios range from  $\delta^{11}\text{B} = -9.8 \pm 1.1$  to  $-2.2 \pm 1.7\text{‰}$  (Table 1), with the majority of samples ranging from  $-9$  to  $-5\text{‰}$  (42 of the 53 analysed samples). Only four samples show  $\delta^{11}\text{B}$  values lower than  $-9\text{‰}$ , but none of them are significantly below  $-9\text{‰}$  within their two standard error uncertainties (Fig. 5). These low- $\delta^{11}\text{B}$  samples are not restricted to one particular location or subset of samples. High  $\delta^{11}\text{B} \geq -6\text{‰}$  values were found for most of the samples from the EPR  $10-12^\circ\text{N}$  section and for the Kolbeinsey Ridge samples. Three samples from the MAR  $26^\circ\text{S}$  section and two samples from the EPR  $9-10^\circ\text{N}$  section also show elevated  $\delta^{11}\text{B}$  values, but these are not significantly above  $-6\text{‰}$  within their two standard error uncertainties (Fig. 5).

The samples from the SWIR ( $57^\circ\text{E}$ ) show a range of B concentrations from  $1.5$  to  $2.5\text{ }\mu\text{g/g}$ , but only an insignificant and unsystematic variation in their B isotopic compositions from  $-8.8 \pm 1.6$  to  $-7.0 \pm 1.2\text{‰}$ , not related to B concentrations or other geochemical indicators of differentiation (Table 3; Fig. 5). The error-weighted mean of the five SWIR samples is  $\delta^{11}\text{B} = -7.6 \pm 1.5\text{‰}$  (2SD; Table 3). The enriched-MORB sample from the Siqueiros Fault Zone shows an equally high B content to the SWIR samples, and also an indistinguishable B isotopic composition to those samples of  $\delta^{11}\text{B} = -6.6 \pm 1.6\text{‰}$  (Table 3).

The on- and off-axis samples from the EPR  $10-12^\circ\text{N}$  section show a trend of increasing  $\delta^{11}\text{B}$  with increasing B content (Fig. 5a) and other incompatible trace elements and with decreasing MgO content. Some of the highest  $\delta^{11}\text{B}$  samples also show the highest  $\delta^7\text{Li}$  values (Fig. 5b). Furthermore, the enrichment of isotopically heavy boron is connected to a strong enrichment in chlorine (Fig. 5c) and elevated  $\text{Cl/K}$  (Fig. 5d). The same combination of isotopically heavy boron, high  $[\text{Cl}]$ , and high  $\text{Cl/K}$  was found in the Kolbeinsey Ridge samples (Fig. 5). Only one sample from the EPR  $10-12^\circ\text{N}$  section was found to have  $\text{Cl/K} < 0.08$  and it has a  $\delta^{11}\text{B} = -7.0 \pm 3.4\text{‰}$  (Table 3; Fig. 7). The two Kolbeinsey Ridge samples both have very high  $\text{Cl/K}$  (Table 1).

All remaining samples show boron contents below  $1.2\text{ }\mu\text{g/g}$  (Fig. 5a). Among these, the lowest B contents were found in the depleted MORB samples from the Siqueiros Fault Zone with  $0.40-0.43\text{ }\mu\text{g/g}$  B and a mean  $\delta^{11}\text{B}$  value of  $-7.0 \pm 3.3\text{‰}$  for the low- $\text{Cl/K}$  samples (Table 3; Fig. 7). The MAR  $26^\circ\text{S}$  section samples all have  $\text{Cl/K} < 0.08$ ,  $0.6-1.1\text{ }\mu\text{g/g}$  B and a mean  $\delta^{11}\text{B}$  value of  $-7.0 \pm 2.5\text{‰}$  (Table 3; Fig. 7). Most of the EPR  $9-10^\circ\text{N}$  section samples show  $\text{Cl/K} < 0.08$  and B contents of  $0.7-1.0\text{ }\mu\text{g/g}$  with a mean  $\delta^{11}\text{B}$  value of  $-7.8 \pm 3.1\text{‰}$ , excluding three high- $\text{Cl/K}$  samples (Table 3; Fig. 7).

The mean of all investigated samples with  $\text{Cl/K} < 0.08$  is  $-7.3 \pm 2.6\text{‰}$  (2SD;  $n=41$ ; Table 3). The mean does not change significantly if only samples with very low  $\text{Cl/K} < 0.025$  are considered, resulting in a mean of  $\delta^{11}\text{B} = -7.6 \pm 2.5\text{‰}$  ( $n=13$ ; Table 3). The mean of the six different investigated ridge sections ( $\text{Cl/K} < 0.08$  only) is  $-7.1 \pm 0.9\text{‰}$  (2SD; Table 3; Fig. 7).

No correlation was found between  $\delta^{11}\text{B}$  and geochemical parameters that indicate the degree of depletion or enrichment of the mantle source of the MORB magmas, such as  $\text{La/Sm}$ ,  $\text{Ba/TiO}_2$ , or  $\text{Zr/Y}$ . Boron isotopes also do not show any systematic variation with radiogenic isotope ratios, such as those of Sr, Nd or Pb (Fig. 4c,d; Supplement). Yet equivalent to the Li isotopes discussed above, the highest  $\delta^{11}\text{B}$  values were found in samples, which show elevated  $^{87}\text{Sr}/^{86}\text{Sr}$  and significantly elevated Cl and  $\text{Cl/K}$  (Fig. 4c,d, 5). And as discussed above, these samples do not differ from lower- $\delta^{11}\text{B}$  samples in Nd or Pb isotopes (Fig. 4d; Supplement).

The positive correlation between the boron and lithium isotopic compositions of the full dataset is very weak ( $R^2 = 0.09$ ; Fig. 5b). Samples from EPR  $9-10^\circ\text{N}$  show a range of  $\delta^{11}\text{B}$  values ( $-9.3$  to  $-3.3\text{‰}$ ), but have dominantly high  $\delta^7\text{Li}$  above  $+4\text{‰}$ . Also, most of the high- $\text{Cl/K}$  samples from all localities are enriched in isotopically heavy B, but show highly variable Li isotopic compositions (Fig. 5b).

## 5 Discussion

Magma contamination through assimilation, as well as isotope fractionation among various Earth reservoirs can only be quantified with good knowledge of the elemental distribution that determines mass balance and flux, and therefore impacts the magnitude by which various differentiation mechanisms affect isotope fractionation. Unfortunately, elemental abundances of Li and B in the bulk silicate earth and the depleted mantle are still a matter of debate and require further evaluation, which we address first, followed by a discussion of the isotopic composition of the MORB source mantle.

### 5.1 Abundances of Li in MORB and the depleted mantle

Lithium, as well as B and Be, shows incompatible behaviour during mantle melting and fractional crystallisation of basaltic magmas (e.g., Ryan & Langmuir, 1987, 1988, 1993; Brenan *et al.*, 1998). This is expressed in the positive correlation of light element concentrations with the concentrations of other incompatible elements in MORB glasses, and their negative correlation with MgO content, as discussed above. The set of MORB glasses investigated here shows a relatively constant Li/Yb ratio ( $1.64 \pm 0.30$ , 2SD; Cl/K < 0.08 only) that does not vary systematically with Li concentration, nor with MgO content, nor with La/Sm. Ryan & Langmuir (1987) showed that Li/Yb is relatively constant among MORB at approximately 1.7 and suggested that fractional crystallization at mid-ocean ridges does not fractionate this ratio. However, they demonstrated that Li/Yb shows some fractionation during MORB melting. Gale *et al.* (2013) determined average abundances of MORB from the large global data set published for basalt samples from all ridges and derived a value of Li/Yb = 1.79 ([Li] = 6.5 µg/g) for 'all MORB', which included all samples apart from back-arc centres.

Salters & Stracke (2004) used Li/Yb = 1.75 and the established Yb abundances to determine a depleted-MORB mantle (DMM) abundance of [Li] = 0.70 µg/g. However, the constant Li/Yb observed in MORB does not necessarily mean that Li and Yb have the same compatibility during mantle melting; it may be a fortuitous result of a limited range in the degree of melting and the distribution of the elements among various mineral hosts. It has, in fact, been established that Li and Yb are respectively hosted by different minerals in peridotites: Li shows the highest abundances in olivine, followed by clinopyroxene and orthopyroxene and is low in spinel and garnet (Ryan & Langmuir, 1987; Seitz *et al.*, 2003; Ottolini *et al.*, 2004; Paquin *et al.*, 2004). The major host of Li in mantle rocks is, therefore, olivine independent of pressure and the degree of melt extraction. Ytterbium, in contrast, is most compatible in garnet and clinopyroxene (e.g., McDade *et al.*, 2003). Its compatibility will, therefore, vary with the degree and depth of melting. MOR melting appears to produce a relatively constant Li/Yb in MORB, whereas ocean island basalts that show lower-degree melt extraction from garnet peridotites show a more compatible behaviour of Yb and relatively constant Li/Dy instead (Ryan & Langmuir, 1987). Extraction of some magmas, such as the ocean island basalts, from the mantle may occur by smaller degrees of melting compared to a MOR scenario, with a contribution of melts that coexisted with garnet and, therefore, produced higher-Li/Yb melts. This may have contributed to the elevated Li/Yb = 8.2 of the continental crust. However, the major contribution to the Li enrichment of the continental crust probably occurred in geological processes that involve material transport by hydrous fluids, such as in subduction zones. Here, preferential extraction of Li from the slab results in very high Li/Yb of arc magmas (Ryan & Langmuir, 1987).

MORB is generated from the depleted mantle by partial melting, and the best estimate for [Li] in the depleted mantle may be determined through modelling of this partial melting process. The model employed here uses experimentally determined mineral/melt partition coefficients for Li and Yb, the established REE abundances for the depleted mantle (Salters & Stracke, 2004), and it is anchored on the relatively constant Li/Yb ratios of MORB. Little variability is seen among the large set of MORB analyses now available, with an estimated Li/Yb = 1.64 for our samples. This value is close to previous estimates of 1.7 (Ryan & Langmuir, 1987), 1.75 (Salters & Stracke, 2004), and 1.79 (Gale *et al.*, 2013).

A number of studies have determined partition coefficients for lithium between peridotite minerals or

phenocrysts and basaltic melt (summarised in Tomascak *et al.*, 2016a). These partition coefficients (i.e.,  $c(\text{Li})_{\text{mineral}}/c(\text{Li})_{\text{melt}}$ ) range widely from 0.01 – 1 for olivine, clinopyroxene, orthopyroxene and plagioclase, depending on temperature, mineral and melt composition and other parameters. However, studies that investigated all three major mantle minerals consistently found the highest Li partition coefficients for olivine, followed by clinopyroxene and orthopyroxene (Brenan *et al.*, 1998; McDade *et al.*, 2003; Ottolini *et al.*, 2009, see Supplement). A simple model is employed here to provide an estimate of the effects of peridotite partial melting and fractional crystallisation of basaltic melt on Li abundances and Li isotopic composition.

Low-pressure partial melting of depleted spinel peridotite was modelled to estimate the abundances of Li (and B) in the depleted mantle, using batch melting models and Rayleigh fractional melting with accumulation of the extracted melt batches (see Supplement). Published experimental mineral-melt partition coefficients are used (listed in Supplement) together with the REE contents (Yb and Pr) of the depleted mantle from Salters & Stracke (2004), which serve as the initial composition of the mantle source prior to melting. Lithium and B contents of the initial mantle composition (= depleted mantle) are adjusted such that the Li/Yb and B/Pr ratios of the resulting melts generated by approximately 2 to 20% partial melting are close to the target values of  $\text{Li/Yb} = 1.64 \pm 0.30$  and  $\text{B/Pr} = 0.57 \pm 0.09$  (Fig. 8; see Supplement for details). Batch and Rayleigh models both require that the Li abundance of the MORB-source mantle is  $[\text{Li}] = 1.20 \pm 0.10 \mu\text{g/g}$  and  $[\text{B}] = 0.077 \pm 0.010 \mu\text{g/g}$  (Fig. 8). This estimate does not rely on the assumption of similar compatibility of light elements and REE nor on unfractionated element ratios during mantle melting; in fact, it rejects this notion and is instead based on non-modal melting models and experimentally determined partition coefficients, which contrast strongly between Li and Yb and between B and Pr among the major mantle phases (see Supplement). We, therefore, argue against the depleted mantle  $[\text{Li}]$  value proposed by Salters & Stracke (2004) and suggest the new estimate of  $[\text{Li}] = 1.20 \pm 0.10 \mu\text{g/g}$  determined through partial melting models.

The Li abundances predicted for highly depleted mantle after extraction of 2 to 20% MORB ranges from 1.1 to 0.7  $\mu\text{g/g}$  depending on model and degree of melting. The Li/Yb ratio of the mantle residues range from 3.2 to 9.1, and increase with the degree of melt depletion. This is consistent with the record of Li/Yb in unmetasomatised mantle rocks (see Supplement), and it is approximately twice to five times as high as the ratio observed in MORB.

## 5.2 Abundance of Li in the primitive mantle

Estimates of element abundances in the bulk silicate earth (BSE; =primitive mantle) are generally based on four different approaches: (1) through a crust–mantle mass balance calculation, (2) through a cosmochemical approach, (3) through direct analyses of mantle rocks, and (4) by using trace-element ratios in mantle-derived basalts and elements of similar compatibility with well-established mantle abundances.

Here, we estimate the Li abundance in the BSE through mass balance of all the components of the mantle, crust and hydrosphere. Uncertainties in this method arise mainly from uncertainties in abundances in the individual components and in the possibility of unaccounted (hidden) reservoirs. In a simple model, we use the abundances of Li in the continental crust (18  $\mu\text{g/g}$ ; Rudnick & Gao, 2003; Teng *et al.*, 2008), oceanic crust (4  $\mu\text{g/g}$ ; Ryan & Langmuir, 1987), altered oceanic crust (7.6  $\mu\text{g/g}$ ; Chan *et al.*, 1992), pelagic sediments (50  $\mu\text{g/g}$ ; Bouman *et al.*, 2004), seawater (0.18  $\mu\text{g/g}$ ; Broecker & Peng, 1982; Jeffcoate *et al.*, 2004), and the depleted mantle (1.2  $\mu\text{g/g}$ ; this study, see above). In addition, a portion of ancient subducted altered oceanic crust is required to balance the Earth's Li isotope budget (see below). The mass proportions for most reservoirs are well constrained, with the exceptions of the ancient subducted crust and the portion of mantle that is depleted. The Li abundance for the MORB-source mantle can be estimated with reasonable uncertainty, but no agreement exists on what proportion of the mantle shows a level of trace-element depletion similar to this MORB source. The crust is thought to represent the material extracted from the depleted mantle, and reintegration of these complimentary reservoirs will result in the composition of the BSE (Hofmann, 1988). Estimates for the mass fraction of the mantle that is depleted range from 0.27 (Chaussidon

& Jambon, 1994) to 0.62 (Yanagi, 2011) to 1 (Hofmann, 1997), representing depletion of only the upper mantle, upper mantle and half of the lower mantle, or of the entire mantle, respectively. These three proportions of mantle depletion lead to estimates for Li abundances of the BSE (or primitive mantle) of 1.62, 1.39 and 1.32  $\mu\text{g/g}$ , respectively. Values exceeding 2  $\mu\text{g/g}$  could only be reached by assuming unrealistically high abundances in the bulk continental crust ( $> 40 \mu\text{g/g}$ ), or through further unaccounted reservoirs with very-high Li concentrations.

Our preferred estimate for the primitive mantle is  $[\text{Li}] = 1.39 \pm 0.10 \mu\text{g/g}$ , which is derived from mass balance assuming extraction of the crust from depletion of 62% of the mantle, i.e. the depletion proportion of Yanagi (2011). We recommend that these values for the depleted mantle ( $[\text{Li}] = 1.20 \pm 0.10 \mu\text{g/g}$ ) and primitive mantle ( $[\text{Li}] = 1.39 \pm 0.10 \mu\text{g/g}$ ) should be used in the geochemical reference frame (Table 4).

The cosmochemical approach derives the BSE Li abundances from the moderately volatile character of Li during condensation of the solar nebular. The primitive-mantle abundances of the moderately volatile, lithophile elements (e.g., alkali metals, Zn) relative to their abundances in CI chondrites show an exponential correlation to their 50% condensation temperature,  $T_{50}$  (e.g., McDonough & Sun, 1995). The abundances of the moderately volatile elements (Mn, K, Na, Rb, Cs, Zn), Mg and Si in CI chondrites and the primitive mantle relative to Mg (Palme & O'Neill, 2003) and their  $T_{50}$  values (Lodders, 2003) define a calibration line, which can be used to estimate the primitive-mantle abundance of the moderately volatile Li from its  $T_{50}$  and its abundance in CI chondrites. This method has large uncertainties that stem from the scatter of the elements along the calibration line, and from uncertainties in the CI abundance and the  $T_{50}$  of Li (e.g., Wasson, 1985; Lodders, 2003). Lithium abundances in CI chondrites have been estimated between 1.45 and 1.57  $\mu\text{g/g}$  (e.g., Palme, 1988; Wasson & Kallemeyn, 1988; Anders & Grevesse, 1989; Palme & Jones, 2003). Recent analyses of the Orgueil CI chondrite have revealed Li abundances that are generally consistent with these estimates (1.2 – 1.6  $\mu\text{g/g}$ ; James & Palmer, 2000; Seitz *et al.*, 2007; Pogge von Strandmann *et al.*, 2011). We use a value of  $[\text{Li}] = 1.49 \mu\text{g/g}$  here (Palme & Jones, 2003). The  $T_{50}$  of Li has been estimated to 1142 K (at 10 Pa) assuming that it substituted for Mg in olivine and pyroxene during condensation of the solar nebular (Lodders, 2003). A primitive-mantle abundance of 1.27  $\mu\text{g/g}$  would be consistent with this condensation temperature. Our preferred primitive mantle value of  $[\text{Li}] = 1.39 \mu\text{g/g}$  converts to a depletion factor of 0.40 relative to Mg and CI chondrites. The  $T_{50}$  consistent with this Li abundance would be  $1145 \pm 15 \text{ K}$ , which is indistinguishable from the independent volatility estimate of 1142 K listed by Lodders (2003).

Jagoutz *et al.* (1979) analysed six peridotite xenoliths from kimberlites and alkali basalts and used them to derive abundances of major and trace elements for the primitive mantle by extrapolating Mg/Si and Al/Si ratios to their intersection with the cosmochemical fractionation line. However, this method does not work well for Li, as Li abundances vary from 1.20 – 2.07  $\mu\text{g/g}$  among the six samples, but do not correlate with any of the partial melting indicators, such as Ca, Al or Cr content or Mg number. Jagoutz *et al.* (1979) tentatively used the Li concentration of their San Carlos peridotite sample (2.07  $\mu\text{g/g}$ ) as their estimate for the primitive mantle. This would result in a relatively high Li/Yb of 4.9 for the primitive mantle.

The abundance of Li given by McDonough & Sun (1995) for the primitive mantle is 1.6  $\mu\text{g/g}$  based on the range of Li abundances in the six samples of Jagoutz *et al.* (1979). However, it is a 'preferred value' that represents neither the mean (1.52  $\mu\text{g/g}$ ) nor the median (1.48  $\mu\text{g/g}$ ), and it is lower than the value preferred by the authors of the original work. McDonough & Sun (1995) argue for Li partitioning behaviour similar to the heavy REE during melt extraction from the mantle following Ryan & Langmuir (1987), but their [Li] and [Yb] estimates result in a Li/Yb of 3.6 for the primitive mantle, which is approximately twice as high as the MORB value.

More recently, the detailed investigation of Li abundances and distribution in mantle xenoliths, as well as Li isotope studies on these rocks have revealed a complex behaviour of Li at high temperatures and during eruption and cooling (e.g., Nishio *et al.*, 2004; Rudnick & Ionov, 2007; Magna *et al.*, 2008; Ionov & Seitz, 2008; Aulbach *et al.*, 2008; Aulbach & Rudnick, 2009; Pogge von Strandmann *et al.*, 2011). It is now clear that the high diffusivity of Li and its mobility in fluids and melts commonly lead to enrichment or depletion of Li in bulk xenoliths, individual minerals or zones and domains of minerals in the xenoliths

without necessarily affecting the abundance of major elements or the REE (e.g., Seitz *et al.*, 2004; Wagner & Deloule, 2007; Rudnick & Ionov, 2007; Pogge von Strandmann *et al.*, 2011). In particular, the xenoliths from San Carlos (Arizona), from which sample SC1 was taken by Jagoutz *et al.* (1979) to best represent the Li content of the primitive mantle, show extreme disturbance in Li isotopes together with Li intra-mineral zonation and disequilibrium inter-mineral partitioning (Jeffcoate *et al.*, 2007). Sample SC1 itself has an unusual Li isotopic composition (see Supplement; Seitz *et al.*, 2004). These observations suggest that Li is influenced strongly by metasomatic effects in these xenoliths, including an influence of the host magma on Li abundances and distribution. Thus, they discredit most kimberlite and alkali-basalt hosted xenoliths as providers of useful information on the Li abundance in the primitive or depleted mantle. A more detailed summary of Li abundances in mantle rocks is given in the Supplement.

Li/Yb ratios of 1.6 – 2.0 applied to the primitive mantle in combination with the established Yb abundances would result in a very low estimate of  $[Li] = 0.7 - 0.9 \mu\text{g/g}$  for the primitive mantle, and the assumption of constant Li/Yb ratios during mantle melting has to be rejected, as discussed above. For mass balance reasons, the high Li/Yb of the continental crust compared to the depleted mantle requires that the primitive mantle had a higher Li/Yb than the depleted mantle has today, and the depleted mantle has a much higher Li/Yb ( $\approx 3.0$ ) than MORB, as discussed above.

### 5.3 Boron compatibility during MORB generation

The compatibility of boron during mantle melting and crystallisation of basaltic magmas relative to other trace elements has been discussed previously, but the historic development of analytical capabilities has to be kept in mind when evaluating data from studies that were conducted several decades ago. Earlier workers had no access to in-situ analyses of REE and many other trace elements in small glass samples.  $K_2O$  analyses by EPMA were afflicted with larger uncertainties, and boron analyses suffered from relatively large analytical blank contributions, in particular for data from depleted MORB samples. Evaluation of the relative compatibility of B and other incompatible elements at today's level of precision and accuracy were, therefore, not accessible in the early 1990s.

Most previous studies have employed a ratio of  $B/K = 0.0010$  to estimate the B abundances of the depleted and primitive mantle based on the better established K contents of these reservoirs. It was initially assumed that B/K is not fractionated during peridotite partial melting and fractional crystallisation of basalts, and that the MORB-source mantle (=depleted mantle) and the primitive mantle all had  $B/K = 0.0010$  (Ryan & Langmuir, 1993; Chaussidon & Jambon, 1994). The use of this ratio was proposed by Ryan & Langmuir (1993) and Chaussidon & Jambon (1994), who found that B/K in N-MORB (MORB with  $(La/Sm)_N < 1$ ) ranged from 0.0005 to 0.0018 with averages estimated by the two studies of 0.0008 and 0.0012, respectively. Yet they also found significantly lower values in enriched-type MORB and ocean-island basalts.

Salters & Stracke (2004) estimated  $[B]$  of depleted-MORB mantle (DMM) from  $B/K = 0.0010$ , resulting in a DMM abundance of  $[B] = 0.060 \mu\text{g/g}$ . Ryan & Langmuir (1993) estimated  $[B] = 0.085 - 0.170 \mu\text{g/g}$  for the depleted mantle using models of partial melting and their MORB boron data in comparison with the more incompatible Ba. Chaussidon & Marty (1995) estimated very low depleted mantle abundances of  $[B] = 0.010 - 0.015 \mu\text{g/g}$  from crust–mantle mass balance, assuming that their estimate for the ocean island basalt source ( $[B] = 0.090 - 0.110 \mu\text{g/g}$ ) represented primitive mantle abundances and that a fraction of 0.27 of the mantle was depleted to form the continental crust.

Trace-element ratios in MORB may be influenced by variable abundances of the elements in the mantle source, by fractionation during partial melting due to contrasting compatibilities, and by fractionation during magma differentiation, again due to contrasting partition behaviour of the trace elements. Fractionation during magma differentiation can be monitored by investigating sets of samples that show ranges of Mg/Fe ratios. Our low-Cl/K sample sets from the SWIR 57°E, the MAR 26°S and from the EPR 9.5°N all show ranges of Mg numbers of approximately ten units and can thus be used to monitor the evolution of trace-element ratios as a result of magma differentiation. B/Ce and B/Pr ratios are both constant, and B/K shows only small variation within these individual sample sets (see Fig. 3e,h; Supplement). This demonstrates



that these trace-element ratios are not fractionated during MORB differentiation, at least for magmas with  $Mg\# \geq 48$ . Hence, variations in B/K as observed among the set of global MORB has to be a result of B/K fractionation during the partial melting event that produced these basalts, or has to reflect heterogeneities in B/K among the various mantle sources, or both.

Variations in B/K in our set of MORB glasses arise from the large differences in K together with other highly-incompatible element abundances (e.g., Ba, Nb, U) that characterise the different MORB types, which contrasts with their relatively small variation in B concentrations. No variability exists in B/Ce and B/Pr, which are constant among all low-Cl/K samples from all investigated localities.

Our data set shows a systematic variation of B/K with  $(La/Sm)_N$  in global MORB, ranging from  $B/K = 0.0020$  in N-MORB with  $(La/Sm)_N = 0.3 - 0.5$  to  $B/K = 0.0004$  in E-MORB with  $(La/Sm)_N = 1.8$ . The array of La/Sm in the global MORB array arguably reflects variable degrees of depletion in the mantle sources of these basalts, with high La/Sm in the mantle source of enriched MORB and low La/Sm in the depleted MORB mantle. The negative correlation of B/K with La/Sm, therefore, shows that variations in B/K (and B/Nb) in the global MORB array also reflect variability of B/K (and B/Nb) in the mantle. These mantle heterogeneities could reflect the addition of recycled materials to the enriched mantle source. However, this would require addition of materials that were enriched in K and all other highly incompatible trace elements, but depleted in boron, so that melt generated from these enriched domains would show anomalously low B/K (and B/Nb, etc.). Also, at the same time the global set of samples shows near-constant B/Pr (and B/Ce), which is very difficult to reconcile with a disturbance of trace-element ratios by recycling processes. It is, hence, more likely that the heterogeneities reflect ancient melt extraction and melt impregnation processes in the depleted and enriched mantle sources, respectively, rather than enrichment through recycling of fractionated material. The observed global variability in B/K and the lack of variability in B/LREE is thus best explained by a much higher incompatibility of K (and Nb) compared to B during partial melting in the upper mantle, and similar compatibility of B and Pr (or Ce) in the same process.

The evaluation of element compatibility from global MORB trends is, nonetheless, afflicted with uncertainties, because variations in element abundance ratios among mantle domains may be caused by processes other than melt extraction or impregnation. It would, therefore, be ideal to focus the evaluation only on melts extracted from a single mantle domain with a homogeneous composition. In such an ideal case, variations in trace-element contents would strictly reflect the degree of partial melting, and trace-element ratios would be governed by relative peridotite–melt partitioning. Initially, models of such “cogenetic MORB melting suites” were thought to be represented by high-Mg samples from individual mid-ocean ridge segments that show little variation in their radiogenic isotope compositions (e.g., Ryan & Langmuir, 1993). Today, models of magma transport and storage at mid-ocean ridges include a multitude of interaction processes, such as porous melt flow, replenishment and tapping, diffusional exchange between phenocrysts and melt, and combined assimilation–fractional crystallisation (O’Neill & Jenner, 2012; Lissenberg *et al.*, 2013; Coogan & O’Hara, 2015). These processes all lead to the fractionation of trace elements and of trace-element ratios that deviate from the simple-model predictions. The conclusions drawn from sets of MORB samples are, therefore, generalised and simplify the processes that may occur in nature, even if they are relatively undifferentiated and come from one ridge section. Nonetheless, the influence of processes other than mantle melting that influence trace-element ratios is reduced, if only high-Mg samples from individual ridge sections are considered. Our sets of samples also include low-Cl/K Mg-rich glasses with  $Mg\# \geq 60$  or  $MgO > 8 \text{ wt } \%$  in three different ridge sections: two highly-depleted samples form the Siqueiros Transform Fault, a set of eight samples from the EPR 9 – 10°N section, and a set of nine samples from the MAR 26°S section. The Siqueiros samples are too few and the spread in trace-element contents in the EPR 9 – 10°N is too restricted for a meaningful evaluation of geochemical trends from these sets. We, therefore, focus on the sample set of high-Mg, low-Cl/K samples from the MAR.

The relative compatibility of boron during mantle melting can be established from plots showing the logarithm of [B] versus the logarithms of the abundances of other trace elements (Fig. 9), as has been established by Hémond *et al.* (2006) based on earlier work (e.g., Jochum *et al.*, 1983; Niu & Batiza, 1997).

The slopes of the linear regression lines of the low-Cl/K, high-Mg samples from the MAR 26°S (red lines in Fig. 9b,d) indicate that B is more compatible than K (slope < 1; Fig. 9b), but similar in compatibility to Ce, Pb, Pr, P, and Be (slopes ≈ 1; Fig. 9d,f; Supplement). The slope in log[B]–log[Nd] and log[B]–log[Sm] plots are significantly larger than 1, showing that B is more incompatible than Nd and Sm (Supplement). The slopes of a large range of trace elements can be used to place B on a multi-element plot (‘spidergram’; see Supplement), and the sample set investigated here shows that B compatibility is similar to the light REE (Ce, Pr) and to Pb, Be, and P (Fig. 9f). Interestingly, the selected MAR samples also show a relatively large scatter on the log[B]–log[K] plot ( $R^2 = 0.36$ ; Fig. 9b) and the log[B]–log[Nb] plot ( $R^2 = 0.56$ ; Supplement), whereas the linear correlations are well defined for log[B]–log[Pr] ( $R^2 = 0.95$ ; Fig. 9d) and log[B]–log[Ce] plot ( $R^2 = 0.93$ ; Supplement). A third observation concerns the relative variation among the three ridge sections with high-Mg samples: they show a large scatter for log[B]–log[K] and log[B]–log[Nb], but all fall on the same correlation line for log[B]–log[Pr] and log[B]–log[Ce] (Fig. 9b,d; Supplement). These three observations together show that (i) K and Nb are more incompatible than B during MORB melting, (ii) that B is similar in incompatibility to the light REE, Pb, P and Be, and (iii) that the mantle heterogeneities that exist among different ridge sections did not fractionate B from the light REE and are, thus, consistent with generation by melt extraction and impregnation events that followed the same partition behaviour than modern MORB melting.

For the global data set, variations in trace-elements and trace-element ratios may arise for various reasons, such as fractional crystallisation, partial melting, and variations in element abundances in the mantle sources of the basalts. The high-Cl/K samples are excluded from the discussion, because their trace-element abundances are likely affected by assimilation of seawater-altered materials. Fractional crystallisation does not significantly fractionate incompatible trace elements from one another until high degrees of fractionation are reached, and it did not affect B/K nor B/Pr in our sample set, as discussed above. Low to moderate degrees of fractional crystallisation will mostly lead to a translation of data points towards the upper right corner of the Hémond diagrams, more or less parallel to the 1:1 line. It will, thus, lead to stronger apparent similarities in compatibility than would be reflected by partial melting alone. For mantle heterogeneities, the Hémond diagrams still accurately reflect relative element compatibilities, if the heterogeneities were caused by previous melt depletion, as argued above (see also discussion in Hémond *et al.*, 2006). Only in cases where mantle heterogeneities were caused by a process other than melt extraction or melt infiltration would the data points be scattered around the diagrams for such elements that were affected by that particular process. Hence, elements that show large scatter in concentration with random anomalies on multi-element plots (‘spidergrams’; see Supplement) are not likely to accurately reflect compatibility during melting. Boron, Be, Li and the REE, however, are not outliers of this type. The light elements and the REE show very systematic patterns on all plots, supporting the idea that the Hémond plots accurately reflect the relative compatibility of boron and many other trace elements during mantle melting and MORB generation, even if the global data set is evaluated. The plots including the global data set show the same results as the plots for the high-Mg MAR 26°S samples. The linear correlations are weak and show slopes < 1 for log[B]–log[K] and log[B]–log[Nb], but are strong and show slopes close to 1 for log[B]–log[Pr] and log[B]–log[Ce] (Fig. 9a,c; Supplement).

We conclude that the compatibility of B is close to that of Ce, Pr, Pb, P and Be (see Supplement). It has previously been established that Be behaves similarly to the light REE and to Zr during MORB melting and fractional crystallisation (Ryan & Langmuir, 1988; Brenan *et al.*, 1998; Ryan, 2002). Be/Nd and Be/Zr ratios have been reported to be nearly constant in mantle-derived magmatic rocks (Ryan & Langmuir, 1988; Ryan, 2002). The element ratios established from our dataset are  $B/Ce = 0.10 \pm 0.02$ ,  $B/Pr = 0.57 \pm 0.09$  and  $B/Be = 2.0 \pm 0.4$  for the mean and 2SD of the low-Cl/K (< 0.08) samples.

Models that uphold the notion of a highly incompatible behaviour of B and constant B/K during partial melting would need to account for the formation of the systematic global MORB array with its negative correlation of B/K and La/Sm, and they would need to explain how ratios of B over allegedly more compatible trace elements (e.g., B/Pr, B/Be, B/Pb) do not show any variability among the global MORB array.

The latter would require that relative partitioning of B and the other trace elements during MORB generation would have to exactly compensate the pre-existing mantle heterogeneities in each and every locality investigated here. This would seem highly fortuitous and unlikely.

#### 5.4 Abundances of B in MORB and the depleted mantle

The partial melting models applied here to determine the Li abundance of the depleted mantle (see above) are also applied to B, based on partition coefficients for boron between peridotite minerals and basaltic melt (e.g., Chaussidon & Libourel, 1993; Brenan *et al.*, 1998; Ottoloni *et al.*, 2009, see Supplement). The B abundance for the depleted mantle is adjusted, such that the B/Pr ratios of the melts extracted from approximately 2 to 20% partial melting are close to the target values of  $B/Pr = 0.57 \pm 0.09$ , as observed in MORB. For the same fraction of melting the melts show  $Li/Yb = 1.64 \pm 0.30$ , if the depleted-mantle Li content of  $1.20 \mu\text{g/g}$  is used (Fig. 8; Supplement). A boron abundance of  $0.077 \pm 0.010 \mu\text{g/g}$  is established here for the depleted mantle (Table 4; Fig. 8). This value is close to the estimate of  $0.060 \mu\text{g/g}$  given by Salters & Stracke (2004) and to the estimate of  $0.063 \mu\text{g/g}$  of Kamenetsky & Eggins (2012), but in contrast to these models, our estimate does not rely on the assumption of unfractionated trace-element ratios. Indeed, the B/Pr ratio of the mantle residues modelled here are very different from the values observed in MORB and range from 0.61 to 13 (see Supplement).

The constant B/Pr of MORB allows us to provide B abundance estimates for existing MORB models. For example, [B] in the N-MORB model of Hofmann (1988) is computed here as  $1.19 \mu\text{g/g}$ , and the estimate for the average MORB of Gale *et al.* (2013) is set here to  $[B] = 1.28 \mu\text{g/g}$  (Table 4) based on the Pr concentrations given in these models. These models comprise basalts that underwent a certain degree of fractional crystallisation and have higher B contents than many of our samples.

#### 5.5 Abundance of B in the primitive mantle

Estimates of B abundances have been derived by the same methods as described for Li above. For the mass balance calculation we use the abundances of B in the continental crust ( $11 \mu\text{g/g}$ ; Taylor & McLennan, 1995; Rudnick & Gao, 2003), oceanic crust ( $1 \mu\text{g/g}$ ; Ryan & Langmuir, 1993; Chaussidon & Jambon, 1994), altered oceanic crust ( $26 \mu\text{g/g}$  in the top 500m; Smith *et al.*, 1995), pelagic sediments ( $53 \mu\text{g/g}$ ; You *et al.*, 1995; Smith *et al.*, 1995), seawater ( $4.4 \mu\text{g/g}$ ; Broecker & Peng, 1982; Spivack & Edmond, 1987), and the depleted mantle ( $0.077 \mu\text{g/g}$ ; this study, see above). Ancient subduction is assumed to not efficiently recycle boron into the mantle, and the B mass fraction of this component is small (see below). The mass fractions of depleted mantle of 0.27, 0.62 and 1 discussed above result in estimates for B abundances of the BSE (or primitive mantle) of 0.32, 0.19 and  $0.15 \mu\text{g/g}$ , respectively.

The global MORB array depicted in Fig. 3f crosses the primitive mantle La/Sm value at  $B/K = 0.0006 \pm 0.0002$ . Boron is less incompatible than K, as established above, and partial melting will hence produce melts with lower B/K ratios compared to their mantle source. The global-MORB-array value of B/K at primitive-mantle La/Sm may thus be used in combination with the established K abundance of the primitive mantle ( $240 \mu\text{g/g}$ ; McDonough & Sun, 1995) to provide a minimum estimate for the B abundance of the primitive mantle of  $0.14 \pm 0.05 \mu\text{g/g}$ .

Our preferred estimate for the primitive mantle is  $[B] = 0.19 \pm 0.02 \mu\text{g/g}$ , which is derived from mass balance assuming extraction of the crust from depletion of the upper and part of the lower mantle, favouring the fraction of depleted mantle of Yanagi (2011). We recommend that these values for the depleted mantle ( $[B] = 0.077 \pm 0.010 \mu\text{g/g}$ ) and primitive mantle ( $[Li] = 0.19 \pm 0.02 \mu\text{g/g}$ ) should be used in the geochemical reference frame (Table 4).

Boron, like Li, is a moderately volatile, lithophile element, and Cameron *et al.* (1973) completed thermodynamic calculations on the main boron species that would condense in the solar nebular. Formation of these borides and borates result in a  $T_{50}$  of  $\sim 750 \text{ K}$  (Cameron *et al.*, 1973). The primitive-mantle abundance predicted for this temperature is  $[B] = 0.103 \mu\text{g/g}$  from the calibration discussed above and a CI

abundance of  $[B] = 0.690 \mu\text{g/g}$  (estimate from Zhai & Shaw, 1994; Palme & Jones, 2003). However, higher condensation temperatures of 908 – 910 K were estimated subsequently (Zhai, 1995; Lodders, 2003), which would be consistent with  $[B] = 0.207 \mu\text{g/g}$  in the primitive mantle. Chaussidon & Robert (1995, 1997) stated that the concept of a single condensation temperature is not meaningful for B. They argue that B in chondrites presents a mix of isotopically heavy boron from pre-solar grains and isotopically light boron produced by spallation in the solar nebular (Chaussidon & Robert, 1995, 1997). In addition, estimates for the boron abundances in CI chondrites vary widely and range from 0.27 to  $1.2 \mu\text{g/g}$  (e.g., Palme, 1988; Wasson & Kallemeyn, 1988; Anders & Grevesse, 1989; Palme & Jones, 2003). We use a reference value of  $[B] = 0.69 \mu\text{g/g}$  here (Palme & Jones, 2003).

A primitive mantle value of  $[B] = 0.19 \pm 0.02 \mu\text{g/g}$  as preferred here (Table 4) converts to a depletion factor of 0.12 relative to Mg and CI chondrites. The  $T_{50}$  for B consistent with this primitive-mantle abundance of B is  $898 \pm 20 \text{ K}$ , which is indistinguishable from the independent volatility estimate of 908 K listed by Lodders (2003).

Higgins & Shaw (1984) estimated primitive mantle abundances of B by analyses of what were considered ‘fertile’ peridotite samples. They used the same six samples from Jagoutz *et al.* (1979) described above and found abundances of  $[B] = 0.44 - 0.64 \mu\text{g/g}$ , yet with no correlation to any chemical indicator of partial melting or fertility. Their primitive mantle value of  $[B] = 0.5 \mu\text{g/g}$  would require a much more refractory character of B and would translate to a  $T_{50}$  of 1095 K. Higgins & Shaw (1984) suggested that the bulk of the B may have condensed as a solid-solution component in major silicates, mostly anorthite, at high temperatures. However, this is unlikely given the incompatible behaviour and low abundance of B in the relevant silicates, and the hypothesis was dismissed by others (Chaussidon & Jambon, 1994). It seems likely that the abundances measured by Higgins & Shaw (1984) suffered from contamination in the lab, from B-rich secondary phases, or from metasomatic enrichment of boron in the samples.

More recently, Menard *et al.* (2013) analysed a suite of mantle xenoliths (spinel and garnet lherzolites and harzburgites) and compared estimates of whole-rock boron abundances derived from analyses of the constituent minerals with measured bulk-rock concentrations. They found that the bulk-rock analyses typically have 300 – 600 % of the B estimated from the mineral content, and analyses of some samples showed extreme B enrichment ( $0.6 - 10 \mu\text{g/g}$ ) that far exceeded the mineral-based estimates and were discarded as not representative of abundances present in any mantle domain (Menard *et al.*, 2013). The authors estimated primitive mantle abundances of B from the most fertile, least contaminated, least metasomatised xenoliths and derived two different estimates: based on the mean concentrations calculated from the mineral separates of three samples, a primitive mantle estimate of  $0.14 \pm 0.05 \mu\text{g/g}$  is given, whereas the measured whole-rock analyses of three samples resulted in an estimate of  $0.26 \pm 0.04 \mu\text{g/g}$ , which is favoured by the authors (Menard *et al.*, 2013). In-situ measurements of B abundances in orogenic mantle peridotites by Ottolini *et al.* (2004) have revealed lower values for estimated whole-rock abundances and led to an estimate for the primitive mantle of  $[B] = 0.07 - 0.10 \mu\text{g/g}$  by these authors.

Primitive-mantle estimates for B based on canonical element ratios include those of Lyubetskaya & Korenaga (2007), who averaged estimates from the ratios  $B/K = 0.0010$  and  $B/Rb = 0.4$ , resulting in a primitive mantle abundance of  $[B] = 0.17 \mu\text{g/g}$ . Palme & Jones (2003) estimated  $[B] = 0.260 \mu\text{g/g}$  for the primitive mantle from  $B/K = 0.0010$ . McDonough & Sun (1995) pointed to the large variations in  $B/K$  observed among mantle-derived magmas and in estimates for the crust, and they tentatively estimated  $[B] = 0.30 \mu\text{g/g}$  for the primitive mantle. Chaussidon & Marty (1995) estimated  $[B] = 0.090 \mu\text{g/g}$  for the primitive mantle from  $B/K = 0.00024$  in their ocean island basalt samples ( $[B] = 1.1 \mu\text{g/g}$ ) based on the idea that ocean island basalts would be sourced from an undepleted (primitive) source. Kamenetsky & Eggins (2012) established a B abundance of  $0.12 \mu\text{g/g}$  for the primitive mantle from constant  $B/Nd = 0.09$  and the  $[Nd]$  estimate of  $1.25 \mu\text{g/g}$  of McDonough & Sun (1995). As discussed above, the assumption of constant  $B/K$  or  $B/Nd$  ratios among MORB and any mantle source does not appear robust, weakening the premise of all of these estimates. Instead, a primitive mantle value of  $[B] = 0.19 \pm 0.02 \mu\text{g/g}$  is suggested here.

## 5.6 Lithium isotopic composition of MORB

The Li isotopic composition of MORB was investigated by Tomascak *et al.* (2008), who also investigated samples from the EPR 9.5°N section, in addition to samples from 15.5°N on the EPR, from the MAR near the Azores hot-spot, and from the South-East Indian Ridge (SEIR). These authors found that the mean  $\delta^7\text{Li}$  value for MORB was  $+3.4 \pm 1.4\text{‰}$  ( $2\sigma$ ), but that measurable differences existed in their sample set between different localities. However, no global correlation was found between  $\delta^7\text{Li}$  and radiogenic isotopes or trace-element indicators of mantle depletion. The results from this study confirm these findings, but at an improved analytical precision. Tomascak *et al.* (2008) presented data with a precision of  $\pm 1.1\text{‰}$  ( $2\sigma$ ), whereas most of the data presented here have a precision of better than  $\pm 0.3\text{‰}$  (Table 1).

In contrast to the lack of global correlations between Li isotopic composition and other geochemical tracers, there exist certain correlations on the local scale that have also been observed in previous studies (Elliott *et al.*, 2006; Tomascak *et al.*, 2008). For example, Elliott *et al.* (2006) observed a correlation between the Li isotopic composition and Sr and Nd isotopic compositions and with La/Sm in the sample set collected at the EPR north of the Clipperton Fault Zone. Their set of samples was also investigated here, and the majority of their samples were re-analysed in order to check for possible effects of analysts and methods biases (see Supplement for details). Elliott *et al.* (2006) argued that the isotopically heavy Li was derived from a recycled mantle component that was ultimately generated in the mantle wedge of an ancient subduction zone. Tomascak *et al.* (2008) tentatively followed this interpretation for the samples from the EPR 15.5°N section, whereas they argue for shallow assimilation of a seawater component for their EPR 9.5°N samples.

The distinction between these two contrasting processes – melting of ancient mantle heterogeneities vs. shallow contamination of the magma at the ridge – is important, but not easy to demonstrate. The best geochemical tools to distinguish these two possible processes may be chlorine contents and Nd and Pb isotopes. Chlorine abundances are elevated by assimilation of seawater, brines, or seawater-altered oceanic crust (Michael & Schilling, 1989; Michael & Cornell, 1998; le Roux *et al.*, 2006; Kendrick *et al.*, 2013). There may also be some Cl enrichment expected from recycled subduction-zone components, but not as severe as in an assimilation scenario beneath the ridge (Tomascak *et al.*, 2008). Enrichments in radiogenic Sr may be expected from assimilation of seawater or altered oceanic crust, as well as from recycling of ancient subducted components, so that this parameter may not be diagnostic. The isotopic compositions of Nd and Pb, however, are not easily influenced by seawater alteration, and may thus be used to identify recycled materials or, more generally, heterogeneities in the mantle source of the MORB magmas.

The correlations of  $\delta^7\text{Li}$  with  $^{87}\text{Sr}/^{86}\text{Sr}$  at the EPR 10 – 12°N section observed by Elliott *et al.* (2006) was also observed here through repeat  $\delta^7\text{Li}$  analyses of their samples. Yet, the correlation is weak ( $R^2 = 0.49$ ), no significant correlations exist with Nd isotopes ( $R^2 = 0.18$ ) nor any systematic of the Pb isotope ratios. Moreover, the existing correlations are not defined by a continuous array, but by two more or less distinct sub-groups (Fig. 4): (1) three on-axis samples from 11.4°N with high  $\delta^7\text{Li}$  ( $+4.2$  to  $+5.1\text{‰}$ ), high  $^{87}\text{Sr}/^{86}\text{Sr}$  (0.70266–0.70282), and lower  $^{143}\text{Nd}/^{144}\text{Nd}$  (0.513053–0.513138), and (2) all other samples from this section including off-axis samples from 11.4°N and on- and off-axis samples from 10.5°N with low  $\delta^7\text{Li}$  ( $+2.8$  to  $+3.7\text{‰}$ ), low  $^{87}\text{Sr}/^{86}\text{Sr}$  (0.70247–0.70255), and higher  $^{143}\text{Nd}/^{144}\text{Nd}$  (0.513105–0.513180). The two groups overlap in their Nd and Pb isotope ratios, and the samples from this section are more differentiated than the other samples investigated here, with MgO contents of 3.90 – 7.49 wt %. Cl contents are relatively high, and the highest Cl contents in excess of 1000  $\mu\text{g/g}$  are found in the on-axis samples at 11.4°N that define the isotopically heavy-Li end of the correlations. This suggests that contamination of the EPR 11.4°N lavas by a seawater component occurred at the ridge during the differentiation of these magmas. The only two samples from the EPR 10 – 12°N section with MgO contents above 7 wt % have low  $\delta^7\text{Li}$  values ( $+2.8$  and  $+3.2\text{‰}$ ).

Heterogeneities perpendicular to the ridge represent different ages of on-axis volcanism, as well as younger off-axis volcanism. The latter shows more enriched-type mantle sources, but also higher proportions of assimilation, and it would take a more focused effort to investigate the Li and B isotope systematics of this particular section of ocean floor.

No correlation between Li isotopes and any radiogenic isotopes were observed for the MAR segment samples (Fig. 4a,b), and no such correlation was observed by Tomascak *et al.* (2008) in their sample sets from the MAR or from the SEIR. Our relatively large sample set from the EPR 9.5°N section shows a large range in  $\delta^7\text{Li}$  values (+2.9 to +4.7‰), but again does not show any correlation of the Li isotopes and the radiogenic isotopes. The fact that correlations of Li isotopes and other geochemical parameters are only observed in some parts of the EPR, but are absent in most other places, and the fact that no global correlation exists, suggests that large-scale long-lived heterogeneities of the depleted mantle are probably not the cause of the observed variation in Li isotopes. Instead, Li isotopes seem to be decoupled from other elemental and isotopic tracers, and may, therefore, be related to processes operating beneath the ridge. These processes may include assimilation of seawater-altered materials that would lead to elevated  $\delta^7\text{Li}$  values coupled with variable enrichments in Cl, high Cl/K, and elevated  $^{87}\text{Sr}/^{86}\text{Sr}$ , depending on the amount and type of assimilated material (see below; Tomascak *et al.*, 2008). Assimilation at the ridge was interpreted to be the cause of elevated  $\delta^7\text{Li}$  values of some EPR 9.5°N samples investigated by Tomascak *et al.* (2008), and is our preferred interpretation for the EPR 11.4°N samples. There is no requirement to invoke the involvement of mantle heterogeneities, such as old recycled components, to explain the Li isotope data set from these sites. This conclusion is in contrast to the findings of Elliott *et al.* (2006), a study that was completed on a much smaller sample set.

The indicators of combined assimilation and fractional crystallisation (high [Cl], low MgO), are strong in the EPR 11.4°N samples. However, assimilation cannot explain the observed range of  $\delta^7\text{Li}$  values in all samples investigated here. A group of samples from very recent lava flows (erupted between 1991 and 2002) from the EPR 9.5°N section shows very high  $\delta^7\text{Li}$  values (+3.9 to +4.7‰), but low [Cl] ( $\leq 62 \mu\text{g/g}$ ), low  $^{87}\text{Sr}/^{86}\text{Sr}$  (0.70244–0.70250), and high MgO (7.9 – 8.9 wt %). These features render it unlikely that these glasses were affected by assimilation–differentiation processes. Instead, it has to be considered that the mantle source of these lavas may be isotopically different in its Li isotopic composition, but without being distinct in its trace-element composition or radiogenic isotope composition. Two samples investigated from the same ridge section have much lower  $\delta^7\text{Li}$  values (+2.9 and +3.0‰), but overlap with the high- $\delta^7\text{Li}$  group in their radiogenic isotope ratios. These two samples are from slightly older lavas that erupted earlier in the twentieth century (Sims *et al.*, 2002). This shows that Li isotopic heterogeneities at opposite ends of the total variation observed in the global MORB data set are preserved in lavas erupted at the same ridge section within a few decades from each other without any changes in other geochemical parameters.

The above observations lead to the conclusion that some process must have generated diverse Li isotopic excursions in lavas extracted from a possibly homogenous mantle source without affecting their radiogenic or trace element compositions. Kinetic fractionation of Li isotopes during melt-rock interaction would be a possible process of this type (Lundstrom *et al.*, 2005; Jeffcoate *et al.*, 2007; Tomascak *et al.*, 2008). It has been demonstrated in peridotite xenoliths and in orogenic peridotites that diffusive enrichment of Li in mantle rocks during interaction with basaltic melt has the capacity to strongly alter their Li isotopic composition and induce very low  $\delta^7\text{Li}$  values in the peridotites (Lundstrom *et al.*, 2005; Rudnick & Ionov, 2007; Tang *et al.*, 2007; Kaliwoda *et al.*, 2008; Lai *et al.*, 2015). The diffusive fractionation that leads to the enrichment of the peridotites in isotopically light Li correspondingly has to deplete the passing magmas in this component and consequently drive these magmas to higher  $\delta^7\text{Li}$  values (see Supplement for details). This fractionation mechanism could be responsible for a shift of the erupted basalts to higher  $\delta^7\text{Li}$  values (Supplement; Jeffcoate *et al.*, 2007) that would not correlate with indicators of mantle source depletion or degree of melting. Kinetic Li isotope fractionation may also affect the magmas as they pass through the crust and during storage in the crustal magma lens; this is where Li could diffusively exchange with the host rock, leading to further isotopic excursions. The multistage interaction between magma and host rock and the complex mixing and replenishment processes now envisaged for mid-ocean ridge magma chambers and conduit systems (O'Neill & Jenner, 2012; Lissenberg *et al.*, 2013; Coogan & O'Hara, 2015) provide a range of scenarios that would create Li chemical potential gradients in a number of ways and, hence, are expected to induce diffusional fractionation.

Tomascak *et al.* (2008) argued that the homogenisation of magmas in the plumbing system beneath the ridge would erase isotopic excursions produced by kinetic processes, and these authors, therefore, dismissed the possibility that the  $\sim 1.5\%$  spread in  $\delta^7\text{Li}$  values observed in lavas at the seafloor would be preserved if it was generated by diffusion processes during melt–rock interaction in the mantle. However, such isotopic excursions would only be levelled out and erased, if the different magma batches had excursions in opposite directions of the mean MORB value. Yet, in cases in which the rising magmas are too rich in Li to be in equilibrium with the surrounding mantle, all these magma batches would be diffusively driven towards high  $\delta^7\text{Li}$  values, resulting in a high mean  $\delta^7\text{Li}$  value that may be preserved in the erupted lavas. This signature could be further enhanced in the crustal magma lens, if more Li is diffusively lost to the host rock. The high  $\delta^7\text{Li}$  values of the very recent EPR 9.5°N lavas investigated here may be the result of such a process. They are not distinct in their radiogenic isotopic composition, their trace-element patterns, are not enriched in Cl, and they do not show elevated  $\delta^{11}\text{B}$  values (see below). These features together argue against seawater assimilation and against geochemical heterogeneities in the mantle, leaving kinetic processes as the most likely cause of the high  $\delta^7\text{Li}$  values in these samples.

## 5.7 Assimilation and the boron isotopic composition of MORB

The B isotopic composition of unaltered MORB glasses has been investigated in several studies starting with Spivack & Edmond (1987). These authors analysed two samples from the EPR resulting in a  $\delta^{11}\text{B}$  of  $-3.0 \pm 2.0\%$ . Ishikawa & Nakamura (1992) investigated a number of altered basaltic rocks from ODP Hole 504B (Galapagos Spreading Center). They extrapolated the alteration trend back to the least altered sample and argued that  $\delta^{11}\text{B} = +0.2\%$  was representative of fresh MORB.

The largest number of samples of any previously published study have been investigated by Chaussidon & Jambon (1994), who analysed 17 MORB glasses from the EPR, MAR and the Red Sea and found  $\delta^{11}\text{B}$  to range from  $-6.5$  to  $-1.2\%$  with a mean of  $-3.9 \pm 3.3\%$ . These authors observed a similar range of values in back-arc basin basalts and OIB. Based on a number of geochemical parameters, they argued that the range observed in the oceanic basalts did not reflect mantle source heterogeneities, but was due to the assimilation of seawater-altered materials by the magmas prior to eruption. Chaussidon & Jambon (1994) argued that  $\delta^{11}\text{B} = -7.0 \pm 1.0\%$  is most representative of the upper mantle. However, the authors discuss the possibility that the MORB-source mantle could contain recycled materials derived from subducted altered oceanic crust enriched in isotopically heavy boron, and that the higher  $\delta^{11}\text{B}$  observed in MORB may be derived from this recycled component in the mantle. In a subsequent study, Chaussidon & Marty (1995) have argued that the primitive mantle and uncontaminated mantle-derived basalts really have a  $\delta^{11}\text{B}$  value of  $-10 \pm 2\%$ , and that higher values were generated by the assimilation of altered oceanic materials into the magma during ascent.

Other studies with more restricted numbers of samples include Moriguti & Nakamura (1998) with two samples from ODP Hole 648B (MAR) with  $\delta^{11}\text{B} = -5.3 \pm 0.2\%$ , and le Roux *et al.* (2004) with four samples from the EPR resulting in  $\delta^{11}\text{B} = -7.3 \pm 0.8\%$ . Roy-Barman *et al.* (1998) investigated Os and B isotopes of six MORB glasses from the MAR, Central Indian Ridge and the EPR, and three OIB glasses from Lo'ih. They showed that radiogenic Os is found in samples that also show isotopically heavy B, most likely introduced by assimilation of altered crust. Their two MORB samples with  $^{187}\text{Os}/^{188}\text{Os} < 0.135$  have a  $\delta^{11}\text{B}$  value of  $-10.3 \pm 2.2\%$ , which they take as representative of the uncontaminated mantle, following Chaussidon & Marty (1995).

Any comparison of all these  $\delta^{11}\text{B}$  values published by a number of authors from different laboratories and determined by various analytical techniques need to take the historic analytical limitations into account. Well-established silicate reference materials for B isotope analysis only became available relatively recently (e.g., Jochum *et al.*, 2006), and analytical protocols have been improved over the past two decades (e.g., Aggarwal *et al.*, 2009; Foster *et al.*, 2013; Marschall & Monteleone, 2015). Discrepancies at the level of 5% or less among the different studies from the 1980s and 1990s cited above are not significant, given the level of accuracy, inter-laboratory comparability and lack of internationally distributed B isotope reference

materials. Nonetheless, these studies established that the  $\delta^{11}\text{B}$  value of fresh, uncontaminated MORB had to be between  $-12$  and  $0\text{‰}$ , most likely between  $-10$  and  $-5\text{‰}$ , and that assimilation of seawater or seawater-altered materials could explain elevated  $\delta^{11}\text{B}$  values observed in some MORB samples (Chaussidon & Jambon, 1994; Roy-Barman *et al.*, 1998).

The availability of well-characterised international reference materials and the advancement in analytical methods provides the tools to determine the B isotopic composition of MORB with a much improved accuracy and precision (see method section, and Marschall & Monteleone, 2015). The data presented here will, therefore, be used to discuss the influence of crustal assimilation and fractional crystallisation on the B isotopic composition of MORB, and to deduct an accurate  $\delta^{11}\text{B}$  value for uncontaminated MORB.

The lack of a global correlation between B isotopes and any trace element or radiogenic isotope compositions, and the indistinguishable  $\delta^{11}\text{B}$  value of all investigated ridge sections (low-Cl/K samples only) show that pristine MORB has a homogenous B isotopic composition. Mantle heterogeneities that were identified through radiogenic isotopes and an enrichment in incompatible trace elements do not appear to possess anomalous B isotope compositions. The subset of samples from EPR 9.5°N that show high  $\delta^7\text{Li}$  values ( $+3.9$  to  $+4.7\text{‰}$ ) do not have elevated  $\delta^{11}\text{B}$  values ( $-6.8 \pm 0.9\text{‰}$ ); however, it should be noted that the analytical precision in this study is much better for Li isotopes ( $\pm 0.3\text{‰}$ ) than for B isotopes ( $\pm 2\text{‰}$ ), and that a possible excursion by approximately  $1\text{‰}$ , as seen in  $\delta^7\text{Li}$ , may still go undetected in  $\delta^{11}\text{B}$ .

Boron diffuses slower than Li, and kinetic fractionation of boron isotopes by diffusion in melts (or fluids) is insignificant (Chakraborty *et al.*, 1993), in contrast to Li. However, B and B isotopes are very sensitive to assimilation of seawater, brines, serpentinite, sediment, and low- $T$  altered oceanic crust. All of these components are highly enriched in B compared to pristine mantle-derived basalt, and they all show highly elevated  $\delta^{11}\text{B}$  values (Table 5). It has also been suggested that stoping in MOR magma chambers may lead to the assimilation of brine-rich roof rocks (Michael & Schilling, 1989), which would lead to a combined assimilation of brine and altered oceanic crust. High-temperature altered oceanic crust, although it also shows elevated  $\delta^{11}\text{B}$  values, is depleted in B relative to MORB (Ishikawa & Nakamura, 1992). The effects of fractional crystallisation and of assimilation of various components on the Li and B isotopic composition and the Li, B and Cl abundance of MORB is quantified here assuming bulk mixing (Fig. 10). Fractional crystallisation has a negligible effect on the Li and B isotopic composition of the magma (Fig. 10), due to the incompatible behaviour of both elements and the small isotope fractionation between solids and liquid at magmatic temperatures (also see discussion below). In contrast, Li, B and Cl contents will increase with fractional crystallisation (Fig. 10).

The geochemical effects of assimilation are displayed in Fig. 10 in comparison to the samples from the EPR 10.5°N and 11.4°N section, which show the largest isotopic and elemental variability. Assimilation of only  $2 - 3\%$  of either seawater, brine, serpentinite or low- $T$  altered crust would be sufficient to produce the observed elevation in  $\delta^{11}\text{B}$  from the sample with the lowest Cl/K to the most Cl-rich sample with the highest  $\delta^{11}\text{B}$  value (Fig. 10a,c). In combination with some degree of fractional crystallisation (which is evident in these samples from their low MgO content), this would also produce the range in Li and B contents. However, the elevated Cl contents require assimilation of either seawater or brine in all samples with elevated  $\delta^{11}\text{B}$  (Fig. 10c). Elevated  $\delta^7\text{Li}$  values are only expected from the assimilation of low- $T$  altered crust, since seawater, brine and serpentinites all have very low Li contents (Table 5; Fig. 10b,d). The model results show that the 10.4°N samples may have assimilated seawater or brine, leading to an enrichment in Cl and isotopically heavy B without affecting their Li isotopic composition. The three samples collected from the volcanic axis at 11.4°N may have been affected by assimilation of low- $T$  altered oceanic crust, leading to an enrichment in Li, B and Cl and elevated  $\delta^7\text{Li}$  and  $\delta^{11}\text{B}$  values. Alternatively, the elevated  $\delta^7\text{Li}$  in these samples may have been produced independently from the B and Cl signatures, for example through kinetic fractionation, as discussed above for the recent EPR 9.5°N lavas.

Unravelling the effects of assimilation is a prerequisite for the determining the composition of the uncontaminated mantle. The composition of the uncontaminated mantle is required in order to identify contamination signals, but the uncontaminated mantle value can only be determined, if the contamination trend can



be identified and traced back to the composition of pristine MORB. This partially circular problem can only be resolved by including additional tracers into the investigation, such as Li, B and Cl abundances and the Li isotopic composition. Assimilation of seawater or brine leads to a strong increase in Cl abundances and high Cl/K ratios in MORB glasses, even at very small amounts of assimilation (Fig. 10c). Consequently, samples with elevated Cl/K are likely to have experienced brine or seawater assimilation and are excluded from the set of samples used to determine the isotopic composition of pristine MORB.

Assimilation of small amounts of low- $T$  altered oceanic crust is predicted to lead to a strong increase in MORB  $\delta^{11}\text{B}$  without significant changes in Cl contents (Fig. 10c). However, this type of contamination would also lead to elevated  $\delta^7\text{Li}$  values. Samples that show co-enrichment in isotopically heavy Li and heavy B are, therefore, likely to have experienced assimilation of low- $T$  altered oceanic crust (Fig. 10b). This applies to the three samples from the EPR 11.4°N discussed above and to one sample (ALV2351-002) from the EPR 9 – 10°N section (Fig. 5b).

Serpentinite assimilation would lead to a strong elevation of  $\delta^{11}\text{B}$  values, but would be undetectable through Li isotopes and through B, Li or Cl abundances, at least at small mass fractions of assimilation (Fig. 10). However, serpentinite formation is not common in magmatic sections of fast-spreading ridges away from transform faults. It is more abundant along slow-spreading ridges, where some of the spreading is amagmatic and accommodated by normal faults or detachment faults. Consequently, serpentinite assimilation would be expected for the samples from the MAR and SWIR, but not for the EPR, and a systematic off-set of the MAR and SWIR samples to higher  $\delta^{11}\text{B}$  values would be expected. This is not observed, as low-Cl/K samples from all investigated ridge sections are indistinguishable in  $\delta^{11}\text{B}$  (Fig. 7).

The assimilation hyperbolae displayed in Fig. 10 further highlight the difficulty in identifying the B isotopic composition of uncontaminated MORB. Small amounts of assimilation at the level of 2% or less are able to increase the  $\delta^{11}\text{B}$  value of MORB magmas by several per mil. The correlation of  $\delta^{11}\text{B}$  values and Cl abundances, as well as elevated  $\delta^{11}\text{B}$  in combination with elevated  $\delta^7\text{Li}$  suggests that any samples with  $\delta^{11}\text{B} > -6\text{‰}$  have been affected by assimilation and do not represent pristine mantle-derived melts. The remaining samples reach values as low as  $-9.4\text{‰}$ , but values at the low end of the range are rare and only six low-Cl/K samples showed  $\delta^{11}\text{B} < -8.5\text{‰}$ . None of them were significantly below  $-8.5\text{‰}$  within their 2SE precision (Table 1).

The majority of low-Cl/K samples show  $\delta^{11}\text{B}$  values between  $-8.5$  and  $-6.0\text{‰}$  with no significant difference among the various investigated ridge sections, and without any correlation with Cl, Li or B contents. Samples from diverse localities, such as the southern MAR, the SWIR and the various sections of the EPR all show an indistinguishable distribution around the mean value of  $-7.1\text{‰}$  (Fig. 11). These observations taken together render it unlikely that pristine, uncontaminated MORB has a  $\delta^{11}\text{B}$  lower than  $-8\text{‰}$ . For example, if pristine MORB had a  $\delta^{11}\text{B}$  value of  $-10\text{‰}$ , it would require that all analysed low-Cl/K samples had assimilated the same amount of high- $\delta^{11}\text{B}$  material, i.e., approximately 2% low- $T$  altered oceanic crust or 0.1% serpentinite. Assimilation of identical amounts of serpentinite to each sample, independent of spreading rate and magma supply rates is highly unlikely, as discussed above. Assimilation of identical amounts of low- $T$  altered crust would be fortuitous, but not impossible. However, it would not just lead to enrichment in isotopically heavy B, but also to an enrichment in isotopically heavy Li (Fig. 10b,d). The consequence of a pristine MORB  $\delta^{11}\text{B}$  value of  $-10\text{‰}$  would be that its  $\delta^7\text{Li}$  value would need to be between  $+2.5$  and  $+2.8\text{‰}$ , values that have not been observed in equilibrated peridotites and are rarely observed in MORB glass, and which would be in contradiction to all published estimates of the Li isotopic composition of the Earth's mantle (Tomascak *et al.*, 2016a). This possibility is, therefore, also highly unlikely and is rejected here. Assimilation of seawater or brine can be excluded based on the low Cl contents of the samples (Fig. 5c,d).

It is, therefore, concluded here that pristine MORB that has not experienced assimilation of seawater-altered materials is homogenous in boron isotopes on the level of current analytical precision and accuracy, and has a  $\delta^{11}\text{B}$  of  $-7.1 \pm 0.9\text{‰}$  (2SD; Table 3).

## 5.8 The lithium and boron isotopic composition of the mantle

Basalts and basaltic glasses have been used in the past to unravel the B and Li isotopic composition of the mantle (e.g., Chaussidon & Jambon, 1994; Tomascak *et al.*, 2008). It is argued in these studies that the isotope fractionation between rocks and silicate melt is negligible at the high temperatures at which basaltic melts are generated in the mantle, and that the basalts, therefore, faithfully record the unfractionated isotopic composition of their mantle sources.

The degree to which this assumption is justified can be estimated from equilibrium isotope fractionation and element partition coefficients between basaltic liquid and the restitic peridotite. Isotope fractionation factors for Li and B are not well constrained for magmatic processes (see supplement for discussion), but based on the available data it can be estimated that MORB accurately reflects the  $\delta^7\text{Li}$  ( $+3.5 \pm 1.0\text{‰}$ ) and  $\delta^{11}\text{B}$  ( $-7.1 \pm 0.9\text{‰}$ ) values of its mantle source within  $0.4\text{‰}$  (see Supplement).

Nevertheless, MORB is heterogeneous in radiogenic isotopes and trace elements with levels of depletion that vary strongly among the global data set (e.g., Salters, 1996; O'Neill & Jenner, 2012; Gale *et al.*, 2013). Some of the MORB variability is generated during magmatic processes beneath the ridge, but some of it has to reflect heterogeneity of the MORB-source mantle. It is still a matter of debate how much of the variation in mantle composition is generated by melt fractionation processes within the mantle at various times in the past, and how much is due to recycling of subducted materials into the upper mantle (e.g., Allègre *et al.*, 1984; Workman & Hart, 2005; Iwamori *et al.*, 2010).

Boron isotope fractionation is unlikely to occur during internal differentiation processes within the mantle, as stated above (and discussed in the Supplement), so that any variations in the mantle would be strong evidence for input of surface materials into the mantle, most likely by ancient subduction. It could, therefore, be hypothesised that the depleted mantle as a whole has been slowly contaminated by subducted materials over time, and that the  $\delta^{11}\text{B}$  value derived here for the depleted mantle reflects an intermediate composition between the primitive mantle and the recycled material (Chaussidon & Marty, 1995). However, the homogeneity of the relatively large sample set presented here with a lack of correlation to established indicators of mantle source enrichment and heterogeneity render this hypothesis highly unlikely. It would require that boron was stirred into the entire upper mantle on a global scale to homogenise its isotopic composition, but not its elemental abundance. This hypothetical homogenisation process also did not homogenise trace-element abundances or radiogenic isotope ratios, which clearly show local, regional and global variation, also apparent in the sample set studied here. The hypothesis that the primitive mantle had a lower  $\delta^{11}\text{B}$  value (e.g.,  $-10\text{‰}$ ) than the depleted mantle and that the depleted mantle contains a certain portion of recycled isotopically heavy boron is, therefore, not supported. Consequently, the estimate for the  $\delta^{11}\text{B}$  value of the depleted mantle ( $-7.1 \pm 0.9\text{‰}$ ) is extended to the primitive mantle ignoring the small possible fractionation effects of partial melting.

## 5.9 The global Li budget and the B isotopic composition of the continental crust

The mean Li and B isotopic compositions of the continental crust are important parameters in the global budget of these elements, and have been discussed in a number of studies based on the analysis of crustal materials that were thought to represent bulk crustal compositions or from which bulk crustal compositions could be reconstructed. Estimates for the B isotopic composition of the bulk continental crust are  $\delta^{11}\text{B} = -8.8\text{‰}$  based on a study on metamorphic and magmatic rocks from Argentina (Kasemann *et al.*, 2000), and between  $\delta^{11}\text{B} = -13$  and  $-8\text{‰}$  based on a global collection of magmatic tourmalines (Chaussidon & Albarède, 1992). Marschall & Ludwig (2006) also concluded that most tourmaline from granites and pegmatites show  $\delta^{11}\text{B}$  values of  $-10 \pm 3\text{‰}$ , which may be taken as representative of average continental crust. However, it should be noted that magmatic tourmaline is restricted to S-type granites and pegmatites and sampling is, therefore, biased towards metasedimentary sources, which likely show a more extreme influence of weathering than the bulk crust. Weathering preferentially removes the heavy isotopes from the continents, which should lead to sub-mantle  $\delta^{11}\text{B}$  value of the evolved continental crust consistent with the

enrichment of isotopically heavy B in rivers and seawater (Lemarchand *et al.*, 2000, 2002). However, the majority of subduction-zone magmas show elevated  $\delta^{11}\text{B}$  values consistent with a preceding removal of isotopically heavy B from the subducting slab (e.g., Rosner *et al.*, 2003; Marschall *et al.*, 2007a; Ryan & Chauvel, 2014). Subduction-zone volcanism related to apparently deeper inputs from the slab show lower B concentrations and lower  $\delta^{11}\text{B}$  values consistent with an earlier preferential release of isotopically heavy boron from the slab (Ishikawa & Nakamura, 1994; Ryan & Chauvel, 2014). Deeply subducted slabs may thus be similar or even lower in  $\delta^{11}\text{B}$  than unmodified mantle, and are likely to have similarly low B contents as the mantle. Newly added continental crust produced at convergent plate margins may have a mean  $\delta^{11}\text{B}$  value higher than the depleted mantle from the input of high- $\delta^{11}\text{B}$  magmas.

The investigation of the Li isotopic composition of the continental crust is more advanced than for B isotopes, and studies on shales and loess, as well as granulite terrains, lower-crustal xenoliths, and granites have been used to estimate the Li isotopic composition of the bulk continental crust to  $\delta^7\text{Li} = +1.2\text{‰}$  and  $+1.7\text{‰}$  (Teng *et al.*, 2004, 2008, 2009; Sauzéat *et al.*, 2015). It should be noted, however, that the granulite, granite and xenolith data cover a wide range in  $\delta^7\text{Li}$  from approximately  $-18$  to  $+16\text{‰}$  (Teng *et al.*, 2008, 2009; Magna *et al.*, 2010). This renders it difficult to provide a precise average Li isotopic composition of the middle and lower crust, whereas the average of the upper continental crust is probably well represented by shale and loess. Nonetheless, the bulk continental crust can be expected to have a  $\delta^7\text{Li}$  lower than the mantle, as isotopically heavy Li is preferentially removed during weathering, leading to low- $\delta^7\text{Li}$  weathering residues and high- $\delta^7\text{Li}$  rivers (e.g., Huh *et al.*, 2001; Rudnick *et al.*, 2004; Pogge von Strandmann *et al.*, 2006, 2012; Vigier *et al.*, 2008, 2009; Liu *et al.*, 2013, 2015). Subduction-related magmas do not show strong Li isotopic deviations from MORB (see Tomascak *et al.*, 2016b) and it can, therefore, be assumed that continental crust newly formed at subduction zones has a  $\delta^7\text{Li}$  value similar to that of MORB and the depleted mantle.

Uncertainties with the method of determining the bulk composition of the continental crust from a collection of samples arise from the difficulty to select samples that are representative of the crust or of quantifiable parts of it, and from the immense heterogeneity of this reservoir. An alternative way to determine the mean composition of the continents is through mass balance. This requires that all other reservoirs are well defined in terms of their elemental abundances and isotopic composition for the element of interest. The Li and B abundances of the major mantle, crustal and surface reservoirs have been discussed above and are listed in Table 6. The Li and B isotopic compositions of altered oceanic crust, pelagic sediment, and seawater have been previously determined (see Table 6 for values and references), and the fresh oceanic crust is taken from the mean MORB value established above.

A mass-balance based estimate for the Li isotopic composition of the continental crust based on these reservoirs would be very close to that of MORB ( $+3.5\text{‰}$ ), if no ancient subducted altered oceanic crust is invoked. This is in contrast to the low  $\delta^7\text{Li}$  value estimated by Teng *et al.* (2008, 2009), and it is in conflict with the effect that weathering has on the extraction of isotopically heavy Li from the continents (Huh *et al.*, 2001). Hence, the bulk continental crust most likely has a  $\delta^7\text{Li}$  value lower than the mantle, and may be best represented by the estimates of Teng *et al.* (2008, 2009), i.e.,  $\delta^7\text{Li} = +1.7\text{‰}$  (Table 6). The mass fraction of the isotopically heavy-Li reservoirs that counter-balance the isotopically light crust (and marine sediments) are seawater and altered oceanic crust, which together carry less than 0.1 % of the total Li of the BSE. This contrasts with 6.7 % of the BSE lithium in the continental crust (Fig. 12). Hence, the presence of material enriched in isotopically heavy Li is required to balance the  $^6\text{Li}$ -enriched surface reservoirs.

Subduction of oceanic crust is expected to introduce isotopically heavy Li into the mantle (Marschall *et al.*, 2007b). Ancient subducted altered oceanic crust could be stored in the deep mantle and could be occasionally tapped by deep plumes that feed ocean island volcanism. High  $\delta^7\text{Li}$  values in ocean island basalts are correlated with radiogenic isotope indicators of deep recycling (e.g., Ryan & Kyle, 2004; Nishio *et al.*, 2005; Vlastélic *et al.*, 2009; Chan *et al.*, 2009; Krienitz *et al.*, 2012); although near-surface processes, such as assimilation and kinetic fractionation, may have a similar effect on OIB as they have on MORB, which may complicate their interpretation. The size of this reservoir is estimated here by assuming Li abun-

dances and isotopic composition of present-day average altered oceanic crust for the subducted component (Table 6) and from the Li isotope mass balance required to balance the low- $\delta^7\text{Li}$  continental crust. A mass fraction of 0.3% of the BSE of such a reservoir would balance the continental crust, containing  $\sim 2\%$  of the total Li of the BSE (Fig. 12; Table 6). This mass is equivalent to 33 times the amount of altered oceanic crust present on the surface today (Table 6). The current rate of subduction of oceanic crust is  $60 \times 10^{12} \text{ kg/a}$  (Peacock, 1990) and a constant portion of alteration of the upper 500 m, as assumed for present-day oceanic crust, requires 3.7 billion years of subduction to build up a reservoir of the size estimated here. Alternative to a distinct reservoir, the subducted isotopically heavy Li may have been homogenised with the upper mantle or with the bulk mantle. These scenarios would have led to an increase in the  $\delta^7\text{Li}$  values of these reservoirs by 0.22 and 0.13‰, respectively, i.e., values that would not currently be detectable.

The mass balance budget is different for B, which shows much higher concentrations in seawater and altered oceanic crust. Also, pelagic sediments are enriched in the heavy isotope compared to MORB, and these three high- $\delta^{11}\text{B}$  reservoirs together contain approximately 4% of the B of the BSE (Table 6). The continental crust is estimated to contain one third of the Earth's boron, compared to only one quarter in the depleted mantle (Fig. 12; Table 6). Hence, a large portion of B has been extracted from the mantle and has been further fractionated among the surface reservoirs, with preferential enrichment of the lighter isotope in the continental crust (Fig. 12). The B isotopic composition of the continental crust resulting from mass balance is  $\delta^{11}\text{B} = -9.1 \pm 2.4\text{‰}$ . This estimate for the bulk continental crust agrees with previous estimates (see above), but provides a more robust and precise assessment.

The isotopically light B in the continental crust is counter-balanced by isotopically heavy B in the marine realm, with the mantle and the BSE showing intermediate values (Fig. 12; Table 6). No significant subduction of B is required to balance the previously estimated composition of the continental crust. This is consistent with estimates of the low efficiency of subduction to return B into the mantle: boron is largely removed from the slab in the fore-arc during dehydration and returned to the overriding plate via fluids and magmas, and only a small fraction is recycled into the deep mantle (Moran *et al.*, 1992; Savov *et al.*, 2005; Marschall *et al.*, 2007a). In addition, strong B isotope fractionation during dehydration is predicted to lead to a loss of isotopically heavy B from the slab, which in turn approaches low  $\delta^{11}\text{B}$  values close to that of the normal mantle (Peacock & Hervig, 1999; Rosner *et al.*, 2003; Marschall *et al.*, 2007a; Ryan & Chauvel, 2014). The mass balance calculation presented here, therefore, assumes low abundances of B and a MORB-like B isotopic composition in the ancient subducted altered oceanic crust (Table 6) with no influence on the continental crust  $\delta^{11}\text{B}$  estimate (Fig. 12). Alternatively, much less B isotope fractionation may be assumed during slab dehydration and B loss, and in an extreme case the deep subducted oceanic crust may reflect the unfractionated B isotopic composition of the altered oceanic crust ( $\delta^{11}\text{B} = +0.8\text{‰}$ ). Still, the low B concentrations of the dehydrated slab will restrict the impact of this component on the mass balance. The predicted  $\delta^{11}\text{B}$  value of the continental crust would only be 0.5‰ lower than in the case of dehydration fractionation discussed above. We thus consider our estimate of  $\delta^{11}\text{B} = -9.1 \pm 2.4\text{‰}$  for the bulk continental crust reliable. However, if evidence for a large, B-rich anomalous- $\delta^{11}\text{B}$  reservoirs in the mantle emerged in future studies, the continental crust estimate would have to be adjusted.

## 6 Conclusions

Lithium and B isotopic compositions of a selection of global MORB glass samples at improved precision and accuracy compared to previously published data allowed estimates to be made for the Li and B abundances of MORB, depleted and primitive mantle. Mass balance for the bulk silicate Earth was used to estimate the B isotopic compositions of the continental crust and portions of Li and B in ancient subducted oceanic crust that likely reside in the mantle. A number of conclusions are drawn:

1. The apparent incompatibility of B during mantle melting and basalt fractional crystallisation is lower than that of K and Nb, and is similar to those of Ce, Pr, Pb, P, Be and Zr, with relatively constant

B/Ce =  $0.10 \pm 0.02$  and B/Pr =  $0.57 \pm 0.09$  in MORB. However, the relative partitioning of B and the LREE varies strongly with the modal composition of the mantle, and the constant B/LREE ratio observed in MORB does not reflect the mantle ratio. The abundance of B in the primitive mantle is estimated to be  $0.19 \pm 0.02 \mu\text{g/g}$ , and that of the depleted MORB-source mantle is estimated to be  $0.077 \pm 0.010 \mu\text{g/g}$ .

2. The Li/Yb ratio of the global MORB data set is relatively constant, but it does not reflect the Li/Yb ratio of the primitive or depleted mantle. It is a result of moderate melt extraction and non-modal melting (decrease of clinopyroxene) combined with the relative partitioning among different mantle minerals and basaltic melt. The Li abundance of the depleted MORB-source mantle is estimated here from melting models to be  $1.20 \pm 0.10 \mu\text{g/g}$ . Mass balance for the bulk silicate Earth leads to an estimate for the abundance of Li in the primitive mantle of  $1.39 \pm 0.10 \mu\text{g/g}$ ,
3. Pristine MORB that has not experienced assimilation of seawater-altered materials shows a resolvable heterogeneity in lithium isotopes ranging from  $\delta^7\text{Li} = +2.9 \pm 0.2\text{‰}$  to  $+4.3 \pm 0.5\text{‰}$ . This variation does not correlate with radiogenic isotope or trace-element signatures and is most likely not related to assimilation nor mantle heterogeneity. Instead, it may be caused by kinetic fractionation of Li isotopes during melt transport and storage between the mantle and the surface.
4. Fractionated, low-MgO MORB glass samples with high  $\delta^7\text{Li} > +4\text{‰}$ , high Cl contents and high  $^{87}\text{Sr}/^{86}\text{Sr}$  are unlikely to reflect Li isotope heterogeneities of their mantle source, but probably reflect assimilation of low- $T$  altered oceanic crust into the magma chamber beneath the ridge.
5. The B isotopic composition of MORB glass is highly sensitive to assimilation of low- $T$  altered oceanic crust, seawater, brine, and serpentinites, which increase the  $\delta^{11}\text{B}$  value of MORB glass by several per mil even at small ( $\leq 3\%$ ) fractions of assimilation. Values of  $\delta^{11}\text{B} > -6\text{‰}$  are interpreted to reflect assimilation processes at the ridge. Boron isotopes could, therefore, be used in combination with Cl contents in future studies to detect and quantify assimilation processes in MORB.
6. Pristine MORB that has not experienced assimilation of seawater-altered materials is homogenous in boron isotopes on the level of current analytical precision and accuracy, and has a  $\delta^{11}\text{B}$  of  $-7.1 \pm 0.9\text{‰}$  (2SD). No variation was detected between N-MORB and E-MORB, or as a function of degree of melting or spreading rate.
7. Lithium and B equilibrium isotope fractionation during partial melting is very small, and MORB glass from uncontaminated magmas accurately reflect the Li and B isotopic compositions of their mantle source within  $0.4\text{‰}$ . However, the effects of kinetic fractionation by diffusion possibly caused the  $\delta^7\text{Li}$  of some lavas to shift to higher values by approximately  $1\text{‰}$ .
8. The boron isotopic composition of the bulk continental crust is estimated based on global mass balance and is  $\delta^{11}\text{B} = -9.1 \pm 2.4\text{‰}$ . No reservoir is invoked in the mantle that contains isotopically fractionated B significantly different from that of the ambient mantle. However, subducted material with a fractionated B isotopic composition could exist in the mantle without significantly affecting the mass balance estimate, as long as its B content is as low as predicted from subduction-zone studies.
9. The enrichment of isotopically light lithium in the continental crust is not balanced by the small high- $\delta^7\text{Li}$  surface reservoirs, such as seawater and altered oceanic crust. The presence of isotopically heavy lithium is, therefore, required in the mantle. Such a reservoir could have formed between the Archaean and the present at the current rate of subduction of altered oceanic crust. It may be present in distinct domains to be tapped by ocean island volcanism, or it may have been homogeneously stirred into the mantle. In the latter case it would have changed the isotopic composition of the bulk mantle by an amount that would not currently be measurable.

Uncertainties in the conclusions presented here arise from the still limited number of investigated samples. Future studies should apply the analytical methods available now to larger sets of MORB glasses to study local variations as a function of differentiation and other magma chamber processes, and to study global variations in more detail with relations to plume activity, spreading rate or ridge depth, for example. Experimental studies should focus on the determination of Li and B equilibrium stable isotope fractionation at magmatic temperatures. These data are needed to better quantify the isotope fractionation during mantle partial melting. Diffusion modelling may be employed in melt extraction, transport, and storage models to investigate the effects of Li isotope kinetic fractionation in more detail.

The estimates for Li and B abundances and isotopic compositions of the primitive and depleted mantle presented in this study can be used to detect anomalies in ocean island basalts and island-arc basalts to detect and quantify recycled materials in the mantle source of these rocks and, therefore, provide evidence for deep recycling and the path ways of long-term mantle convection.

## Acknowledgments

HRM would like to thank Veronique Le Roux, Glenn Gaetani, Sune Nielsen and Ralf Dohmen for discussion. We thank Ken Sims, Yaoling Niu, Cynthia Robinson and Colin Devey for providing a selection of MORB glass samples, and Gretchen Swarr for assistance with laser-ablation ICP-MS analysis. The paper benefited from constructive and insightful reviews by Roberta Rudnick, Jeff Ryan, Peter Michael and a fourth reviewer, as well as from editorial handling by Janne Blichert-Toft, which is much appreciated. This study was in part financially supported by the NSF ocean sciences program (OCE grant #1232996 to VDW and HRM), and by a WHOI internal grant provided by the Andrew W. Mellon Foundation to HRM and NS (#27005261). TE was partially supported by NERC grant NE/M000427/1.

## References

- Aggarwal, J., Böhm, F., Foster, G., Halas, S., Hönisch, B., Jiang, S. Y., Košler, J., Liba, A., Rodushkin, I., Sheehan, T., Shen, J. J. S., Tonarini, S., Xie, Q., You, C. F., Zhao, Z. Q. & Zuleger, E. (2009) How well do non-traditional stable isotope results compare between different laboratories: results from interlaboratory comparison of boron isotope measurements. *J Analyt Atom Spectrom* **24**: 825–831
- Allègre, C. J., Hamelin, B. & Dupré, B. (1984) Statistical analysis of isotopic ratios in MORB: the mantle blob cluster model and the convective regime of the mantle. *Earth Planet Sci Lett* **71**: 71–84
- Anders, E. & Grevesse, N. (1989) Abundances of the elements; meteoritic and solar. *Geochim Cosmochim Acta* **53**: 197–214
- Arevalo, R. & McDonough, W. F. (2008) Tungsten geochemistry and implications for understanding the Earth's interior. *Earth Planet Sci Lett* **272**: 656–665
- Aulbach, S. & Rudnick, R. L. (2009) Origins of non-equilibrium lithium isotopic fractionation in xenolithic peridotite minerals: examples from Tanzania. *Chem Geol* **258**: 17–27
- Aulbach, S., Rudnick, R. L. & McDonough, W. F. (2008) Li-Sr-Nd isotope signatures of the plume and cratonic lithospheric mantle beneath the margin of the rifted Tanzanian craton (Labait). *Contrib Mineral Petrol* **155**: 79–92
- Barnes, J. D. & Cisneros, M. (2012) Mineralogical control on the chlorine isotope composition of altered oceanic crust. *Chem Geol* **326-327**: 51–60
- Batiza, R., Melson, W. G. & O'Hearn, T. (1988) Simple magma supply geometry inferred beneath a segment of the Mid-Atlantic Ridge. *Nature* **335**: 428–431

- 1307 Batiza, R., Fox, P. J., Vogt, P. R., Cande, S. C., Grindlay, N. R., Melson, W. G. & O'Hearn, T. (1989)  
1308 Morphology, abundance, and chemistry of near-ridge seamounts in the vicinity of the Mid-Atlantic Ridge  
1309 ~ 26° S. *J Geol* **97**: 209–220
- 1310 Batiza, R., Niu, Y., Karsten, J. L., Boger, W., Potts, E., Norby, L. & Butler, R. (1996) Steady and non-steady  
1311 state magma chambers below the East Pacific Rise. *Geophys Res Lett* **23**: 221–224
- 1312 Bonifacie, M., Busigny, V., Mével, C., Philippot, P., Agrinier, P., Jendrzewski, N., Scambelluri, M. &  
1313 Javoy, M. (2008) Chlorine isotopic composition in seafloor serpentinites and high-pressure metaperi-  
1314 dotites. Insights into oceanic serpentinization and subduction processes. *Geochim Cosmochim Acta* **72**:  
1315 126–139
- 1316 Bouman, C., Elliott, T. & Vroon, P. Z. (2004) Lithium inputs to subduction zones. *Chem Geol* **212**: 59–79
- 1317 Boynton, W. V. (1985) *Developments in Geochemistry*, chap. Rare Earth Element Geochemistry, 115. Else-  
1318 vier, Amsterdam
- 1319 Brenan, J. M., Neroda, E., Lundstrom, C. C., Shaw, H. F., Ryerson, F. J. & Phinney, D. L. (1998) Be-  
1320 havior of boron, beryllium and lithium during melting and crystallization: constraints from mineral-melt  
1321 partitioning experiments. *Geochim Cosmochim Acta* **62**: 2129–2141
- 1322 Broecker, W. S. & Peng, T. H. (1982) *Tracers in the sea*. Lamont-Doherty Geological Observatory, Pal-  
1323 isades, New York (USA)
- 1324 Cameron, A. G. W., Colgate, S. A. & Grossman, L. (1973) Cosmic abundance of boron. *Nature* **243**: 204–  
1325 207
- 1326 Carbotte, S. & Macdonald, K. (1992) East Pacific Rise 8° – 10°30' N: evolution of ridge segments and  
1327 discontinuities from SeaMARC II and three-dimensional magnetic studies. *J Geophys Res* **B 97**: 6959–  
1328 6982
- 1329 Carbotte, S. M., Welch, S. M. & Macdonald, K. C. (1991) Spreading rate, rift valley propagation, and frac-  
1330 ture zone offset history during the past 5 my on the Mid-Atlantic Ridge: 25° – 27°30' S and 31° – 34°30' S.  
1331 *Marine Geophys Res* **13**: 51–80
- 1332 Castillo, P. & Batiza, R. (1989) Strontium, neodymium and lead isotope constraints on near-ridge seamount  
1333 production beneath the South Atlantic. *Nature* **342**: 262–265
- 1334 Catanzaro, E. J., Champion, C. E., Garner, E. L., Marinenko, G., Sappenfield, K. M. & Shields, W. R. (1970)  
1335 Boric acid: isotopic and assay standard reference materials. *NBS (US) Spec Publ* **260-17**: 1–71
- 1336 Chakraborty, S., Dingwell, D. B. & Chaussidon, M. (1993) Chemical diffusivity of boron in melts of haplo-  
1337 granitic composition. *Geochim Cosmochim Acta* **57**: 1741–1751
- 1338 Chan, L. H., Edmond, J. M., Thompson, G. & Gillis, K. (1992) Lithium isotopic composition of submarine  
1339 basalts: Implications for the lithium cycle in the ocean. *Earth Planet Sci Lett* **108**: 151–160
- 1340 Chan, L. H., Alt, J. C. & Teagle, D. A. H. (2002) Lithium and lithium isotope profiles through the upper  
1341 oceanic crust: a study of seawater–basalt exchange at ODP Sites 504B and 896A. *Earth Planet Sci Lett*  
1342 **201**: 187–201
- 1343 Chan, L. H., Leeman, W. P. & Plank, T. (2006) Lithium isotopic composition of marine sediments. *Geochem*  
1344 *Geophys Geosys* **7**: 10.1029/2005GC001 202

- 1345 Chan, L. H., Lassiter, J. C., Hauri, E. H., Hart, S. R. & Blusztajn, J. (2009) Lithium isotope systematics of  
1346 lavas from the Cook–Austral Islands: constraints on the origin of HIMU mantle. *Earth Planet Sci Lett*  
1347 **277**: 433–442
- 1348 Chaussidon, M. & Albarède, F. (1992) Secular boron isotope variations in the continental crust: an ion  
1349 microprobe study. *Earth Planet Sci Lett* **108**: 229–241
- 1350 Chaussidon, M. & Jambon, A. (1994) Boron content and isotopic composition of oceanic basalts: Geo-  
1351 chemical and cosmochemical implications. *Earth Planet Sci Lett* **121**: 277–291
- 1352 Chaussidon, M. & Libourel, G. (1993) Boron partitioning in the upper mantle: an experimental and ion  
1353 microprobe study. *Geochim Cosmochim Acta* **57**: 5053–5062
- 1354 Chaussidon, M. & Marty, B. (1995) Primitive boron isotope composition of the mantle. *Science* **269**: 383–  
1355 386
- 1356 Chaussidon, M. & Robert, F. (1995) Nucleosynthesis of  $^{11}\text{B}$ -rich boron in the pre-solar cloud recorded in  
1357 meteoritic chondrules. *Nature* **374**: 337–339
- 1358 Chaussidon, M. & Robert, F. (1997) Comment on “Boron cosmochemistry II: Boron nucleosynthesis and  
1359 condensation temperature” by M. Zhai. *Meteor Planet Sci* **32**: 321–326
- 1360 Coogan, L. A. & O’Hara, M. J. (2015) MORB differentiation: *In situ* crystallization in replenished-tapped  
1361 magma chambers. *Geochim Cosmochim Acta* **158**: 147–161
- 1362 Cooper, K. M., Eiler, J. M., Sims, K. W. W. & Langmuir, C. H. (2009) Distribution of recycled crust within  
1363 the upper mantle: insights from the oxygen isotope composition of MORB from the Australian–Antarctic  
1364 Discordance. *Geochem Geophys Geosys* **10**: Q12004
- 1365 Crane, K. (1976) The intersection of the Siqueiros Transform Fault and the East Pacific Rise. *Marine Geol*  
1366 **21**: 25–46
- 1367 Danyushevsky, L. V., Eggins, S. M., Falloon, T. J. & Christie, D. M. (2000)  $\text{H}_2\text{O}$  abundance in depleted to  
1368 moderately enriched mid-ocean ridge magmas; part I: incompatible behaviour, implications for mantle  
1369 storage, and origin of regional variations. *J Petrol* **41**: 1329–1364
- 1370 Danyushevsky, L. V., Perfit, M. R., Eggins, S. M. & Falloon, T. J. (2003) Crustal origin for coupled  
1371 ‘ultra-depleted’ and ‘plagioclase’ signatures in MORB olivine-hosted melt inclusions: evidence from  
1372 the Siqueiros Transform Fault, East Pacific Rise. *Contrib Mineral Petrol* **144**: 619–637
- 1373 Devey, C. W., Garbe-Schönberg, C. D., Stoffers, P., Chauvel, C. & Mertz, D. F. (1994) Geochemical effects  
1374 of dynamic melting beneath ridges: reconciling major and trace element variations in Kolbeinsey (and  
1375 global) mid-ocean ridge basalt. *J Geophys Res (B)* **99**: 9077–9095
- 1376 Duncan, R. A. & Hogan, L. G. (1994) Radiometric dating of young MORB using the  $^{40}\text{Ar} - ^{39}\text{Ar}$  incremen-  
1377 tal heating method. *Geophys Res Lett* **21**: 1927–1930
- 1378 Elliott, T., Jeffcoate, A. & Bouman, C. (2004) The terrestrial Li isotope cycle: light-weight constraints on  
1379 mantle convection. *Earth Planet Sci Lett* **220**: 231–245
- 1380 Elliott, T., Thomas, A., Jeffcoate, A. & Niu, Y. (2006) Lithium isotope evidence for subduction-enriched  
1381 mantle in the source of mid-ocean-ridge basalts. *Nature* **443**: 565–568
- 1382 Flesch, G. D., Anderson, A. R. & Svec, H. J. (1973) A secondary isotopic standard for  $^6\text{Li}/^7\text{Li}$  determina-  
1383 tions. *Internat J Mass Spectrom Ion Proc* **12**: 265–272



- 1384 Fornari, D. J., Haymon, R. M., Perfit, M. R., Gregg, T. K. P. & Edwards, M. H. (1998) Axial summit  
1385 trough of the East Pacific Rise 9°–10°N: geological characteristics and evolution of the axial zone on fast  
1386 spreading mid-ocean ridge. *J Geophys Res* **103**: 9827–9855
- 1387 Foster, G. L., Pogge von Strandmann, P. A. E. & Rae, J. W. B. (2010) Boron and magnesium isotopic  
1388 composition of seawater. *Geochem Geophys Geosys* **11**: Q08 015
- 1389 Foster, G. L., Hönisch, B., Paris, G., Dwyer, G. S., Rae, J. W. B., Elliott, T., Gaillardet, J., Hemming, N. G.,  
1390 Louvat, P. & Vengosh, A. (2013) Interlaboratory comparison of boron isotope analyses of boric acid,  
1391 seawater and marine CaCO<sub>3</sub> by MC-ICPMS and NTIMS. *Chem Geol* **358**: 1–14
- 1392 Gale, A., Dalton, C. A., Langmuir, C. H., Su, Y. & Schilling, J. G. (2013) The mean composition of ocean  
1393 ridge basalts. *Geochem Geophys Geosys* **14**: 489–518
- 1394 Genske, F. S., Turner, S. P., Beier, C., Chu, M. F., Tonarini, S., Pearson, N. J. & Haase, K. M. (2014)  
1395 Lithium and boron isotope systematics in lavas from the Azores islands reveal crustal assimilation. *Chem*  
1396 *Geol* **373**: 27–36
- 1397 Goldstein, S. J., Perfit, M. R., Batiza, R., Fornari, D. J. & Murrell, M. T. (1994) Off-axis volcanism at the  
1398 East Pacific Rise detected by uranium-series dating of basalts. *Nature* **367**: 157–159
- 1399 Gonfiantini, R., Tonarini, S., Gröning, M., Adorni-Braccesi, A., Al-Ammar, A. S., Astner, M., Bächler,  
1400 S., Barnes, R. M., Basset, R. L., Cocherie, A., Deyhle, A., Dini, A., Ferrara, G., Gaillardet, J., Grimm,  
1401 J., Guerrot, C., Krähenbühl, U., Layne, G., Lemarchand, D., Meixner, A., Northington, D. J., Pennisi,  
1402 M., Reitznerová, E., Rodushkin, I., Sugiura, N., Surberg, R., Tonn, S., Wiedenbeck, M., Wunderli, S.,  
1403 Xiao, Y. & Zack, T. (2003) Intercomparison of boron isotope and concentration measurements. Part II:  
1404 evaluation of results. *Geostand News* **27**: 41–57
- 1405 Goss, A. R., Perfit, M. R., Ridley, W. I., Rubin, K. H., Kamenov, G. D., Soule, S. A., Fundis, A. & Fornari,  
1406 D. J. (2010) Geochemistry of lavas from the 2005–2006 eruption at the East Pacific Rise, 9°46' N–9°56' N:  
1407 implications for ridge crest plumbing and decadal changes in magma chamber compositions. *Geochem*  
1408 *Geophys Geosys* **11**: Q05T09
- 1409 Graham, D. W., Castillo, P. R., Lupton, J. E. & Batiza, R. (1996) Correlated He and Sr isotope ratios in  
1410 South Atlantic near-ridge seamounts and implications for mantle dynamics. *Earth Planet Sci Lett* **144**:  
1411 491–50
- 1412 Gurenko, A. A. & Schmincke, H. U. (2002) Orthopyroxene-bearing tholeiites of the Iblean Plateau (Sicily):  
1413 constraints on magma origin and evolution from glass inclusions in olivine and orthopyroxene. *Chem*  
1414 *Geol* **183**: 305–331
- 1415 Hahm, D., Castillo, P. R. & Hilton, D. R. (2009) A deep mantle source for high <sup>3</sup>He/<sup>4</sup>He ocean island  
1416 basalts (OIB) inferred from Pacific near-ridge seamount lavas. *Geophys Res Lett* **36**: L20 316
- 1417 Halama, R., McDonough, W. F., Rudnick, R. L. & Bell, K. (2008) Tracking the lithium isotopic evolution  
1418 of the mantle using carbonatites. *Earth Planet Sci Lett* **265**: 726–742
- 1419 Hart, S. R. (1984) A large-scale isotope anomaly in the Southern Hemisphere mantle. *Nature* **309**: 753–757
- 1420 Hauri, E., Wang, J., Dixon, J., King, P., Mandeville, C. & Newman, S. (2002) SIMS analysis of volatiles in  
1421 silicate glasses: 1. Calibration, matrix effects and comparisons with FTIR. *Chem Geol* **183**: 99–114
- 1422 Hay, W. W., Sloan, J. L. & Wold, C. N. (1988) Mass/age distribution and composition of sediments on the  
1423 ocean floor and the global rate of sediment subduction. *J Geophys Res* **93**: 14 933–14 940

- Hémond, C., Hofmann, A. W., Vlastélic, I. & Nauret, F. (2006) Origin of MORB enrichment and relative trace element compatibilities along the Mid-Atlantic Ridge between 10° and 24°N. *Geochem Geophys Geosys* **7**: Q12 010
- Higgins, M. D. & Shaw, D. M. (1984) Boron cosmochemistry interpreted from abundances in mantle xenoliths. *Nature* **308**: 172–173
- Hofmann, A. W. (1988) Chemical differentiation of the Earth: the relationship between mantle, continental crust, and oceanic crust. *Earth Planet Sci Lett* **90**: 297–314
- Hofmann, A. W. (1997) Mantle geochemistry: the message from oceanic volcanism. *Nature* **385**: 219–229
- Huang, Y., Chubakov, V., Mantovani, F., Rudnick, R. L. & McDonough, W. F. (2013) A reference Earth model for the heat producing elements and associated geoneutrino flux. *Geochem Geophys Geosys* **14**: 2003–2029
- Huh, Y., Chan, L. H. & Edmond, J. M. (2001) Lithium isotopes as a probe of weathering processes: Orinoco River. *Earth Planet Sci Lett* **194**: 189–199
- Ionov, D. A. & Seitz, H. M. (2008) Lithium abundances and isotopic compositions in mantle xenoliths from subduction and intra-plate settings: mantle sources vs. eruption histories. *Earth Planet Sci Lett* **266**: 316–331
- Ishikawa, T. & Nakamura, E. (1992) Boron isotope geochemistry of the oceanic crust from DSDP/ODP Hole 504B. *Geochim Cosmochim Acta* **56**: 1633–1639
- Ishikawa, T. & Nakamura, E. (1994) Origin of the slab component in arc lavas from across-arc variation of B and Pb isotopes. *Nature* **370**: 205–208
- Iwamori, H., Albarède, F. & Nakamura, H. (2010) Global structure of mantle isotopic heterogeneity and its implications for mantle differentiation and convection. *Earth Planet Sci Lett* **299**: 339–351
- Jagoutz, E., Palme, H., Baddenhausen, H., Blum, K., Cendales, M., Dreibus, G., Spettel, B., Lorenz, V. & Wänke, H. (1979) The abundances of major, minor and trace elements in the Earth's mantle as derived from primitive ultramafic nodules. *Proc 10<sup>th</sup> Lunar Planet Sci Conf* 2031–2050
- James, R. H. & Palmer, M. R. (2000) The lithium isotope composition of international rock standards. *Chem Geol* **166**: 319–326
- Jeffcoate, A. B., Elliott, T., Thomas, A. & Bouman, C. (2004) Precise, small sample size determinations of lithium isotopic compositions of geological reference materials and modern seawater by MC-ICP-MS. *Geostand Geoanal Res* **28**: 161–172
- Jeffcoate, A. B., Elliott, T., Kasemann, S. A., Ionov, D., Cooper, K. & Brooker, R. (2007) Li isotope fractionation in peridotites and mafic melts. *Geochim Cosmochim Acta* **71**: 202–218
- Jestin, F., Huchon, P. & Gaulier, J. M. (1994) The Somalia plate and the East African Rift System: present-day kinematics. *Geophys J Intern* **116**: 637–654
- Jochum, K. P., Hofmann, A. W., Ito, E., Seufert, H. M., & White, W. M. (1983) K, U and Th in mid-ocean ridge basalt glasses and heat production, K/U and K/Rb in the mantle. *Nature* **306**: 431–436
- Jochum, K. P., Dingwell, D. B., Rocholl, A., Stoll, B., Hofmann, A., Becker, S., Bessette, D., Dietze, H. J., Dulski, P., Erzinger, J., Hellebrand, E., Hoppe, P., Horn, I., Janssens, K., Jenner, G. A., Klein, M., McDonough, W. F., Maetz, M., Mezger, K., Münker, C., Nikogosian, I. K., Pickhardt, C., Raczek, I., Rhede,

- 1463 D., Seufert, H. M., Simakin, S. G., Sobolev, A. V., Spettel, B., Straub, S., Vincze, L., Wallianos, A.,  
1464 Weckwerth, G., Weyer, S., Wolf, D. & Zimmer, M. (2000) The preparation and preliminary character-  
1465 isation of eight geological MPI-DING reference glasses for in-situ microanalysis. *Geostand Newsl* **24**:  
1466 87–133
- 1467 Jochum, K. P., Stoll, B., Herwig, K., Willbold, M., Hofmann, A., Amini, M., Aarburg, S., Abouchami, W.,  
1468 Hellebrand, E., Mocek, B., Raczek, I., Stracke, A., Alard, O., Bouman, C., Becker, S., Dücking, M.,  
1469 Brätz, H., Klemm, R., de Bruin, D., Canil, D., Cornell, D., de Hoog, C. J., Dalpé, C., Danyushevsky, L. V.,  
1470 Eisenhauer, A., Gao, Y., Snow, J. E., Groschopf, N., Günther, D., Latkoczy, C., Giullong, M., Hauri,  
1471 E. H., Höfer, H. E., Lahaye, Y., Horz, K., Jacob, D. E., Kasemann, S. A., Kent, A. J. R., Ludwig, T., Zack,  
1472 T., Mason, P. R. D., Meixner, A., Rosner, M., Misawa, K., Nash, B. P., Pfänder, J. A., Premo, W. R.,  
1473 Sun, W. D., Tiepolo, M., Vannucci, R., Vennemann, T., Wayne, D. & Woodhead, J. D. (2006) MPI-DING  
1474 reference glasses for in situ microanalysis: New reference values for element concentrations and isotope  
1475 ratios. *Geochem Geophys Geosys* **7**: Q02 008, doi:10.1029/2005GC001 060
- 1476 Kaliwoda, M., Ludwig, T. & Altherr, R. (2008) A new SIMS study of Li, Be, B and  $\delta^7\text{Li}$  in mantle xenoliths  
1477 from Harrat Uwayrid (Saudi Arabia). *Lithos* **106**: 261–279
- 1478 Kamenetsky, V. S. & Eggins, S. M. (2012) Systematics of metals, metalloids, and volatiles in MORB melts:  
1479 effects of partial melting, crystal fractionation and degassing (a case study of Macquarie Island glasses).  
1480 *Chem Geol* **302-303**: 76–86
- 1481 Kasemann, S., Erzinger, J. & Franz, G. (2000) Boron recycling in the continental crust of the central Andes  
1482 from the Paleozoic to Mesozoic, NW Argentina. *Contrib Mineral Petrol* **140**: 328–343
- 1483 Kendrick, M. A., Arculus, R. J., Burnard, P. & Honda, M. (2013) Quantifying brine assimilation by subma-  
1484 rine magmas: examples from the Galápagos Spreading Centre and Lau Basin. *Geochim Cosmochim Acta*  
1485 **123**: 150–165
- 1486 Key, K., Constable, S., Liu, L. & Pommier, A. (2013) Electrical image of passive mantle upwelling beneath  
1487 the northern East Pacific Rise. *Nature* **495**: 499–502
- 1488 Kobayashi, K., Tanaka, R., Moriguti, T., Shimizu, K. & Nakamura, E. (2004) Lithium, boron, and lead  
1489 isotope systematics of glass inclusions in olivines from Hawaiian lavas: evidence for recycled components  
1490 in the Hawaiian plume. *Chem Geol* **212**: 143–161
- 1491 Krienitz, M. S., Garbe-Schönberg, C. D., Romer, R. L., Meixner, A., Haase, K. M. & Stroncik, N. A.  
1492 (2012) Lithium isotope variations in ocean island basalts – implications for the development of mantle  
1493 heterogeneities. *J Petrol* **53**: 2333–2347
- 1494 Lai, Y. J., Pogge von Strandmann, P. A. E., Dohmen, R., Takazawa, E. & Elliott, T. (2015) The influence  
1495 of melt infiltration on the Li and Mg isotopic composition of the Horoman Peridotite Massif. *Geochim*  
1496 *Cosmochim Acta* **164**: 318–332
- 1497 Leeman, W. P. & Sisson, V. B. (1996) Geochemistry of boron and its implications for crustal and mantle  
1498 processes. In: Grew, E. S. & Anovitz, L. M. (eds.) *Boron: mineralogy, petrology and geochemistry*,  
1499 vol. 33 of *Rev. Mineral.*, 645–695, Mineral. Soc. Am.
- 1500 Lemarchand, D., Gaillardet, J., Lewin, É. & Allègre, C. J. (2000) The influence of rivers on marine boron  
1501 isotopes and implications for reconstructing past ocean pH. *Nature* **408**: 951–954
- 1502 Lemarchand, D., Gaillardet, J., Lewin, É. & Allègre, C. J. (2002) Boron isotope systematics in large rivers:  
1503 implications for the marine boron budget and paleo-pH reconstruction over the Cenozoic. *Chem Geol*  
1504 **190**: 123–140

- 1505 Lissenberg, C. J., MacLeod, C. J., Howard, K. A. & Godard, M. (2013) Pervasive reactive melt migration  
1506 through fast-spreading lower oceanic crust (Hess Deep, equatorial Pacific Ocean). *Earth Planet Sci Lett*  
1507 **361**: 436–447
- 1508 Liu, X. M., Rudnick, R. L., McDonough, W. F. & Cummings, M. (2013) Influence of chemical weathering  
1509 on the composition of the continental crust: insights from Li and Nd isotopes in bauxite profiles developed  
1510 on Columbia River Basalts. *Geochim Cosmochim Acta* **115**: 73–91
- 1511 Liu, X. M., Wanner, C., Rudnick, R. L. & McDonough, W. F. (2015) Processes controlling  $\delta^7\text{Li}$  in rivers  
1512 illuminated by a study of streams and ground waters draining basalts. *Earth Planet Sci Lett* **409**: 212–224
- 1513 Lodders, K. (2003) Solar system abundances and condensation temperatures of the elements. *Astrophys J*  
1514 **591**: 1220–1247
- 1515 Lundstrom, C. C., Sampson, D. E., Perfit, M. R., Gill, J. & Williams, Q. (1999) Insights into mid-ocean  
1516 ridge basalt petrogenesis: U-series disequilibria from the Siqueiros Transform, Lamont Seamounts, and  
1517 East Pacific Rise. *J Geophys Res (B)* **104**: 13 035–13 048
- 1518 Lundstrom, C. C., Chaussidon, M., Hsui, A. T., Kelemen, P. & Zimmerman, M. (2005) Observations of Li  
1519 variations in the Trinity Ophiolite: evidence for isotopic fractionation by diffusion during mantle melting.  
1520 *Geochim Cosmochim Acta* **69**: 735–751
- 1521 Lyubetskaya, T. & Korenaga, J. (2007) Chemical composition of Earth’s primitive mantle and its variance:  
1522 1. Method and results. *J Geophys Res* **112**: B03 211
- 1523 Magna, T., Ionov, D. A., Oberli, F. & Wiechert, U. (2008) Links between mantle metasomatism and lithium  
1524 isotopes: evidence from glass-bearing and cryptically metasomatized xenoliths from Mongolia. *Earth*  
1525 *Planet Sci Lett* **276**: 214–222
- 1526 Magna, T., Janoušek, V., Kohút, M., Oberli, F. & Wiechert, U. (2010) Fingerprinting sources of orogenic  
1527 plutonic rocks from Variscan belt with lithium isotopes and possible link to subduction-related origin of  
1528 some A-type granites. *Chem Geol* **274**: 94–107
- 1529 Marschall, H. R. & Ludwig, T. (2004) The Low-Boron contest: minimising surface contamination and  
1530 analysing boron concentrations at the ng/g-level by secondary ion mass spectrometry. *Mineral Petrol* **81**:  
1531 265–278
- 1532 Marschall, H. R. & Ludwig, T. (2006) Re-examination of the boron isotopic composition of tourmaline  
1533 from the Lavicky granite, Czech Republic, by secondary ion mass spectrometry: back to normal. Critical  
1534 comment on “Chemical and boron isotopic composition of tourmaline from the Lavicky leucogranite,  
1535 Czech Republic” by S.-Y. Jiang et al., *Geochemical Journal*, 37, 545-556, 2003. *Geochem J* **40**: 631–638
- 1536 Marschall, H. R. & Monteleone, B. D. (2015) Boron isotope analysis of silicate glass with very-low boron  
1537 concentrations by secondary-ion mass spectrometry. *Geostand Geoanal Res* **39**: 31–46
- 1538 Marschall, H. R., Altherr, R., Ludwig, T., Kalt, A., Gméling, K. & Kasztovszky, Z. (2006) Partitioning and  
1539 budget of Li, Be and B in high-pressure metamorphic rocks. *Geochim Cosmochim Acta* **70**: 4750–4769
- 1540 Marschall, H. R., Altherr, R. & Rüpke, L. (2007a) Squeezing out the slab – modelling the release of Li, Be  
1541 and B during progressive high-pressure metamorphism. *Chem Geol* **239**: 323–335
- 1542 Marschall, H. R., Pogge von Strandmann, P. A. E., Seitz, H. M., Elliott, T. & Niu, Y. (2007b) The lithium  
1543 isotopic composition of orogenic eclogites and deep subducted slabs. *Earth Planet Sci Lett* **262**: 563–580

- McDade, P., Blundy, J. D. & Wood, B. J. (2003) Trace element partitioning between mantle wedge peridotite and hydrous MgO-rich melt. *Am Mineral* **88**: 1825–1831
- McDonough, W. F. & Sun, S. S. (1995) The composition of the Earth. *Chem Geol* **120**: 223–253
- Menard, G., Vlastélic, I., Ionov, D. A., Rose-Koga, E. F., Piro, J. L. & Pin, C. (2013) Precise and accurate determination of boron concentration in silicate rocks by direct isotope dilution ICP-MS: insights into the B budget of the mantle and B behavior in magmatic systems. *Chem Geol* **354**: 139–149
- Mertz, D. F., Devey, C. W., Todt, W., Stoffers, P. & Hofmann, A. W. (1991) Sr-Nd-Pb isotope evidence against plume-asthenosphere mixing north of Iceland. *Earth Planet Sci Lett* **107**: 243–255
- Michael, P. J. & Cornell, W. C. (1998) Influence of spreading rate and magma supply on crystallization and assimilation beneath mid-ocean ridges: evidence from chlorine and major element chemistry of mid-ocean ridge basalts. *J Geophys Res* **103**: 18 325–18 356
- Michael, P. J. & Schilling, J. (1989) Chlorine in mid-ocean ridge magmas: evidence for assimilation of seawater-influenced components. *Geochim Cosmochim Acta* **53**: 3131–3143
- Moran, A. E., Sisson, V. B. & Leeman, W. P. (1992) Boron depletion during progressive metamorphism: implications for subduction processes. *Earth Planet Sci Lett* **111**: 331–349
- Moriguti, T. & Nakamura, E. (1998) Across-arc variation of Li-isotopes in lavas and implications for crust/mantle recycling at subduction zones. *Earth Planet Sci Lett* **163**: 167–174
- Nishio, Y., Nakai, S., Yamamoto, J., Sumino, H., Matsumoto, T., Prikhod'ko, V. S. & Arai, S. (2004) Lithium isotopic systematics of the mantle-derived ultramafic xenoliths: implications for EM1 origin. *Earth Planet Sci Lett* **217**: 245–261
- Nishio, Y., Nakai, S., Kogiso, T. & Barszczus, H. G. (2005) Lithium, strontium, and neodymium isotopic compositions of oceanic island basalts in the Polynesian region: constraints on a Polynesian HIMU origin. *Geochem J* **39**: 91–103
- Nishio, Y., Nakai, S., Ishii, T. & Sano, Y. (2007) Isotopic systematics of Li, Sr, Nd, and volatiles in Indian Ocean MORBs of the Rodrigues Triple Junction: constraints on the origin of the DUPAL anomaly. *Geochim Cosmochim Acta* **71**: 745–759
- Niu, Y. & Batiza, R. (1994) Magmatic processes at a slow spreading ridge segment: 26°S Mid-Atlantic Ridge. *J Geophys Res* **B 99**: 19 719–19 740
- Niu, Y. & Batiza, R. (1997) Trace element evidence from seamounts for recycled oceanic crust in the Eastern Pacific mantle. *Earth Planet Sci Lett* **148**: 471–483
- Niu, Y., Collerson, K. D., Batiza, R., Wendt, J. I. & Regelous, M. (1999) Origin of enriched-type mid-ocean ridge basalt at ridges far from mantle plumes: the East Pacific Rise at 11°20'N. *J Geophys Res* **B 104**: 7067–7087
- O'Neill, H. S. C. & Jenner, F. E. (2012) The global pattern of trace-element distributions in ocean floor basalts. *Nature* **491**: 698–704
- Ottolini, L., Le Fèvre, B. & Vannucci, R. (2004) Direct assessment of mantle boron and lithium contents and distribution by SIMS analyses of peridotite minerals. *Earth Planet Sci Lett* **228**: 19–36
- Ottolini, L., Laporte, D., Raffone, N., Devidal, J. L. & Le Fèvre, B. (2009) New experimental determination of Li and B partition coefficients during upper mantle partial melting. *Contrib Mineral Petrol* **157**: 313–325

- 1584 Palme, H. (1988) Chemical abundances in meteorites. In: Klare, G. (ed.) *Cosmic Chemistry*, vol. 1 of *Rev.*  
1585 *Modern Astron.*, 28–51, Springer, Berlin
- 1586 Palme, H. & Jones, A. (2003) Solar system abundances of the elements. In: Davis, A. M. (ed.) *Meteorites,*  
1587 *Comets and Planets*, vol. 1 of *Treat. Geochem.*, chap. 3, 41–61, Elsevier
- 1588 Palme, H. & O'Neill, H. S. C. (2003) Cosmochemical estimates of mantle composition. In: Carlson, R. W.  
1589 (ed.) *The Mantle and the Core*, vol. 2 of *Treat. Geochem.*, chap. 1, 1–38, Elsevier
- 1590 Pan, Y. & Batiza, R. (2003) Magmatic processes under mid-ocean ridges: a detailed mineralogic study of  
1591 lavas from East Pacific Rise 9°30'N, 10°30'N, and 11°20'N. *Geochem Geophys Geosys* **4**: 8623
- 1592 Paquin, J., Altherr, R. & Ludwig, T. (2004) Li-Be-B systematics in the ultrahigh-pressure garnet peridotite  
1593 from Alpe Arami (Central Swiss Alps): implications for slab-to-mantle transfer. *Earth Planet Sci Lett*  
1594 **218**: 507–519
- 1595 Parkinson, I. J., Hammond, S. J., James, R. H. & Rogers, N. W. (2007) High-temperature lithium isotope  
1596 fractionation: Insights from lithium isotope diffusion in magmatic systems. *Earth Planet Sci Lett* **257**:  
1597 609–621
- 1598 Peacock, S. M. (1990) Fluid processes in subduction zones. *Science* **248**: 329–337
- 1599 Peacock, S. M. & Hervig, R. L. (1999) Boron isotopic composition of subduction-zone metamorphic rocks.  
1600 *Chem Geol* **160**: 281–290
- 1601 Pearce, N. J. G., Perkins, W. T., Westgate, J. A., Gorton, M. P., Jackson, S. E., Neal, C. R. & Chenery, S. P.  
1602 (1997) A compilation of new and published major and trace element data for NIST SRM 610 and NIST  
1603 SRM 612 glass reference materials. *Geostand Newsl* **21**: 115–144
- 1604 Perfit, M. R., Fornari, D. J., Ridley, W. I., Kirk, P. D., Casey, J., Kastens, K. A., Reynolds, J. R., Edwards,  
1605 M., Desonie, D., Shuster, R. & Paradis, S. (1996) Recent volcanism in the Siqueiros transform fault:  
1606 picritic basalts and implications for MORB magma genesis. *Earth Planet Sci Lett* **141**: 91–108
- 1607 Regelous, M., Niu, Y., Wendt, J. I., Batiza, R., Greig, A. & Collerson, K. D. (1999) Variations in the  
1608 geochemistry of magmatism on the East Pacific Rise at 10°30' N since 800ka. *Earth Planet Sci Lett* **168**:  
1609 45–63
- 1610 Regelous, M., Niu, Y., Abouchami, W. & Castillo, P. R. (2009) Shallow origin for South Atlantic Dupal  
1611 Anomaly from lower continental crust: geochemical evidence from the Mid-Atlantic Ridge at 26°S.  
1612 *Lithos* **112**: 57–72
- 1613 Richter, F. M., Davis, A. M., DePaolo, D. J. & Watson, E. B. (2003) Isotope fractionation by chemical  
1614 diffusion between molten basalt and rhyolite. *Geochim Cosmochim Acta* **67**: 3905–3923
- 1615 Robinson, C. J. (1998) *Mantle melting and crustal generation at the very slow spreading Southwest Indian*  
1616 *Ridge*. Ph.D. thesis, Univ. Cambridge
- 1617 Robinson, C. J., White, R. S., Bickle, M. J. & Minshull, T. A. (1996) Restricted melting under the very  
1618 slow-spreading Southwest Indian ridge. In: MacLeod, C. J., Tyler, P. A. & Walker, C. L. (eds.) *Tectonic,*  
1619 *Magmatic, Hydrothermal and Biological Segmentation of Mid-Ocean Ridges*, vol. 118 of *Spec. Publ.*,  
1620 131–141, Geol. Soc. London
- 1621 Robinson, C. J., Bickle, M. J., Minshull, T. A., White, R. S. & Nichols, A. R. L. (2001) Low degree melting  
1622 under the Southwest Indian Ridge: the roles of mantle temperature, conductive cooling and wet melting.  
1623 *Earth Planet Sci Lett* **188**: 383–398

- 1624 Rosner, M., Erzinger, J., Franz, G. & Trumbull, R. B. (2003) Slab-derived boron isotope signatures in arc  
1625 volcanic rocks from the Central Andes and evidence for boron isotope fractionation during progressive  
1626 slab dehydration. *Geochem Geophys Geosys* **4**: DOI:10.1029/2002GC000438
- 1627 Rosner, M., Ball, L., Peucker-Ehrenbrink, B., Busztajn, J., Bach, W. & Erzinger, J. (2007) A simplified,  
1628 accurate and fast method for lithium isotope analysis of rocks and fluids, and  $\delta^7\text{Li}$  values of seawater and  
1629 rock reference materials. *Geostand Geoanal Res* **31**: 77–88
- 1630 le Roux, P. J., Shirey, S. B., Benton, L., Hauri, E. H. & Mock, T. D. (2004) In situ, multiple-multiplier, laser  
1631 ablation ICP-MS measurement of boron isotopic composition ( $\delta^{11}\text{B}$ ) at the nanogram level. *Chem Geol*  
1632 **203**: 123–138
- 1633 le Roux, P. J., Shirey, S. B., Hauri, E. H., Perfit, M. R. & Bender, J. F. (2006) The effects of variable sources,  
1634 processes and contaminants on the composition of northern EPR MORB (8 – 10°N and 12 – 14°N):  
1635 evidence from volatiles ( $\text{H}_2\text{O}$ ,  $\text{CO}_2$ , S) and halogens (F, Cl). *Earth Planet Sci Lett* **251**: 209–231
- 1636 Roy-Barman, M., Wasserburg, G. J., Papanastassiou, D. A. & Chaussidon, M. (1998) Osmium isotopic  
1637 compositions and Re–Os concentrations in sulfide globules from basaltic glasses. *Earth Planet Sci Lett*  
1638 **154**: 331–347
- 1639 Rubin, K. H., Macdougall, J. D. & Perfit, M. R. (1994)  $^{210}\text{Po}$  –  $^{210}\text{Pb}$  dating of recent volcanic eruptions on  
1640 the sea floor. *Nature* **368**: 841–844
- 1641 Rudnick, R. L. & Gao, S. (2003) Composition of the continental crust. In: Rudnick, R. L. (ed.) *The Crust*,  
1642 vol. 3 of *Treat. Geochem.*, chap. 3, 1–64, Elsevier
- 1643 Rudnick, R. L. & Ionov, D. A. (2007) Lithium elemental and isotopic disequilibrium in minerals from  
1644 peridotite xenoliths from far-east Russia: product of recent melt/fluid-rock reaction. *Earth Planet Sci Lett*  
1645 **256**: 278–293
- 1646 Rudnick, R. L., Tomascak, P. B., Njo, H. B. & Gardner, R. L. (2004) Extreme isotopic fractionation during  
1647 continental weathering revealed in saprolites from South Carolina. *Chem Geol* **212**: 45–58
- 1648 Ryan, J. G. (2002) Trace-element systematics of beryllium in terrestrial materials. In: Grew, E. S. (ed.)  
1649 *Beryllium: Mineralogy, Petrology and Geochemistry*, vol. 50 of *Rev. Mineral.*, 121–145, Mineral. Soc.  
1650 Am.
- 1651 Ryan, J. G. & Chauvel, C. (2014) The subduction-zone filter and the impact of recycled materials on the  
1652 evolution of the mantle. In: Turekian, K. K. (ed.) *The Mantle and Core*, vol. 3 of *Treat. Geochem.*, chap.  
1653 3.13, 479–508, Elsevier, 2<sup>nd</sup> edn.
- 1654 Ryan, J. G. & Kyle, P. R. (2004) Lithium abundance and lithium isotope variations in mantle sources:  
1655 insights from intraplate volcanic rocks from Ross Island and Marie Byrd Land (Antarctica) and other  
1656 oceanic islands. *Chem Geol* **212**: 125–142
- 1657 Ryan, J. G. & Langmuir, C. H. (1987) The systematics of lithium abundances in young volcanic rocks.  
1658 *Geochim Cosmochim Acta* **51**: 1727–1741
- 1659 Ryan, J. G. & Langmuir, C. H. (1988) Be systematics in young volcanic rocks: implications for  $^{10}\text{Be}$ .  
1660 *Geochim Cosmochim Acta* **52**: 237–244
- 1661 Ryan, J. G. & Langmuir, C. H. (1993) The systematics of boron abundances in young volcanic rocks.  
1662 *Geochim Cosmochim Acta* **57**: 1489–1498

- 1663 Saal, A. E., Hauri, E. H., Langmuir, C. H. & Perfit, M. R. (2002) Vapour undersaturation in primitive  
1664 mid-ocean-ridge basalt and the volatile content of Earth's upper mantle. *Nature* **419**: 451–455
- 1665 Salters, V. J. M. (1996) The generation of mid-ocean ridge basalts from the Hf and Nd isotope perspective.  
1666 *Earth Planet Sci Lett* **141**: 109–123
- 1667 Salters, V. J. M. & Stracke, A. (2004) Composition of the depleted mantle. *Geochem Geophys Geosys* **5**:  
1668 10.1029/2003GC000 597
- 1669 Sauzéat, L., Rudnick, R. L., Chauvel, C., Garçon, M. & Tang, M. (2015) New perspectives on the Li isotopic  
1670 composition of the upper continental crust and its weathering signature. *Earth Planet Sci Lett* **428**: 181–  
1671 192
- 1672 Savov, I. P., Ryan, J. G., D'Antonio, M. & Kelley, K. (2005) Geochemistry of serpentized peridotites  
1673 from the Mariana Forearc Conical Seamount, ODP Leg 125: implications for the elemental recycling at  
1674 subduction zones. *Geochem Geophys Geosys* **6**: Q04J15
- 1675 Seitz, H. M., Brey, G. P., Stachel, T. & Harris, J. W. (2003) Li abundances in inclusions in diamonds from  
1676 the upper and lower mantle. *Chem Geol* **201**: 307–318
- 1677 Seitz, H. M., Brey, G. P., Lahaye, Y., Durali, S. & Weyer, S. (2004) Lithium isotopic signatures of peridotite  
1678 xenoliths and isotopic fractionation at high temperature between olivine and pyroxenes. *Chem Geol* **212**:  
1679 163–177
- 1680 Seitz, H. M., Brey, G. P., Zipfel, J., Ott, U., Weyer, S., Durali, S. & Weinbruch, S. (2007) Lithium isotope  
1681 composition of ordinary and carbonaceous chondrites, and differentiated planetary bodies: bulk solar  
1682 system and solar reservoirs. *Earth Planet Sci Lett* **260**: 582–596
- 1683 Shaw, A. M., Behn, M. D., Humphris, S. E., Sohn, R. & Gregg, P. (2010) Deep pooling of low degree melts  
1684 and volatile fluxes at the 85°E segment of the Gakkel Ridge: evidence from olivine-hosted melt inclusions  
1685 and glasses. *Earth Planet Sci Lett* **289**: 311–322
- 1686 Sims, K. W. W., Goldstein, S. J., Blichert-Toft, J., Perfit, M. R., Keleman, P. B., Fornari, D. J., Michael, P. J.,  
1687 Murrell, M. T., Hart, S. R., DePaolo, D. J., Layne, G., Ball, L., Jull, M. & Bender, J. (2002) Chemical  
1688 and isotopic constraints on the generation and transport of magma beneath the East Pacific Rise. *Geochim*  
1689 *Cosmochim Acta* **66**: 3481–3504
- 1690 Sims, K. W. W., Blichert-Toft, J., Fornari, D. J., Perfit, M. R., Goldstein, S. J., Johnson, P., DePaolo, D. J.,  
1691 Hart, S. R., Murrell, M. T., Michael, P. J., Layne, G. D. & Ball, L. (2003) Aberrant youth: chemical  
1692 and isotopic constraints on the origin of off-axis lavas from the East Pacific Rise, 9 – 10°N. *Geochem*  
1693 *Geophys Geosys* **4**: 8621
- 1694 Smith, H. J., Spivack, A. J., Staudigel, H. & Hart, S. R. (1995) The boron isotopic composition of altered  
1695 oceanic crust. *Chem Geol* **126**: 119–135
- 1696 Smith, M. C., Perfit, M. R., Fornari, D. J., Ridley, W. I., Edwards, M. H., Kurras, G. J. & Von Damm,  
1697 K. L. (2001) Magmatic processes and segmentation at a fast spreading mid-ocean ridge: detailed inves-  
1698 tigation of an axial discontinuity on the East Pacific Rise crest at 9°37'N. *Geochem Geophys Geosys* **2**:  
1699 2000GC000 134
- 1700 Soule, S. A., Fornari, D. J., Perfit, M. R. & Rubin, K. H. (2007) New insights into mid-ocean ridge volcanic  
1701 processes from the 2005–2006 eruption of the East Pacific Rise, 9°46'N–9°56'N. *Geology* **35**: 1079–  
1702 1082.



- 1703 Sours-Page, R. L., Nielsen, R. L. & Batiza, R. (2002) Melt inclusions as indicators of parental magma  
1704 diversity on the northern East Pacific Rise. *Chem Geol* **183**: 237–261
- 1705 Spivack, A. J. & Edmond, J. M. (1987) Boron isotope exchange between seawater and the oceanic crust.  
1706 *Geochim Cosmochim Acta* **51**: 1033–1043
- 1707 Pogge von Strandmann, P. A. E., Burton, K. W., James, R. H., van Calsteren, P., Gíslason, S. R. & Mokadem,  
1708 F. (2006) Riverine behaviour of uranium and lithium isotopes in an actively glaciated basaltic terrain.  
1709 *Earth Planet Sci Lett* **251**: 134–147
- 1710 Pogge von Strandmann, P. A. E., Elliott, T., Marschall, H. R., Coath, C., Lai, Y. J., Jeffcoate, A. & Ionov,  
1711 D. A. (2011) Variations of Li and Mg isotope ratios in bulk chondrites and mantle xenoliths. *Geochim  
1712 Cosmochim Acta* **75**: 5247–5258
- 1713 Pogge von Strandmann, P. A. E., Opfergelt, S., Lai, Y. J., Sigfússon, B., Gíslason, S. R. & Burton, K. W.  
1714 (2012) Lithium, magnesium and silicon isotope behaviour accompanying weathering in a basaltic soil  
1715 and pore water profile in Iceland. *Earth Planet Sci Lett* **339–340**: 11–23
- 1716 Tang, Y. J., Zhang, H. F., Nakamura, E., Moriguti, T., Kobayashi, K. & Ying, J. F. (2007) Lithium iso-  
1717 topic systematics of peridotite xenoliths from Hannuoba, North China Craton: implications for melt-rock  
1718 interaction in the considerably thinned lithospheric mantle. *Geochim Cosmochim Acta* **71**: 4327–4341
- 1719 Taylor, S. R. & McLennan, S. M. (1995) The geochemical evolution of the continental crust. *Rev Geophys*  
1720 **33**: 241–265
- 1721 Taylor, S. R. & McLennan, S. M. (2009) *Planetary crusts - their composition, origin and evolution*. Cam-  
1722 bridge University Press
- 1723 Teng, F. Z., McDonough, W. F., Rudnick, R. L., Dalpé, C., Tomascak, P. B., Chappell, B. W. & Gao, S.  
1724 (2004) Lithium isotopic composition and concentration of the upper continental crust. *Geochim Cos-  
1725 mochim Acta* **68**: 4167–4178
- 1726 Teng, F. Z., McDonough, W. F., Rudnick, R. L. & Walker, R. J. (2006) Diffusion-driven extreme lithium  
1727 isotopic fractionation in country rocks of the Tin Mountain pegmatite. *Earth Planet Sci Lett* **243**: 701–710
- 1728 Teng, F. Z., Rudnick, R. L., McDonough, W. F., Gao, S., Tomascak, P. B. & Liu, Y. (2008) Lithium isotopic  
1729 composition and concentration of the deep continental crust. *Chem Geol* **255**: 47–59
- 1730 Teng, F. Z., Rudnick, R. L., McDonough, W. F. & Wu, F. Y. (2009) Lithium isotopic systematics of A-type  
1731 granites and their mafic enclaves: further constraints on the Li isotopic composition of the continental  
1732 crust. *Chem Geol* **262**: 370–379
- 1733 Thompson, G., Bryan, W. B. & Humphris, S. E. (1989) Axial volcanism on the East Pacific Rise, 10 – 12°N.  
1734 In: Saunders, A. D. & Norry, M. J. (eds.) *Magmatism in the ocean basins*, vol. 42 of *Spec. Publ.*, 181–200,  
1735 Geol. Soc. London
- 1736 Tomascak, P. B. (2004) Developments in the understanding and application of lithium isotopes in the earth  
1737 and planetary sciences. In: Johnson, C. M., Beard, B. L. & Albarède, F. (eds.) *Geochemistry of non-  
1738 traditional stable isotopes*, vol. 55 of *Rev. Mineral.*, chap. 5, 153–195, Mineral. Soc. Am., Washington,  
1739 DC
- 1740 Tomascak, P. B., Langmuir, C. H., le Roux, P. J. & Shirey, S. B. (2008) Lithium isotopes in mid-ocean ridge  
1741 basalts. *Geochim Cosmochim Acta* **72**: 1626–1637

- Tomascak, P. B., Magna, T. & Dohmen, R. (2016a) Li partitioning, diffusion and associated fractionation: theoretical and experimental insights. In: Tomascak, P. B., Magna, T. & Dohmen, R. (eds.) *Advances in Lithium Isotope Geochemistry*, vol. 4 of *Advan. Isotope Geochem.*, 47–118, Springer
- Tomascak, P. B., Magna, T. & Dohmen, R. (2016b) Lithium in the deep Earth: mantle and crustal systems. In: Tomascak, P. B., Magna, T. & Dohmen, R. (eds.) *Advances in Lithium Isotope Geochemistry*, vol. 4 of *Advan. Isotope Geochem.*, 119–156, Springer
- Tonardini, S., Pennisi, M., Adorno-Braccisi, A., Dini, A., Ferrara, G., Gonfiantini, R., Wiedenbeck, M. & Gröning, M. (2003) Intercomparison of boron isotope and concentration measurements. Part I: selection, preparation and homogeneity tests of the intercomparison materials. *Geostand Newsl* **27**: 21–39
- Turner, S., Beier, C., Niu, Y. & Cook, C. (2011) U-Th-Ra disequilibria and the extent of off-axis volcanism across the East Pacific Rise at 9°30' N, 10°30' N, and 11°20' N. *Geochem Geophys Geosys* **12**: Q0AC12
- Vigier, N., Decarreau, A., Millot, R., Carignan, J., Petit, S. & France-Lanord, C. (2008) Quantifying Li isotope fractionation during smectite formation and implications for the Li cycle. *Geochim Cosmochim Acta* **72**: 780–792
- Vigier, N., Gislason, S. R., Burton, K. W., Millot, R. & Mokadem, F. (2009) The relationship between riverine lithium isotope composition and silicate weathering in Iceland. *Earth Planet Sci Lett* **287**: 434–441
- Vils, F., Tonardini, S., Kalt, A. & Seitz, H. M. (2009) Boron, lithium and strontium isotopes as tracers of seawater–serpentinite interaction at Mid-Atlantic ridge, ODP Leg 209. *Earth Planet Sci Lett* **286**: 414–425
- Vlastélic, I., Koga, K., Chauvel, C., Jacques, G. & Télouk, P. (2009) Survival of lithium isotopic heterogeneities in the mantle supported by HIMU-lavas from Rurutu Island, Austral Chain. *Earth Planet Sci Lett* **286**: 456–466
- Von Damm, K. L. (2004) Evolution of the hydrothermal system at East Pacific Rise 9°50' N: geochemical evidence for changes in the upper oceanic crust. In: German, C. R., Lin, J. & Parson, L. M. (eds.) *Mid-Ocean Ridges: Hydrothermal Interactions Between the Lithosphere and Oceans*, vol. 148 of *Geophys. Monogr.*, 285–304, Am. Geophys. Union
- Wagner, C. & Deloule, E. (2007) Behaviour of Li and its isotopes during metasomatism of French Massif Central lherzolites. *Geochim Cosmochim Acta* **71**: 4279–4296
- Wanless, V. D. & Shaw, A. M. (2012) Constraining depths of crystallization and crustal accretion on mid-ocean ridges through volatile analyses in olivine-hosted melt inclusions. *Nature Geosci* **5**: 651–655
- Wasson, J. T. (1985) *Meteorites: Their Record of Early Solar-System History*. W. H. Freeman, New York
- Wasson, J. T. & Kallemeyn, G. W. (1988) Composition of chondrites. *Phil Trans Royal Soc London* **A325**: 535–544
- White, S. M., Haymon, R. M. & Carbotte, S. (2006) A new view of ridge segmentation and near-axis volcanism at the East Pacific Rise, 8° – 12° N, from EM300 multibeam bathymetry. *Geochem Geophys Geosys* **7**: Q12005
- Workman, R. K. & Hart, S. R. (2005) Major and trace element composition of the depleted MORB mantle (DMM). *Earth Planet Sci Lett* **231**: 53–72

- 1781 Wunder, B., Meixner, A., Romer, R. L., Wirth, R. & Heinrich, W. (2005) The geochemical cycle of boron:  
1782 constraints from boron isotope partitioning experiments between mica and fluid. *Lithos* **84**: 206–216
- 1783 Yanagi, T. (2011) *Arc volcano of Japan. Generation of continental crust from the mantle*, vol. 136 of *Lect.*  
1784 *Notes Earth Sci.* Elsevier
- 1785 You, C. F., Chan, L. H., Spivack, A. J. & Gieskes, J. M. (1995) Lithium, boron, and their isotopes in  
1786 sediments and pore waters of Ocean Drilling Program Site 808, Nankai Trough: implications for fluid  
1787 expulsion in accretionary prisms. *Geology* **23**: 37–40
- 1788 Zhai, M. (1995) Boron cosmochemistry: Part 2. Boron nucleosynthesis and condensation temperature. *Me-*  
1789 *teoritics* **30**: 733–737
- 1790 Zhai, M. & Shaw, D. M. (1994) Boron cosmochemistry: Part 1. Boron in meteorites. *Meteoritics* **29**: 607–  
1791 615

## Figures

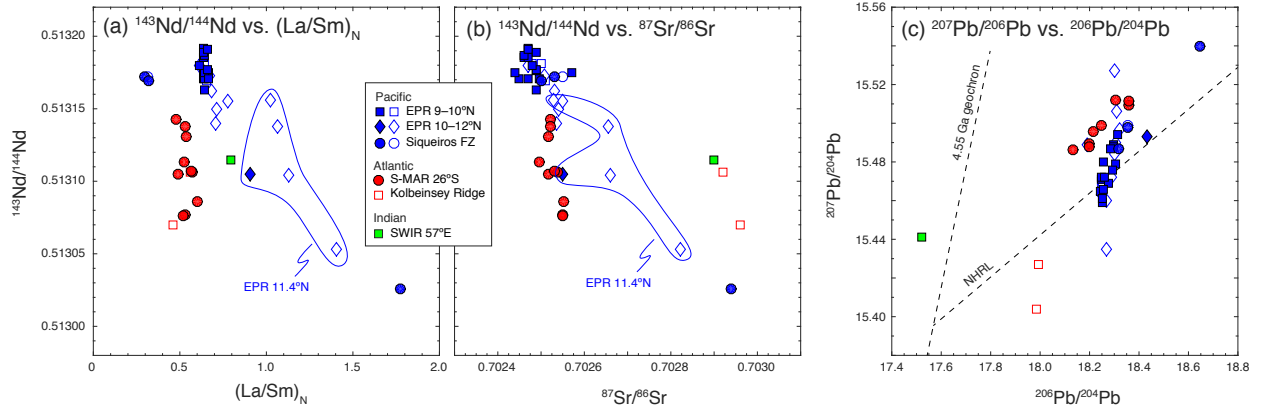


**Fig. 1** Geochemistry of MORB samples from the various ridge sections. Samples with  $\text{Cl}/\text{K} < 0.08$  are shown with filled symbols, and samples with  $\text{Cl}/\text{K} > 0.08$  are shown with open symbols. (a)  $^{143}\text{Nd}/^{144}\text{Nd}$  vs. primitive-mantle normalised  $\text{La}/\text{Sm}$ ; (b)  $^{143}\text{Nd}/^{144}\text{Nd}$  vs.  $^{87}\text{Sr}/^{86}\text{Sr}$ ; (c)  $^{207}\text{Pb}/^{206}\text{Pb}$  vs.  $^{206}\text{Pb}/^{204}\text{Pb}$ . The 4.55 Ga Geochron and the Northern Hemisphere Reference Line (Hart, 1984) are shown for orientation.

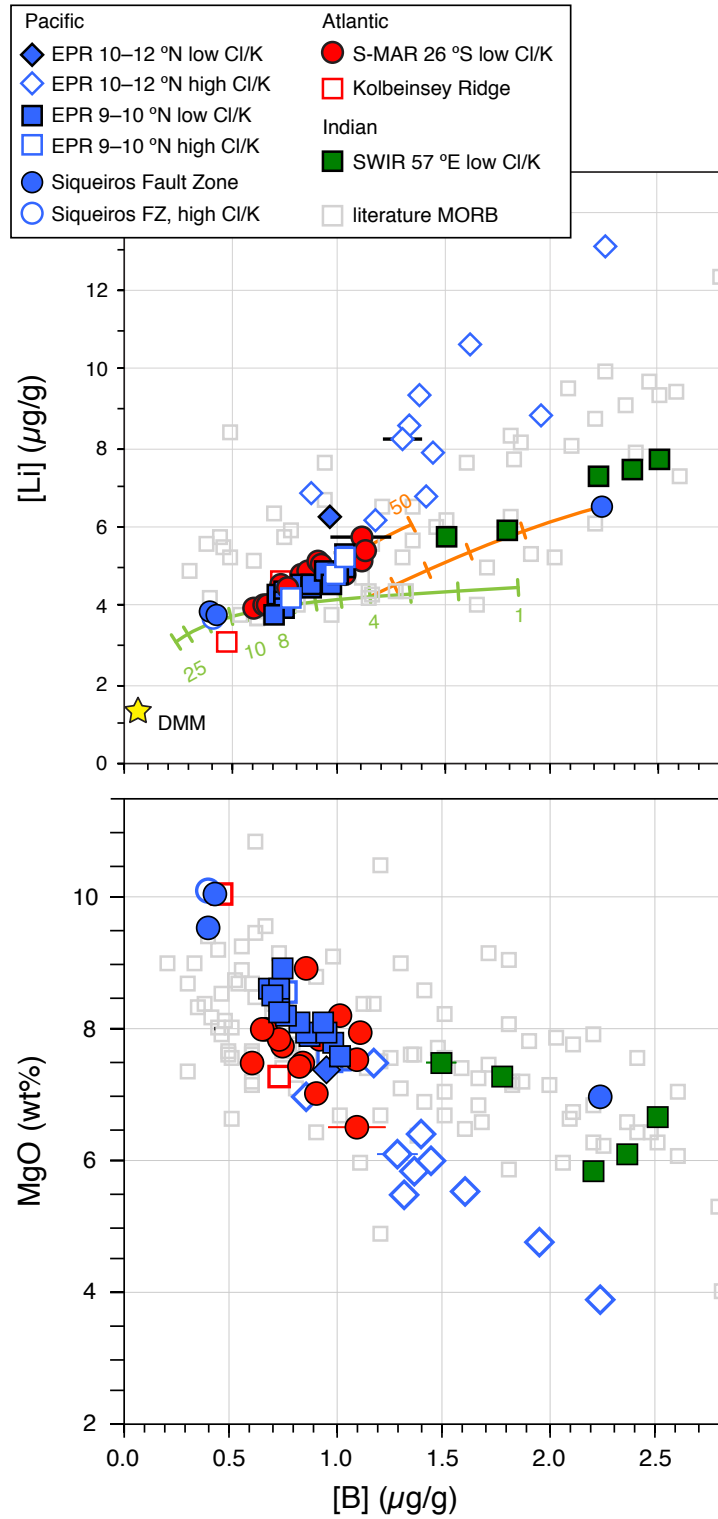


**Fig. 2** Upper panel: boron vs. Li concentrations of MORB glasses analysed in this study. The estimate for the composition of the depleted MORB mantle (DMM) is marked by the yellow star. Partial melting of the DMM produces (accumulated fractional) melts along the green line with numbers marking the degree of melting in percent. Fractional crystallisation of melts generated by 4% and 8% melting of the DMM would evolve along the orange-coloured lines with 10% tick marks and numbers marking the degree of fractional crystallisation. Lower panel: boron concentrations vs. MgO content. Literature values of MORB (from GeoRoc) are shown for comparison. Data sources are listed in Table 1.

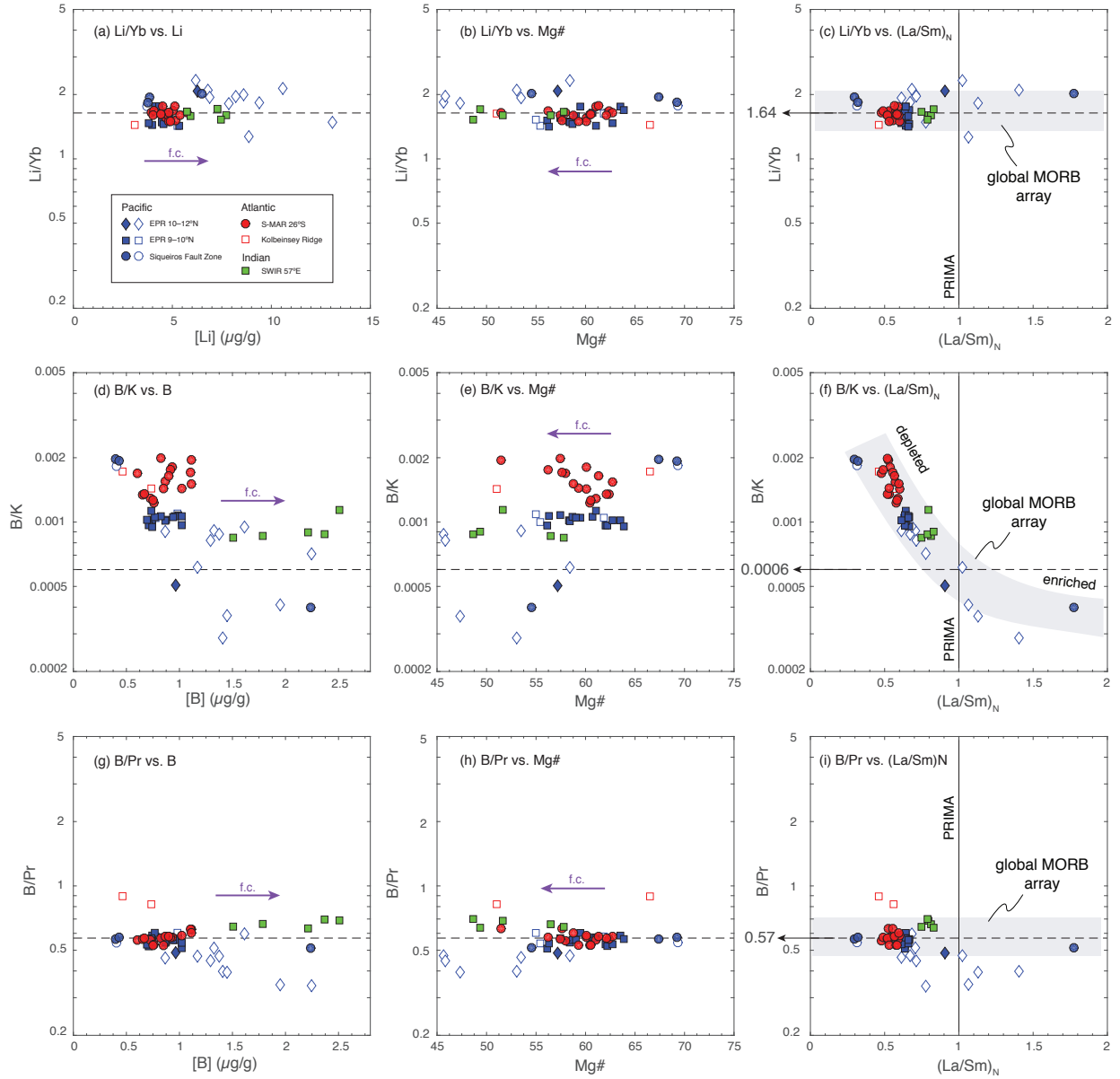


**Fig. 3** (a–c) Li/Yb ratios are relatively constant and do not correlate with [Li], Mg#, nor with primitive-mantle normalised La/Sm. The Li/Yb ratio of the primitive and depleted mantle are estimated at 1.7. Fractional crystallisation (f.c.) does not significantly change Li/Yb. (d–f) B/K ratios of low-Cl/K MORB glasses (filled symbols) vary widely among different ridge segments. Yet, individual ridge segments show relatively constant B/K and little variation with [B] or Mg#. A systematic decrease of B/K with increasing La/Sm is observed that describe a global MORB array (grey field), stretching from B/K = 0.0020 for highly depleted MORB to B/K = 0.0004 for enriched MORB. The array crosses the primitive mantle value ( $\text{La}/\text{Sm} \equiv 1$ ) at  $\text{B}/\text{K} = 0.0006 \pm 0.0002$ . (g–i) B/Pr ratios of low-Cl/K samples are relatively constant at 0.57 and do not show systematic variations with [B], Mg#, nor La/Sm. Filled symbols and open symbols mark samples with Cl/K lower and higher than 0.08, respectively. Four high-Cl/K samples have Mg# between 32 and 42 and are not displayed in panels b, e, and h.

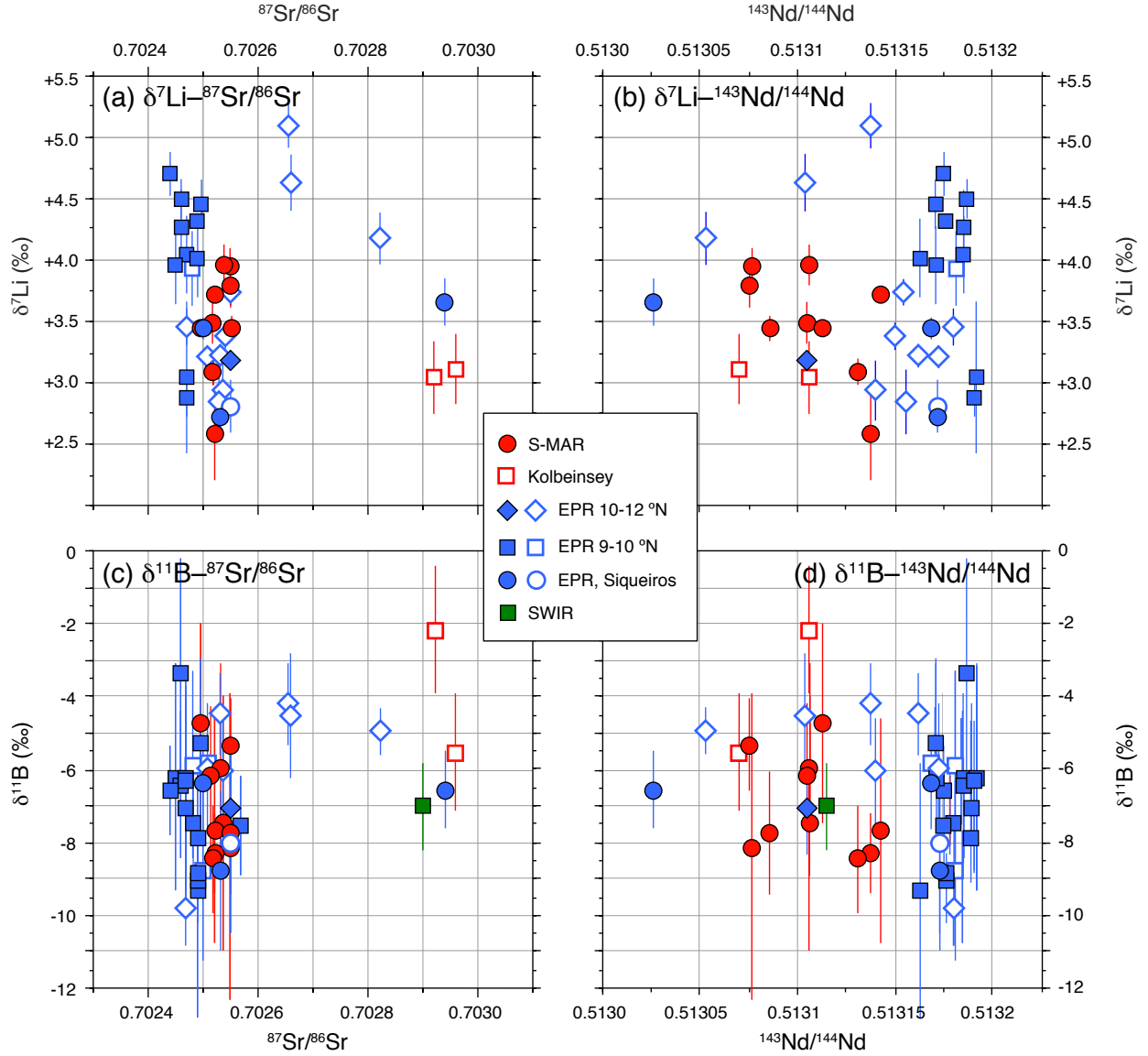


**Fig. 4** Lithium and B isotopic compositions of MORB glass samples plotted vs. radiogenic isotopes of Sr and Nd. (a)  $\delta^7\text{Li}$  vs.  $^{87}\text{Sr}/^{86}\text{Sr}$ ; (b)  $\delta^7\text{Li}$  vs.  $^{143}\text{Nd}/^{144}\text{Nd}$ ; (c)  $\delta^{11}\text{B}$  vs.  $^{87}\text{Sr}/^{86}\text{Sr}$ ; (d)  $\delta^{11}\text{B}$  vs.  $^{143}\text{Nd}/^{144}\text{Nd}$ . Lithium and boron isotopes do not vary systematically with radiogenic isotopes. Lead isotope plots are presented in the Supplement. Nd isotope ratios for EPR 9 – 10°N and the Siqueiros Fault Zone samples from Sims *et al.* (2002) were recalculated based on a CHUR  $^{143}\text{Nd}/^{144}\text{Nd} = 0.51262$  to be consistent with the other literature values. Filled and open symbols represent samples with Cl/K ratios below and above 0.08, respectively.

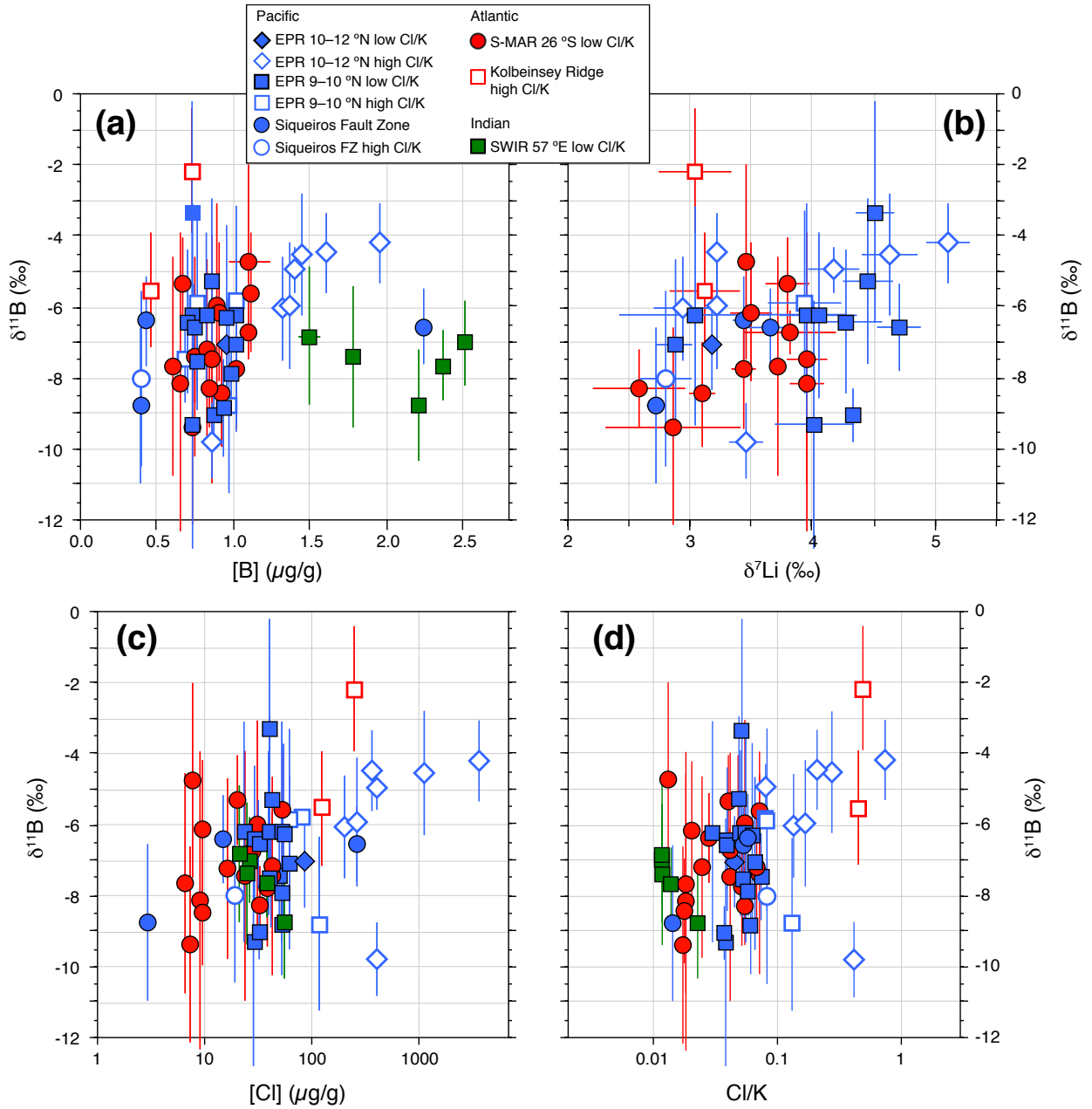


**Fig. 5** (a) Boron isotopic composition vs. boron concentration of investigated MORB samples. Note that the majority of high  $\delta^{11}\text{B}$  samples are enriched in B. SWIR (low degree of melting) and one Pacific E-MORB sample are enriched in B without elevated  $\delta^{11}\text{B}$ . (b) Boron vs. lithium isotopic composition of investigated MORB samples. (c) Boron isotopes vs. Cl concentration of investigated MORB samples showing a trend of high-Cl samples towards  $^{11}\text{B}$  enrichment. (d) Boron isotopes vs. Cl/K ratios of investigated MORB samples showing  $^{11}\text{B}$  enrichment in high-Cl/K samples. Filled and open symbols represent samples with Cl/K ratios below and above 0.08, respectively.



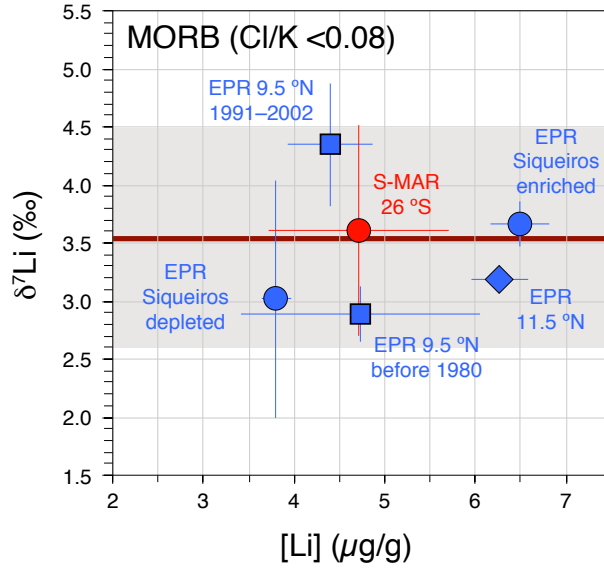


**Fig. 6** Mean lithium isotopic compositions and Li concentrations of mid-ocean ridge sections, excluding high-Cl/K samples. Error bars are 2SD. The EPR 9.5°N samples are subdivided into two groups with eruption ages before and after 1980, respectively. The red line marks the mean of the five investigated sections (+3.5‰) with the grey field showing the 2SD variation ( $\pm 0.9$ ‰). It should be noted that resolvable variation exists among the investigated sample sets.

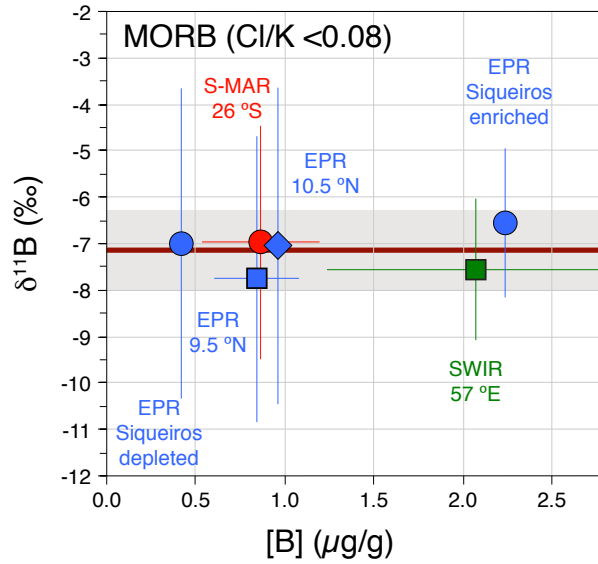


**Fig. 7** Mean boron isotopic compositions and B concentrations of mid-ocean ridge sections, excluding high-Cl/K samples. Error bars are 2SD. The red line marks the mean of the six investigated sections ( $-7.1$ ‰) with the grey field showing the 2SD variation ( $\pm 0.9$ ‰).

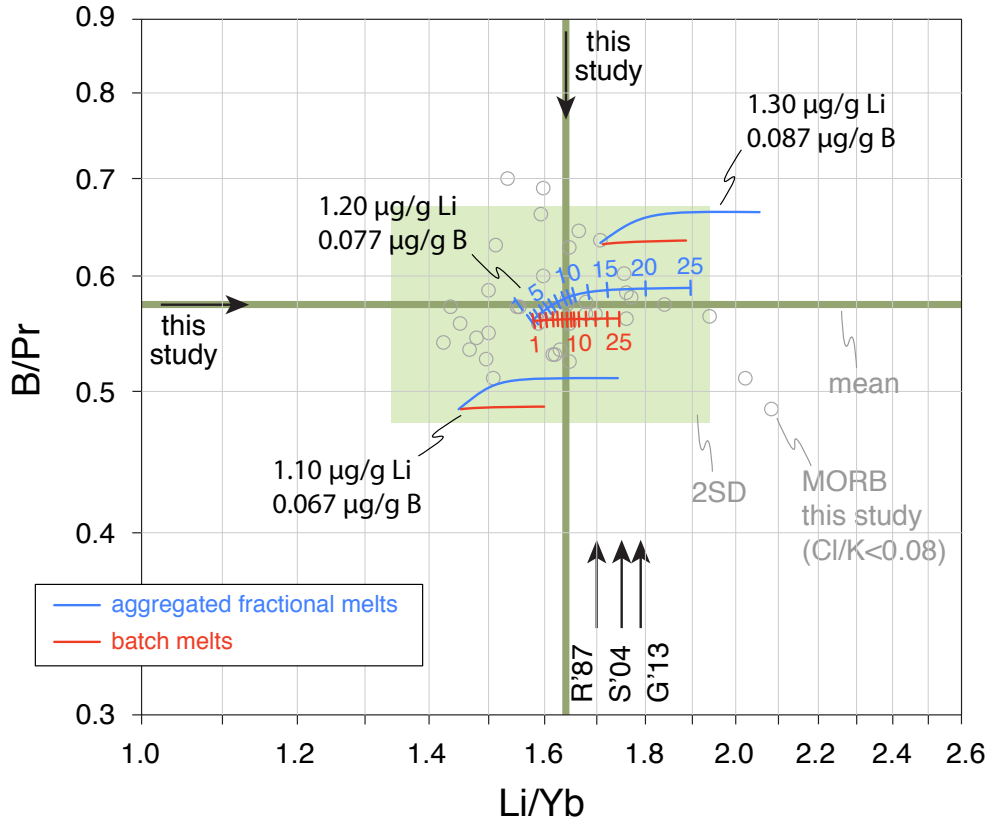


**Fig. 8** Results of mantle melting models to determine the Li and B abundances of depleted MORB mantle (DMM) by matching the Li/Yb and B/Pr ratios (log-log plot), as well as Li and B abundances observed in MORB. Arrows depict published average MORB values: R'87 = Ryan & Langmuir (1987), S'04 = Salters & Stracke (2004), G'13 = Gale *et al.* (2013). The green bars depict the mean Li/Yb and B/Pr ratios of all samples shown in grey circles, and the green box represents the 2SD field. The red curves depict the results of the batch melting calculations, and the blue curves show the composition of accumulated Rayleigh fractional melts with tick marks showing the degree of melting in percent. Three sets of models show the melts generated from three different Li and B abundances in the depleted mantle source. Model details are discussed in the Supplement.

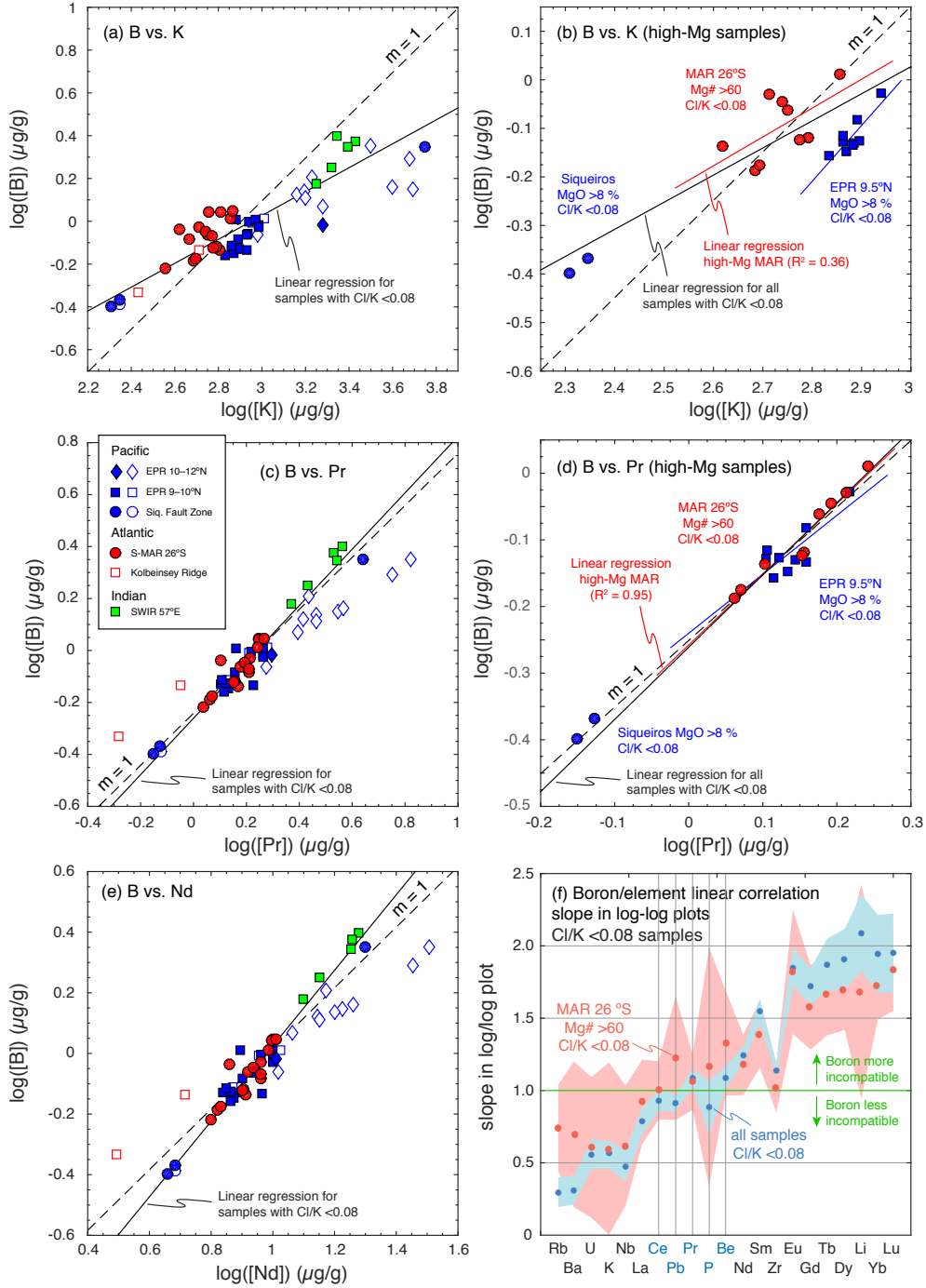


**Fig. 9** Compatibility plots after Hémond *et al.* (2006). (a) Log-log plot (base 10) of [B] vs. [K] for the full data set. The slope of the linear regression line of samples with low Cl/K (black line) is  $< 1$  (dashed line). (b) Log[B]-log[K] plot for high-Mg samples only. The slope of the linear regression line of the high-Mg, low-Cl/K samples from the MAR 26°S section is  $< 1$  (red line), showing that B is more compatible than K; (c) the log[B]-log[Pr] regression line for the global data set is close to slope 1; (d) the log[B]-log[Pr] regression line for the high-Mg, low-Cl/K samples from the MAR 26°S section is close to slope 1; (e) log[B]-log[Nd] regression line is steeper than slope 1. (f) Slopes of the linear regression lines in plots (a)–(e) and respective plots for other trace elements. The blue dots and field show the slopes and their uncertainties (2SD) of the linear regression lines for the low-Cl/K samples from all localities. The red dots and field show the slopes and uncertainties for the high-Mg, low-Cl/K samples from the MAR 26°S section. The slopes of Ce, Pb, Pr, P, Be, and Zr are close to unity, suggesting similar compatibilities of these elements and boron.

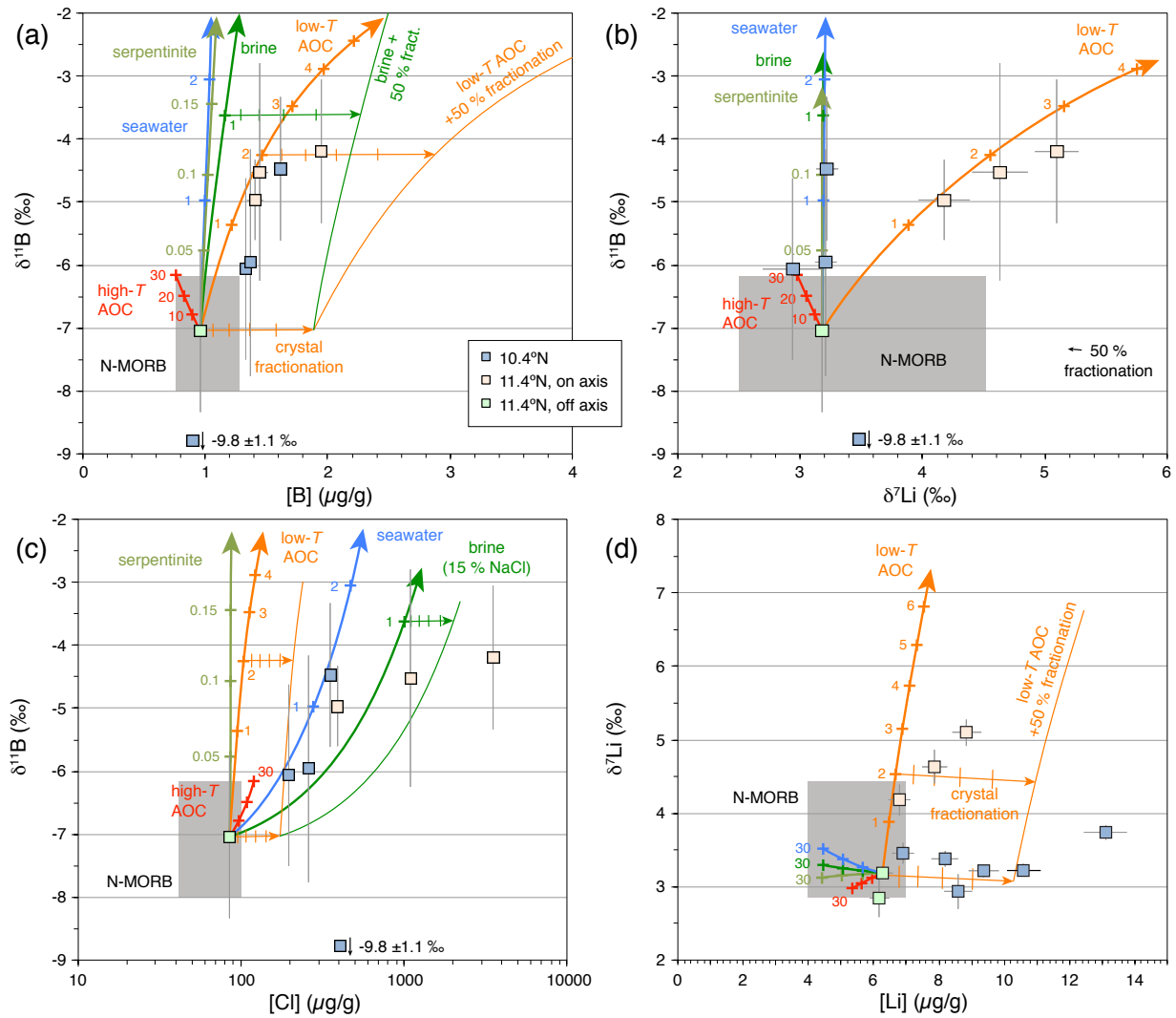


**Fig. 10** Geochemical modelling results of the effect of assimilation of seawater (thick blue lines), hydrothermal brine (thick green lines), serpentinite (yellowish-green lines), low-temperature altered oceanic crust (low-*T* AOC; thick orange lines), and high-temperature altered oceanic crust (high-*T* AOC; thick red lines). All numbers indicate the mass fraction of assimilated material in percent. The near-horizontal arrows indicate crystal fractionation (with tick marks at 10% intervals), and the thin lines indicate the results of combined assimilation and fractional crystallisation assuming equilibrium element and isotope fractionation. (a) Boron isotope ratios vs. B abundances; (b) boron isotope ratios vs. Li isotope ratios. The short black arrow indicates the negligible effect of 50% fractional crystallisation on Li and B isotopic composition of the melt. (c) Boron isotope ratios vs. Cl abundances; (d) lithium isotope ratios vs. Li abundances.

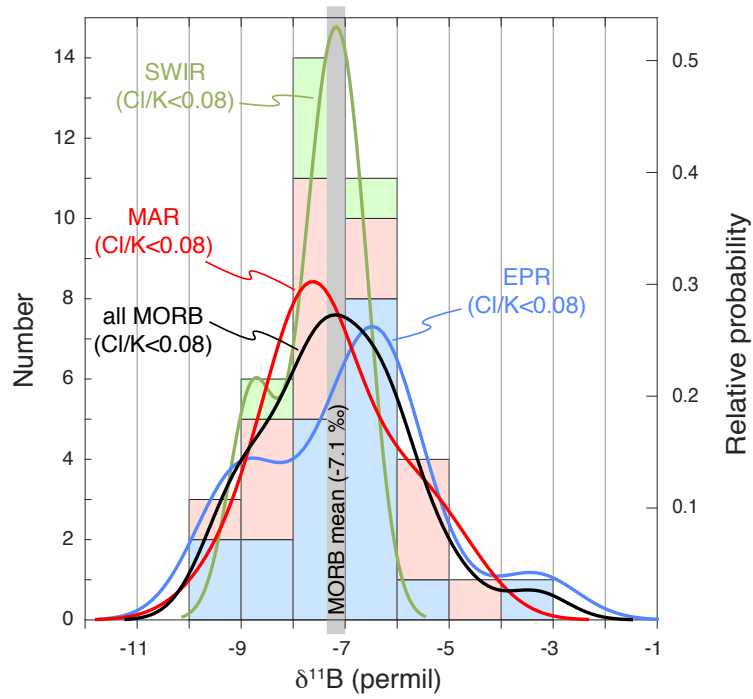


**Fig. 11** Probability-density plots and histogram of B isotope composition of low-Cl/K samples analysed in this study. Colours are: blue = EPR ( $n = 19$ ), red = MAR ( $n = 16$ ), green = SWIR ( $n = 5$ ), black = all samples ( $n = 41$ ). The mean value of the six investigated ridge sections ( $\delta^{11}\text{B} = -7.1\text{‰}$ ) is marked by the grey bar.

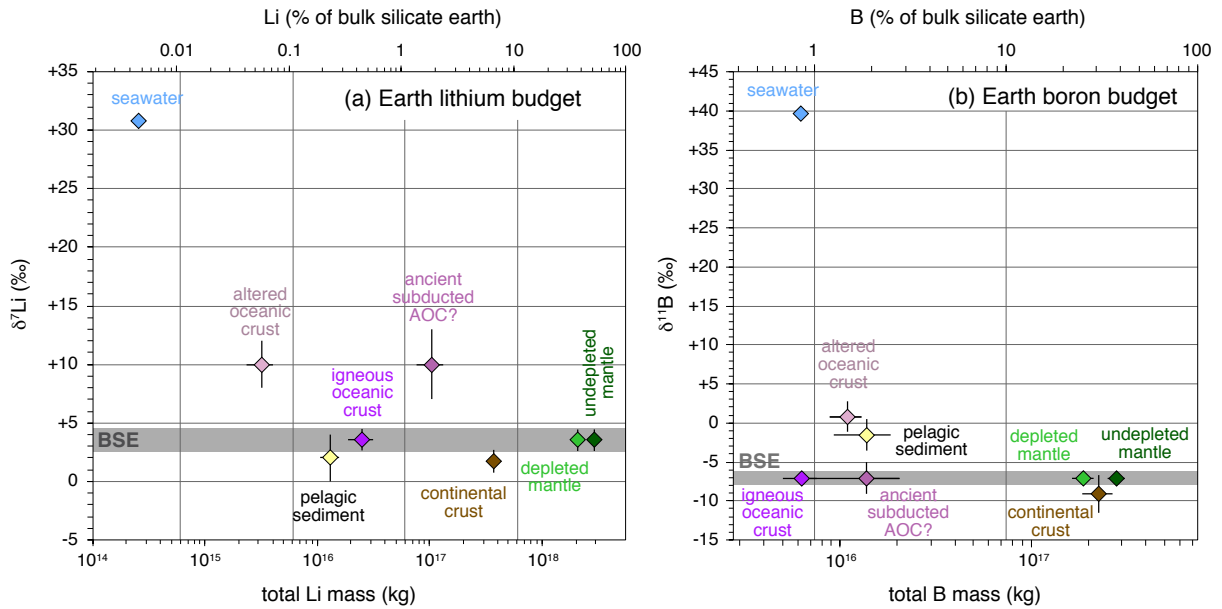


**Fig. 12** Geochemical budget of (a) Li, and (b) B in Earth's major reservoirs. Isotopic compositions on the y-axes, total mass of the element on the bottom x-axes, and fraction of the element of the bulk silicate earth budget on the top x-axes. Note that B has been more efficiently extracted from the mantle than Li. The bulk continental crust is estimated to be enriched in isotopically light Li and B compared to the mantle. This requires the presence of isotopically heavy Li in at least some domains of the mantle, which may be ancient subducted AOC (altered oceanic crust). Displayed values are listed in Table 6.

**Table 1** Investigated MORB glasses

Sample ID	Short ID	Latitude	Longitude	Depth (m)	[B] (μg/g)	$\delta^{11}\text{B}$ (‰)	2SEM (‰)	n	[Li] (μg/g)	$\delta^7\text{Li}$ (‰)	[Be] (μg/g)	[Cl] (μg/g)	[F] (μg/g)	Cl/K	References
East Pacific Rise, 10.5°N and 11.4°N regions (north of the Clipperton fault zone)															
MELPHNX-2-054-003	PH54-3	10.499°	-103.510°	3069	0.867 (44)	-9.8	1.1	8	6.90	+3.46 (15)	0.46	404	180	0.42	1-4
MELPHNX-2-062-001	PH62-1	10.483°	-103.614°	2812	1.291 (96)	n.a.			8.19	+3.38 (11)	0.64	n.a.	n.a.		2-5
MELPHNX-2-064-002	PH64-2	10.456°	-103.626°	3008	1.327 (40)	-6.1	1.4	3	8.60	+2.94 (24)	0.68	197	286	0.14	2,3
MELPHNX-2-065-001	PH65-1	10.453°	-103.635°	2996	1.614 (0)	-4.5	1.1	3	10.6	+3.22 (9)	0.78	353	339	0.21	1-4,6,7
MELPHNX-2-077-006	PH77-6	10.432°	-103.850°	3051	1.372 (51)	-6.0	1.8	3	9.38	+3.21 (9)	0.69	262	322	0.17	2,3
MELPHNX-2-078-002	PH78-2	10.427°	-103.859°	3058	2.245 (53)	n.a.			13.1	+3.74 (10)	1.39	n.a.	n.a.		1-4,8
MELPHNX-2-083-001	PH83-1	11.423°	-103.430°	3014	1.174 (51)	n.a.			6.17	+2.84 (26)	0.68	n.a.	n.a.		4,9
MELPHNX-2-094-001	PH94-1	11.369°	-103.709°	2864	0.961 (35)	-7.0	1.3	3	6.27	+3.18 (4)	0.55	86	182	0.045	1,2,4,9
MELPHNX-2-103-002	PH103-2	11.367°	-103.780°	2560	1.952 (48)	-4.2	1.1	7	8.86	+5.10 (18)	1.38	3525	661	0.74	1,2,4,9
MELPHNX-2-108-001	PH108-1	11.342°	-103.794°	2681	1.407 (65)	-5.0	0.6	3	6.79	+4.18 (21)	0.90	395	369	0.080	1,2,4,5,9,10
MELPHNX-2-GC060	PHGC-60	11.35°	-103.77°	2544	1.448 (67)	-4.5	1.7	3	7.86	+4.63 (23)	0.95	1097	407	0.28	2,9
East Pacific Rise, 9 – 10°N region (south of the Clipperton fault zone)															
ALV2351-002	2351-2	9.836°	-104.291°	2514	0.735 (1)	-3.3	3.1	4	3.97	+4.50 (16)	0.40	40	n.a.	0.052	11,12,13
ALV2352-002	2352-2	9.557°	-104.249°	2565	0.990 (3)	-7.9	0.7	3	4.82	n.a.	0.50	53	n.a.	0.057	11,14
ALV2355-008	2355-8	9.764°	-104.277°	2536	0.960 (13)	-6.3	2.6	3	4.55	n.a.	0.44	54	206	0.063	11,12,14,15
ALV2356-007	2356-7	9.682°	-104.265°	2554	0.939 (6)	-8.8	1.4	6	4.85	n.a.	0.45	53	213	0.061	11,12,14,15
ALV2358-003	2358-3	9.515°	-104.244°	2574	1.022 (41)	-7.1	2.4	6	5.35	+2.87 (15)	0.52	64	167	0.063	11,12,14,15
ALV2358-004	2358-4	9.515°	-104.244°	2574	1.023 (04)	-6.2	3.1	4	4.96	+3.04 (62)	0.52	52	n.a.	0.054	11,12,14
ALV2359-004	2359-4	9.888°	-104.298°	2558	0.876 (6)	-9.1	0.8	3	4.54	+4.32 (5)	0.47	32	n.a.	0.037	11-14
ALV2361-006	2361-6	9.652°	-104.260°	2559	0.696 (8)	-7.5	1.2	4	3.80	n.a.	0.38	50	n.a.	0.073	11,12
ALV2365-003	2365-3	9.280°	-104.218°	2584	1.025 (5)	-5.8	0.2	4	5.24	n.a.	0.54	82	241	0.080	11,12,14,15
ALV2368-004	2368-4	9.849°	-104.294°	2522	0.713 (8)	-6.4	2.0	3	4.27	+4.27 (31)	0.40	29	111	0.039	11,12,13
ALV2370-001	2370-1	9.792°	-104.284°	2523	0.980 (6)	-8.8	2.5	3	4.81	n.a.	0.48	117	n.a.	0.13	11,12,16
ALV2370-006	2370-6	9.792°	-104.284°	2523	0.768 (4)	-7.5	1.4	3	4.31	n.a.	0.38	39	n.a.	0.053	11,12
ALV2372-001	2372-1	9.843°	-104.292°	2521	0.773 (3)	-5.9	2.6	3	4.16	+3.93 (30)	0.41	62	n.a.	0.084	11-14,16,17
ALV2497-001B	2497-1B	9.888°	-104.297°	2555	0.863 (5)	-5.3	2.3	3	4.47	+4.46 (20)	0.45	42	201	0.049	11,13,15,17,18
ALV2504-001	2504-1	9.838°	-104.291°	2515	0.742 (2)	-6.2	3.1	5	4.36	+3.96 (32)	0.45	23	n.a.	0.030	11,12,13,17
ALV2746-003B	2746-3B	9.815°	-104.287°	2514	0.743 (1)	-9.3	3.5	7	4.15	+4.02 (32)	0.41	28	140	0.039	11,12
ALV2746-004	2746-4	9.815°	-104.288°	2515	0.827 (2)	-6.2	2.3	3	4.57	+4.04 (32)	0.42	39	n.a.	0.050	11,12,19
ALV2752-006	2752-6	9.838°	-104.291°	2516	0.747 (3)	-6.6	1.2	3	4.35	+4.70 (18)	0.44	31	113	0.040	11
East Pacific Rise, Siqueiros Fracture Zone															
ALV2384-003	2384-3	8.371°	-103.662°	3751	0.409 (7)	-8.0	2.5	6	3.71	+2.81 (22)	0.19	18	104	0.082	11-13,18,20-23
ALV2384-006	2384-6	8.371°	-103.668°	3707	0.399 (4)	-8.8	2.2	10	3.86	+2.72 (7)	0.22	3	94	0.014	11,12,18,20,22
AH1991-020-020	D20-2	8.348°	-103.649°	3100	0.428 (2)	-6.4	1.3	3	3.75	+3.44 (9)	0.20	13	87	0.058	11,13,20
ALV2390-005	2390-5	8.306°	-104.038°	3003	2.238 (0)	-6.6	1.1	3	6.49	+3.66 (19)	1.23	265	588	0.053	11,12,15

**Table 1** (continued)

Sample ID	Short ID	Latitude	Longitude	Depth (m)	[B] (μg/g)	δ <sup>11</sup> B (‰)	2SEM (‰)	n	[Li] (μg/g)	δ <sup>7</sup> Li (‰)	[Be] (μg/g)	[Cl] (μg/g)	[F] (μg/g)	Cl/K	References
<b>Mid-Atlantic Ridge, Kolbeinsey Ridge</b>															
POLARK5-022-002A	22DS-2A	67.096°	-18.722°	110	0.732 (3)	-2.2	1.7	6	4.67	+3.04 (29)	0.27	249	116	0.49	24,25
POLARK5-037-001	37DS-1	67.077°	-18.747°	170	0.466 (4)	-5.5	1.6	3	3.12	+3.11 (28)	0.18	124	39	0.46	24,25,26
<b>Mid-Atlantic Ridge, 26°S region</b>															
CON2802-012-021	D12-21	-25.700°	-13.911°	3980	1.116 (3)	-5.6	1.7	4	5.40	n.a.	0.50	53	193	0.072	27
CON2802-012-029	D12-29	-25.700°	-13.911°	3980	1.025 (6)	-7.8	1.7	11	4.81	+3.44 (10)	0.52	37	152	0.052	27-30
CON2802-014-001	D14-1	-25.775°	-13.918°	3985	0.917 (5)	-6.2	2.0	3	5.04	+3.49 (17)	0.45	9	141	0.021	27,29,30
CON2802-016-001	D16-1	-25.928°	-13.887°	3465	0.730 (19)	-9.4	2.8	3	4.51	+2.86 (55)	0.38	7	136	0.017	27,29
CON2802-017-004	D17-4	-25.996°	-13.877°	2675	0.826 (12)	-7.2	2.6	3	4.78	n.a.	0.47	16	160	0.025	27
CON2802-018-001	D18-1	-26.020°	-13.868°	2510	0.760 (5)	-7.2	1.5	4	4.42	n.a.	0.43	43	146	0.069	27,31
CON2802-018-002	D18-2	-26.020°	-13.868°	2510	0.753 (4)	-7.4	2.8	6	4.43	n.a.	0.43	43	144	0.072	27
CON2802-019-001	D19-1	-26.014°	-13.844°	2530	0.668 (24)	-5.3	1.3	5	4.02	+3.80 (18)	0.37	20	125	0.040	27,29,30
CON2802-019-002	D19-2	-26.014°	-13.844°	2530	0.650 (41)	-8.1	4.2	5	4.06	+3.95 (14)	0.37	9	122	0.019	27,30
CON2802-021-001	D21-1	-26.118°	-13.862°	3380	0.605 (31)	-7.7	3.1	3	3.95	+3.72 (3)	0.35	6	83	0.018	27,30
CON2802-022-006	D22-6	-26.231°	-13.809°	3785	0.852 (4)	-8.3	1.1	3	4.89	+2.58 (37)	0.43	32	154	0.055	27,30
CON2802-022-010	D22-10	-26.231°	-13.809°	3785	1.109 (141)	-4.7	2.7	3	5.74	+3.45 (5)	0.48	8	160	0.013	27,29,30
CON2802-023-007	D23-7	-26.332°	-13.794°	3705	1.105 (40)	-6.7	0.6	4	5.15	+3.81 (37)	0.47	27	156	0.042	27
CON2802-024-001	D24-1	-26.436°	-13.763°	3480	0.935 (5)	-8.5	1.5	3	4.68	+3.09 (10)	0.45	9	169	0.018	27,29,30,32
CON2802-025-001	D25-1	-26.471°	-13.772°	3760	0.901 (0)	-6.0	2.9	3	5.14	n.a.	0.45	30	165	0.055	27,29,30,32
CON2802-027-003	D27-3	-26.493°	-13.755°	3700	0.868 (2)	-7.5	3.5	3	4.82	+3.96 (16)	0.44	24	158	0.042	27,29,30
<b>South-West Indian Ridge, 57°E region</b>															
DIS0208-004-009M	4/9m(1)	-31.795°	57.557°	4800	2.51 (5)	-7.0	1.2	4	7.72	n.a.	1.09	26	400	0.012	33,34
DIS0208-004-012A	4/12a(1)	-31.795°	57.557°	4800	1.79 (3)	-7.4	2.0	4	5.94	n.a.	0.83	25	285	0.012	33,34
DIS0208-005-015G	5/15g	-31.773°	57.642°	4325	1.51 (7)	-6.8	1.9	4	5.75	n.a.	0.70	21	246	0.012	33,34
DIS0208-007-020A	7/20a	-31.782°	57.593°	4650	2.37 (5)	-7.6	1.0	4	7.46	n.a.	1.02	38	363	0.014	33,34
DIS0208-008-026F	8/26f(1)	-31.838°	57.527°	4600	2.51 (5)	-8.8	1.6	6	7.27	n.a.	1.09	56	369	0.023	33,34

References are: 1: Pan & Batiza (2003); 2: Elliott *et al.* (2006); 3: Regelous *et al.* (1999); 4: Turner *et al.* (2011); 5: Duncan & Hogan (1994); 6: Danyushevsky *et al.* (2000); 7: Sours-Page *et al.* (2002); 8: Batiza *et al.* (1996); 9: Niu *et al.* (1999); 10: Hahn *et al.* (2009); 11: Sims *et al.* (2002); 12: Cooper *et al.* (2009); 13: Goss *et al.* (2010); 14: Goldstein *et al.* (1994); 15: le Roux *et al.* (2006); 16: Smith *et al.* (2001); 17: Rubin *et al.* (1994); 18: Lundstrom *et al.* (1999); 19: Sims *et al.* (2003); 20: Perfit *et al.* (1996); 21: Danyushevsky *et al.* (2003); 22: Saal *et al.* (2002); 23: Arevalo & McDonough (2008); 24: Devey *et al.* (1994); 25: Mertz *et al.* (1991); 26: Salters (1996); 27: Niu & Batiza (1994); 28: Castillo & Batiza (1989); 29: Graham *et al.* (1996); 30: Regelous *et al.* (2009); 31: Batiza *et al.* (1988); 32: Batiza *et al.* (1989); 33: Robinson *et al.* (1996); 34: Robinson (1998).

**Table 2** Geochemical characteristics of investigated samples

MOR section	MgO (wt.%)	Mg#	$^{87}\text{Sr}/^{86}\text{Sr}$		$^{143}\text{Nd}/^{144}\text{Nd}$		$^{206}\text{Pb}/^{204}\text{Pb}$		$^{207}\text{Pb}/^{204}\text{Pb}$		$^{208}\text{Pb}/^{204}\text{Pb}$		Rb <sub>N</sub> , Ba <sub>N</sub> (PRIMA)	(La/Sm) <sub>N</sub> (CI)	References
			low	high	low	high	low	high	low	high	low	high			
Mid-Atlantic Ridge, 26°S	8.9-6.6	63-51	0.702496	0.702605	0.513076	0.513143	18.124	18.372	15.482	15.514	37.721	38.004	0.25-0.54	0.49-0.60	1,2,3,4
Kolbeinsey Ridge, 67°N	10.1-7.3	67-51	0.70292	0.70296	0.513070	0.513106	17.987	17.993	15.404	15.427	37.608	37.653	0.8-1.7	0.46-0.56	5,6
South-West Indian Ridge, 57°E	7.5-5.9	58-49	0.702898	0.703173	0.513051	0.513115	17.441	17.692	15.393	15.478	37.151	37.410	1.7-2.9	0.75-0.83	7
East Pacific Rise, 9 – 10°N	8.9-7.5	64-55	0.70244	0.70257	0.513163*	0.513192*	18.245	18.313	15.459	15.494	37.640	37.750	0.8-1.6	0.62-0.67	10
EPR 10.5°N	7.0-3.9	54-32	0.70247	0.70255	0.513140	0.513180	18.248	18.321	15.460	15.497	37.607	37.762	1.4-7.9	0.61-0.78	8
EPR 11.4°N	7.5-4.8	58-41	0.70253	0.70282	0.513053	0.513156	18.192	18.433	15.435	15.527	37.616	37.890	3.4-16	0.9-1.4	9
EPR, Siqueiros (D-MORB)	10.1-9.6	69-67	0.70250	0.70255	0.513169*	0.513172*	18.316	18.355	15.487	15.499	37.814	37.861	0.17-0.19	0.30-0.32	10,11,12
EPR, Siqueiros (E-MORB)	7.0	55		0.70294		0.513026*		18.646		15.540		38.077	18-21	1.8	10

Rb<sub>N</sub> and Ba<sub>N</sub> (PRIMA) are primitive-mantle normalised Rb and Ba abundances using values from McDonough & Sun (1995). (La/Sm)<sub>N</sub> is the CI chondrite normalised La/Sm ratio using values from Boynton (1985). \*Nd isotope ratios from EPR 9 – 10°N and the Siqueiros Fault Zone for Sims *et al.* (2002) were recalculated based on the CHUR  $^{143}\text{Nd}/^{144}\text{Nd} = 0.51262$  to be consistent with the other literature values. References are: 1 = Niu & Batiza (1994), 2 = Castillo & Batiza (1989), 3 = Graham *et al.* (1996), 4 = Regelous *et al.* (2009), 5 = Mertzt *et al.* (1991), 6 = Devey *et al.* (1994), 7 = (Robinson, 1998), 8 = Regelous *et al.* (1999), 9 = Niu *et al.* (1999), 10 = Sims *et al.* (2002), 11 = Perfit *et al.* (1996), 12 = Saal *et al.* (2002).



**Table 3** Data summary

Locality	[B] ( $\mu\text{g/g}$ )	B/Pr	B/Be	[Li] ( $\mu\text{g/g}$ )	Li/Yb	(La/Sm) <sub>N</sub>	$\delta^{11}\text{B}$ ( $\text{‰}$ )	$\delta^7\text{Li}$ ( $\text{‰}$ )	n	Spreading rate mm/a
East Pacific Rise; 10.5°N and 11.4°N										
All samples	1.4 (8)	0.45	1.77	8.4 (41)	1.90	0.88	-5.6 (37)	3.3 (14)	11	104
Cl/K < 0.08 only	0.96 (3)	0.49	1.75	6.3 (3)	2.08	0.91	-7.0 (34)	3.2 (1)	1	
East Pacific Rise; 9°N–10°N										
All samples	0.9 (2)	0.56	1.91	4.5 (8)	1.56	0.64	-6.3 (30)	4.2 (12)	18	112
Cl/K < 0.08 only	0.8 (2)	0.55	1.91	4.5 (8)	1.57	0.64	-7.8 (31)	4.2 (12)	15	
Cl/K < 0.08; >1980	0.9 (3)	0.55	1.94	4.7 (13)	1.48	0.65	-7.7 (14)	2.9 (2)	4	
Cl/K < 0.08; <1980	0.8 (2)	0.56	1.89	4.4 (5)	1.60	0.64	-7.8 (36)	4.3 (5)	11	
East Pacific Rise; Siqueiros Fracture Zone, depleted MORB										
All samples	0.41 (3)	0.56	2.02	3.8 (2)	1.85	0.31	-7.2 (24)	3.0 (8)	3	
Cl/K < 0.08 only	0.41 (4)	0.57	1.95	3.8 (2)	1.89	0.31	-7.0 (34)	3.0 (10)	2	
East Pacific Rise; Siqueiros Fracture Zone, enriched MORB (Cl/K < 0.08)										
Enriched MORB	2.24 (0)	0.51	1.81	6.5 (1)	2.02	1.8	-6.6 (16)	3.7 (2)	1	
Kolbeinsey Ridge; 67°N (all have Cl/K > 0.08)										
All samples	0.6 (4)	0.86	2.63	3.9 (22)	1.53	0.51	-4.0 (47)	3.1 (1)	2	20
Mid-Atlantic Ridge; 26°S (all have Cl/K < 0.08)										
All samples	0.9 (3)	0.57	1.96	4.7 (10)	1.62	0.55	-7.0 (25)	3.6 (9)	16	26
South-West Indian Ridge; 57°E (all have Cl/K < 0.08)										
All samples	2.1 (8)	0.67	2.19	6.8 (18)	1.62	0.79	-7.6 (15)	n.a.	5	13-16
Global sample set										
All samples	1.1 (10)	0.56	1.95	5.5 (38)	1.67	0.7	-6.4 (32)	3.5 (12)	56	
Cl/K < 0.08 only	1.0 (11)	0.57	1.96	4.9 (20)	1.64	0.6	-7.4 (26)	3.6 (12)	40	
Cl/K < 0.025 only	1.3 (15)	0.61	2.02	5.4 (27)	1.66	0.6	-7.6 (25)	3.5 (9)	13	
Average of localities										
All samples	1.2 (14)	0.60	2.04	5.5 (35)	1.73	0.8	-6.3 (24)	3.5 (9)		
Cl/K < 0.08 only	1.2 (15)	0.56	1.93	5.4 (25)	1.80	0.8	-7.1 (9)	3.5 (9)		

Data summary showing mean values for each ridge segment investigated here, mean values for the full global sample set, and values for the average of all investigated localities. For each category, we list mean values of all samples and for the subset of samples with low Cl/K. Numbers in parentheses give 2SD uncertainties at the last digit.

**Table 4** Lithium and boron abundances in MORB and mantle

Geochemical reservoir	[Li] ( $\mu\text{g/g}$ )	[B] ( $\mu\text{g/g}$ )	comment
primitive mantle	<b>1.39 (10)</b> 0.75	<b>0.19 (2)</b> 0.15	mass balance estimates calculated from constant ratios with Pr and Yb from McDonough & Sun (1995)
depleted mantle	<b>1.20 (10)</b> 0.62	<b>0.077 (10)</b> 0.061	batch and fractional melting models calculated from constant ratios with Pr and Yb from Workman & Hart (2005)
N-MORB	6.63 6.17	1.19 1.28	calculated from constant ratios with Pr and Yb from Hofmann (1988) calculated from constant ratios with Pr and Yb from Gale <i>et al.</i> (2013)

Batch and fractional melting models were calculated using experimentally determined partition coefficients and MORB trace element ratios (see Supplement for details). Employed ratios for MORB are: Li/Yb = 1.7, and B/Pr = 0.573. Preferred values are printed in bold font. Numbers in parentheses give 2SD uncertainties at the last digit.

**Table 5** Parameters and composition of assimilated materials used for geochemical modelling of assimilation

	[B] ( $\mu\text{g/g}$ )	$\delta^{11}\text{B}$ ( $\text{‰}$ )	[Li] ( $\mu\text{g/g}$ )	$\delta^7\text{Li}$ ( $\text{‰}$ )	[Cl] ( $\mu\text{g/g}$ )	data source
pristine melt	0.96	-7.04	6.27	+3.18	86	[1]
low- <i>T</i> AOC	26	+0.8	27	+20	1000	[2]
high- <i>T</i> AOC	0.3	+0.5	3.0	+2.0	200	[3]
serpentine	60	+35	0.10	-5.0	1000	[4]
seawater	4.4	+39.61	0.18	+30.8	19350	[5]
brine (15 % NaCl)	20.2	+12.5	0.15	+15	91000	[6]

[1] the composition of sample PH94-1 was used for the uncontaminated MORB initial composition; [2] data from Smith *et al.* (1995), Chan *et al.* (2002), and Tomascak *et al.* (2008); [3] data from Ishikawa & Nakamura (1992), Chan *et al.* (2002), and Barnes & Cisneros (2012); [4] data from Bonifacie *et al.* (2008), and Vils *et al.* (2009); [5] data from Broecker & Peng (1982), Spivack & Edmond (1987), Rosner *et al.* (2007), and Foster *et al.* (2010); [6] [B] calculated from fluid–mineral partition data from Marschall *et al.* (2006), the B abundance in high-*T* AOC, and an assumed greenschist facies rock composition (albite+chlorite+actinolite+epidote+quartz), which resulted in a rock/fluid partition coefficient for B of 0.015. Boron isotopic composition calculated from fluid–mineral B isotope fractionation data of Wunder *et al.* (2005) for 400°C and the B isotopic composition of high-*T* AOC. [Li] and Li isotope data from Tomascak *et al.* (2008).

**Table 6** Mass balance for Li and B for the silicate Earth

	continental crust	oceanic crust	altered ocean. crust	pelagic sediments	seawater	total of crustal res.	subducted ancient AOC	depleted mantle	undepleted mantle	bulk silicate Earth	data source
Mass ( $10^{21}$ kg)	20.6	6.3	0.42	0.26	1.4	29.0	13.7	2460	1510	4010	[1,2], $\rho$ , $V$
% of BSE	0.51	0.16	0.010	0.007	0.035	0.72	0.34	61	38	$\equiv$ 100	
[Li] ( $\mu\text{g/g}$ )	18 (2)	4 (1)	7.6 (20)	50 (10)	0.18 (1)	14 (1)	7.6 (20)	1.20 (10)	1.39 (10)	1.39 (10)	this study, [3,4,5,6,7,8]
% of BSE	6.7 (9)	0.5 (1)	0.06 (2)	0.24 (5)	0.0046 (4)	7.4 (4)	1.9 (5)	53 (6)	38 (4)	$\equiv$ 100	
$\delta^7\text{Li}$ (‰)	<b>+1.7</b> (10)	<b>+3.5</b> (9)	<b>+10</b> (2)	<b>+2</b> (2)	<b>+30.8</b> (1)	+1.9 (10)	<b>+10</b> (3)	<b>+3.5</b> (9)	<b>+3.5</b> (10)	+3.5 (10)	this study, [3,5,6,7,8,9]
[B] ( $\mu\text{g/g}$ )	11 (2)	1.0 (2)	26 (5)	53 (18)	4.4 (1)	9.1 (12)	1 (5)	0.077 (10)	0.187 (19)	0.187 (19)	this study, [3,4,6,8,12,13]
% of BSE	30 (5)	0.8 (2)	1.5 (3)	1.9 (6)	0.83 (2)	35.3 (1)	1.8 (9)	25 (3)	38 (4)	$\equiv$ 100	
$\delta^{11}\text{B}$ (‰)	-9.1 (24)	<b>-7.1</b> (9)	<b>+0.8</b> (20)	<b>-1.6</b> (20)	<b>+39.61</b> (4)	<b>-7.1</b> (9)	<b>-7.1</b> (9)	<b>-7.1</b> (9)	-7.1 (9)	-7.1 (9)	this study, [8,11,12]

Mass balance input parameters for isotope values are given in bold font. Data sources are: [1] Hay *et al.* (1988); [2] Huang *et al.* (2013); [3] Taylor & McLennan (2009); [4] Rudnick & Gao (2003); [5] Teng *et al.* (2008, 2009); [6] Broecker & Peng (1982); [7] Bourman *et al.* (2004); [8] You *et al.* (1995); [9] Rosner *et al.* (2007); [10] Chan *et al.* (2002); [11] Chan *et al.* (2006); [12] Smith *et al.* (1995); [13] Foster *et al.* (2010). Mass balance models are based on the assumption that Li and B isotopes are not fractionated during mantle melting. The isotopic compositions of the continental crust and of the total of all crustal reservoirs (including continental crust, fresh and altered oceanic crust, pelagic sediments and seawater) result from the mass balance calculation. AOC = altered oceanic crust. Values in parentheses depict estimated or propagated uncertainties in the last digit.